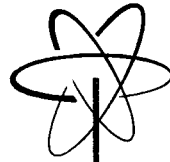# EMERGENCY COOLING
IN BWR's UNDER SIMULATED
LOSS-OF-COOLANT CONDITIONS

(BWR-FLECHT FINAL REPORT)

J. D. DUNCAN
J. E. LEONARD

GENERAL ⨁ ELECTRIC

EMERGENCY COOLING IN
BOILING WATER REACTORS UNDER
SIMULATED LOSS-OF-COOLANT CONDITIONS

(BWR—FLECHT FINAL REPORT)

J. D. Duncan
J. E. Leonard

Approved: _____   Approved: _____

R. G. Bock   F. A. Schraub
Project Engineer   Manager, Core Development

ATOMIC POWER EQUIPMENT DEPARTMENT ● GENERAL ELECTRIC COMPANY
SAN JOSE, CALIFORNIA 95125

GENERAL ⊛ ELECTRIC

NOTICE

TABLE OF CONTENTS

LIST OF ILLUSTRATIONS

List of Illustrations (continued)

List of Illustrations (continued)

List of Illustrations (continued)

LIST OF TABLES

ABSTRACT

The Boiling Water Reactor Full Length Emergency Cooling Heat Transfer (BWR-FLECHT) test program has been completed. This document summarizes the results of that program. Five Zircaloy-clad and five stainless steel-clad full scale BWR bundle mockups were tested under simulated loss-of-coolant conditions. Approximately 150 transient and steady state tests were conducted from 1968 to 1970. The test program has significantly increased the understanding of the heat transfer performance during the emergency cooling phase of the postulated BWR loss-of-coolant accident. The test data and the analysis indicate that both the top-spray and bottom-flooding modes of emergency cooling will terminate the cladding temperature increase and minimize the consequences of the postulated loss-of-coolant accident. The models developed for spray cooling heat transfer allow a conservative prediction of the consequences of the accident. Specifically, the local cladding temperature and local cladding strength can be calculated as a function of time during the accident.

1. SUMMARY

This document is a summary of the Boiling Water Reactor Full Length Emergency Cooling Heat Transfer Program. The subjects covered include:

1.   Spray cooling test results of four stainless steel-clad and five Zircaloy-clad heater bundles. The bundles were tested under simulated loss-of-coolant conditions (Section 4).

2.   Bottom flooding test results of two stainless steel-clad heater bundles tested under simulated loss-of-coolant conditions (Section 5).

3.   A correlation of heat transfer data which will provide conservative predictions of the maximum cladding temperatures in a BWR loss-of-coolant accident (Sections 6 and 7).

A summary of the bundles tested under the FLECHT program is given in Table 1.

2. INTRODUCTION

This is the final report describing the results of the BWR Full Length Emergency Cooling Heat Transfer (FLECHT) program. The loss-of-coolant accident has been investigated in some detail at General Electric[1,2,3] before the FLECHT program was conceived. The FLECHT program was designed to further investigate the significant heat transfer mechanisms during the emergency cooling phase of the postulated BWR loss-of-coolant accident. The effect of the thermal transient on Zircaloy cladding was investigated for the first time in this test program.

The program was funded by the Atomic Energy Commission. Testing and analysis of test results was accomplished by the Core Development Subsection of the General Electric Atomic Power Equipment Department in San Jose, California. Testing extended from July 1968 to October 1970. Technical program management was provided by the Phillips Petroleum Company and Idaho Nuclear Corporation.

Transient and steady state tests were conducted with full length, 49-rod stainless steel-clad heater rod bundles which were designed to simulate Zircaloy-clad fuel bundles. Both General Electric BWR modes of emergency cooling (top spray and bottom flooding) were investigated. In addition, four Zircaloy-clad bundles were tested under spray cooling conditions and a fifth was tested under combined spray and flooding conditions. The primary reason for testing the Zircaloy-clad bundles was to investigate the performance of the cladding under extremely severe loss-of-coolant/emergency cooling conditions. A detailed test plan is included in Reference 4.

Definition of Terms Used—Several terms used frequently in this report are defined here:

a.   *Bundle Power (Full channel power)*—The power at which the corresponding reactor fuel bundle was operating at the time of a loss-of-coolant initiated reactor scram.

b.   *Peak Power*—The maximum power applied to the test bundle, equal to 5% of full power (corresponding to the power level at 30 seconds after the scram).

c.   *Spray Flow Rate*—The rate at which spray flow is introduced at the top of the test bundle.

d.   *Flooding Rate*—The rate at which the bundle and outer channel area would fill if the bundle were unheated and if spray water were not accumulating at the bottom of the bundle.

Table 1
FLECHT TESTING SUMMARY

Bundle Testing Date	Type of Tests	Tests	Peak Power (kW)	Coolant Rate	Initial Temperature (°F)	Reference
SS1N July 68	Flooding	5 Steady State 16 Transient	20-325 240-390	To Hold Level 0.6-3.7 ips	— 1328-2150	GEAP-10117
SS2M Aug-Sept 68	Spray	4 Steady State 15 Transient	200-250 120-390	2.1-2.6 gpm 1.1-3.35 gpm	— 1120-2050	GEAP-10092
SS3M Sept-Dec 68	Spray	4 Steady State 38 Transient	200 120-390	0.6-2.1 gpm 0.4-6.5 gpm	810-1450	GEAP-10092
Zr1M May 69	Spray	1 Transient	200	2.45 gpm	1790	GEAP-10092
SS2N Aug-Oct 69	Spray	3 Steady State 24 Transient 8 Combined Spray & Flooding	150 100-250 250-325	1.0-2.45 gpm 2.45-5.0 gpm 2.0-3.5 gpm 2.0-6.0 ips	— 865-1850 1335-1870	GEAP-13086
Zr2K Dec 69	Spray	1 Transient	195	2.45 gpm	1920	GEAP-13112 NEDG-13064
Zr3M Mar 70	Spray	1 Transient	240	2.45 gpm	2345	GEAP-13174
Zr4M May 70	Spray	1 Transient	240	2.45 gpm	2298	GEAP-13174
Zr5M June 70	Spray with Delayed Flooding	1 Transient	300	3.25 gpm 6.0 ips	2325	GEAP-13174
SS4N Sept-Oct 70	Spray Flooding	10 Transient 11 Transient	250 250	2.45 gpm 1.5-6.0 ips	1076-1718 1300-1600	GEAP-13190

Totals:
5 Zircaloy-Clad Bundle Spray Transient Tests
11 Stainless Steel-Clad Bundle Steady State Spray Tests
95 Stainless Steel-Clad Bundle Spray Transient Tests
5 Stainless Steel-Clad Bundle Steady State Flooding Tests
27 Stainless Steel-Clad Bundle Flooding Transient Tests

e. *Initial Temperature*—The maximum temperature of the cladding at initiation of spray.

f. *Local Convective Heat Transfer Coefficient (or often simply "film coefficient" or "coefficient")*—The coefficient h defined by:

$$q/A = h \ (T \ surface - T \ coolant)$$

where q/A is the calculated heat transfer rate to the coolant including convection and radiation to the coolant and excluding radiation to the wet channel walls, and

T surface is the measured surface temperature and

T coolant is the assumed coolant temperature (taken at the saturation temperature).

g. *Rod Groups*—The rods in the 7 X 7 array are often grouped by these descriptive terms:
  * Corner Rods (Group 1)—The four rods in the corners.
  * Side Rods (Group 2)—The twenty other rods on the outside of the bundle, next to the channel.
  * Outside Rods—Corner and side rods.
  * Inside Rods (Group 3)—The sixteen rods which are one row removed from the channel.
  * Central Rods (Group 4)—The nine rods in the center of the array.

h. *Bundle Designation*—The test bundles were designated descriptively with letters indicating the cladding material (SS for stainless steel and Zr for Zircaloy), a number indicating the order of testing and a letter indicating the heating element material (N for Nichrome, K for Kanthal, M for Molybdenum). Thus, Zr2K was the second Zircaloy-clad test and Kanthal elements were used.

3. EQUIPMENT, INSTRUMENTATION, AND TEST PROCEDURES

The test equipment, instrumentation, and the test procedures are described in detail in the several FLECHT reports. Significant characteristics of the test facilities and the procedures are outlined briefly here.

3.1 HEATER ROD BUNDLES

The test bundles consisted of 49 stainless steel or Zircaloy-clad heater rods held in a 7 X 7 square array on an 0.738 inch pitch by eight BWR spacers. In the atmospheric pressure tests, the heaters were held in place by a top tie plate (which also served as a common electrical ground) and a bottom tie plate. These end restraints allowed relatively little expansion of the heater rods and rod bowing resulted. In the high pressure (SS4N) tests, the heaters were welded to a steel forging at the bottom and allowed to expand through sliding electrical contacts at the top. The test bundles were enclosed by square stainless steel or Zircaloy channels.

3.1.1 Stainless Steel-Clad Heater Rod Design

The stainless steel-clad heaters were double-clad heater rods with Nichrome V or molybdenum heating elements. High purity magnesium oxide powder held the coils in place and insulated them from the cladding. Three heater coil designs were used during FLECHT testing:

a. Molybdenum coils with the pitch varied to produce the desired axial power shape at a specific design temperature distribution (test bundles SS2M and SS3M).

b. Nichrome V coils with the pitch varied to give a 1.37 maximum to average axial power factor (test bundles SS1N and SS2N).

c. Nichrome V coils with the pitch varied to give a 1.47 maximum to average axial local power factor (test bundle SS4N).

The basic heater rod was grooved longitudinally; Chromel-Alumel stainless steel-sheathed thermocouples were placed in the grooves and a second tube was swaged over the first to provide a finished diameter of 0.570 inches.

3.1.2 Zircaloy—Clad Heater Rod Design

The internal construction of the Zircaloy-clad heaters was similar to that of the stainless steel-clad heaters: a heating coil (Kanthal in the case of bundle Zr2K to give a 1.47 peak to average axial power and molybdenum for the other bundles) was insulated from the cladding by Al_2O_3 powder. The Zr1M and Zr2K bundles had thermocouples attached to the inner cladding surface, and all bundles except Zr2K had thermocouples attached to the outer cladding surface.

3.2 TEST FACILITIES

All the bundles except the last (SS4N) were tested in the atmospheric pressure test facility in R tower. The facility consists of a vertical stainless steel channel (the "outer channel") in which the inner channel and test bundles were mounted. Coolant flow was directed to the bottom or sprayed over the top of the test bundles. A supply tank, pump, heat exchanger, throttle valves, and rotometers were used to provide the desired flow rate and inlet water temperature. Bundle SS4N (high pressure) tests were conducted in the building G test loop. This loop is equipped with a steam drum "pressurizer" and additional heaters to provide for pressure control.

3.3 POWER SUPPLIES

All the stainless steel bundles and the first two Zircaloy bundles (Zr1M and Zr2K) were powered with a variable 60-cycle power supply. Local power peaking was provided with a bank of peaking transformers. The last three Zircaloy bundles were powered by a silicon controlled rectifier (SCR) unit. This unit was necessary to minimize power shifting from rod group-to-rod group in the bundles which had molybdenum filaments.

3.4 INSTRUCTION, DATA ACQUISITION, AND DATA REDUCTION

The cladding and channel temperatures were recorded on a Hewlett-Packard Dymec Data Acquisition System and were reduced on a GE-635 digital computer using the SCE data reduction program. During the later stages of the project the data reduction program was improved to provide the data in card form. These data were then input to a second program which calculated individual local heat transfer coefficients.

Other test variables (for example, coolant inlet temperature and flow rate) were recorded in various ways, depending on the test bundle.

3.5 TEST PROCEDURES

Very briefly the bundles were tested as follows:

a. A constant power was applied and the bundle was heated to a particular temperature.

b. The transient was initiated by simultaneously starting the power on the post accident decay curve and initiating coolant flow.

c. In a few cases (bundles SS2N and Zr5M) flooding was initiated at a specified time after spray initiation.

d. The test was completed after all cladding temperatures had been reduced to well below the maximum temperature.

e. In the case of the Zircaloy-clad test bundles, the bundles were removed from the test facility, disassembled, and photographed.

4. SPRAY TEST RESULTS

The results of the FLECHT spray tests are summarized in this section. Detailed results are available in the following FLECHT documents:

Test Bundles	Document
SS2M and SS3M (Stainless steel-clad, molybdenum filaments)	GEAP-10092 (reference 5)
Zr1M (Zircaloy-clad molybdenum filaments)	GEAP-10092 (reference 5)
SS2N (Stainless steel-clad, Nichrome filaments)	GEAP-13086 (reference 6)
SS4N (Stainless steel-clad, Nichrome filaments, high pressure)	GEAP-13190 (reference 7)

Zr2K (Zircaloy-clad,
Kanthal filaments,
internal pressure)

NEDG-13064 Preliminary
Report (reference 8) and
GEAP-13112 (reference 9)

Zr3M, Zr4M, Zr5M (Zircaloy-
clad, molybdenum filaments)

GEAP-13174 (reference 10)

The test data and analysis indicate that:

a. The rugged, double-clad, stainless steel heater design is an excellent test vehicle for investigating the loss-of-coolant accident.[5,6,7]

b. Bundles which employ molybdenum filaments provide an atypical thermal response to the simulated accident. This nontypicality results from molybdenum's high temperature coefficient of electrical resistivity.[5,10]

c. Local heat transfer coefficients calculated using data obtained from stainless steel-clad bundles with constant resistance heating elements (Nichrome) should provide a conservative model for use in predicting the results of a loss-of-coolant accident in a BWR.[6,7,9,10]

d. The high temperature Zircaloy-clad test bundles (Zr3M, Zr4M and Zr5M) were tested under extremely severe conditions (to $\sim$ 2900°F). The resulting damage was confined within the channels[10] enclosing the bundles. The high temperatures resulted from experimental problems, and a fuel bundle would probably not be damaged in exactly the same manner if it were heated to the same temperatures. However, it is likely that fuel bundle damage would also be confined to the channels, even if temperatures as high as 2900°F were attained.

e. Given the thermal response of Zircaloy cladding, the oxidation (and, therefore, the strength of the cladding and energy release rate of the metal-water reaction) can be calculated with reasonable accuracy.[9,10] The Baker-Just[11] Zircaloy-water reaction equation is quite conservative, and a rate constant of approximately one-half the Baker constant is recommended.[10]

f. The effects of Zircaloy-cladding failures (swelling and perforations) on the accident appear to be small.[8,9]

g. Increasing system pressure above atmospheric significantly improves the performance of spray cooling.[7]

4.1 EARLY STAINLESS STEEL-CLAD BUNDLES WITH MOLYBDENUM HEATING ELEMENTS

Pre-FLECHT General Electric funded spray cooling tests[3] indicated that the use of molybdenum coils as heating elements would not severely affect the results of spray cooling tests. The electrical failure of several heater rods in this test series and in the first FLECHT spray bundle (SS2M) biased the results of these tests. That is, unpowered rods in the bundles* provided relatively cool sinks for radiation heat transfer and low maximum temperatures (typically less than 2100°F) resulted. The testing of the second FLECHT spray bundle (SS3M) resulted in significantly higher maximum temperatures. Subsequent analysis indicated that the local axial heater power distribution was distorted by the molybdenum filaments. Molybdenum has a high temperature coefficient of electrical resistivity (the resistance doubles between 1300 and 2500°F, see Figure 1 of reference 5). The variable pitch of the heating elements was selected to give the desired peak-to-average axial power factor (1.37) at a particular axial temperature distribution (Figures 2 and 3 of reference 5). This temperature distribution did not occur in the tests, and as the midplane temperature was increased (as occurred in SS3M testing), the resistance increased which increased the local power and further increased the local temperature. The resulting positive feedback mechanism was limited only by increased radiation from the hot rod surfaces. The fact that the molybdenum filaments were causing the higher test temperatures was confirmed analytically in the following manner. A bundle heat transfer coefficient** for an early stainless steel clad test which had Nichrome (constant resistance filaments) was determined. The local power factors resulting from the skewed temperature profiles in bundle SS3M were calculated. The film coefficient and local power was then used to predict the actual maximum

---

* For example, rods 8, 9, 10, 15 and 16 were unpowered during the SS2M transient testing.[5] Thus, three cold rods adjacent to rod 17 (the highest powered central rod) caused lower maximum temperatures. It should also be noted that electrical failures in the Zr2K (internal pressure) test reduced the maximum temperature of that bundle.[9] The reduction in the later case was relatively small because most of the ten failures occurred slightly before or after the time of maximum temperature and therefore did not effect the maximum bundle temperature.

** This calculation was made using the Tiger V heat transfer program.[3] A single coefficient, variable with time, was determined by trial and assumed to exist on all rods. The coefficient which gave the correct maximum bundle temperature variation with time was used. This technique was later improved[6,7] to provide individual rod heat transfer coefficients.

temperature variation in a single SS3M test (see Figure 1). The prediction was reasonably accurate with the prediction being within 100°F of the data for at least 8 minutes. The implication is that the same heat transfer coefficient (designated h Nichrome) is applicable in both tests and that the increased local power resulting from molybdenum power shifting caused the higher maximum temperatures.

A steady state analysis was presented in reference 5 which provided some insight into the problems which might result from the use of molybdenum filaments. A model was developed which allowed the calculation of the change in maximum test temperature resulting from small changes in one of several test parameters. An example of the results is shown in Figure 2. A particular local center section resistance results when a heater rod is fabricated. An error in fabrication results in a proportional error in local power density if Nichrome elements are used. A change in the maximum temperature results. If molybdenum filaments are used, however, the positive feedback mechansim results in a much larger temperature change as the figure indicates. Other analyses (Figure 30 of reference 5) indicated that with molybdenum filaments the maximum test temperature was quite sensitive to changes in coolant (sink) temperature, the local heat transfer coefficient, and the heater rod coil-to-cladding thermal resistance.

4.2 LATER STAINLESS STEEL-CLAD BUNDLES WITH NICHROME HEATING ELEMENTS

Two test series were run during 1969 (SS2N) and 1970 (SS4N). The stainless steel-clad heater rods used in these tests had Nichrome V heating elements. Since the electrical resistance of Nichrome wire is almost independent of temperature, the power shifting problems encountered with molybdenum filaments (Section 4.1) were avoided. Consequently, the results of these tests series provided the most valuable data in the FLECHT program. Individual local heat transfer coefficients were calculated at the midplane in both bundles. The significant heat transfer mechanisms occurring during the emergency cooling phase of the postulated accident were inferred from the calculated coefficients. A spray cooling model was developed which provides generally conservative predictions of the thermal response of Zircaloy-clad bundles. The model can be expected to provide conservative predictions of a postulated loss-of-coolant accident thermal transient in a General Electric BWR. The model is discussed in detail in Sections 6 and 7 and in Reference 16.

4.2.1 Bundle SS2N (Atmospheric Pressure)

Three series of tests were conducted: steady state spray (3 tests at 150 kW power and variable spray flow rate), transient spray (23 tests at 100 to 250 kW peak power, 2.45 to 5.0 gpm spray rate, and 865°F to 1850°F initial temperature) and combined spray and flooding transients (8 tests at 200 to 325 kW peak power, 2.0 to 3.25 gpm spray rate, 1330°F to 1870°F initial temperature with bottom flooding at 2.0 to 6.0 inches-per-second initiated two minutes after the start of the spray transient). The significant results are summarized here.

The effect of bundle initial temperature and peak power in the spray transient tests are shown in Figure 3. The maximum cladding temperature is plotted against initial temperature with peak power as a parameter. Data from earlier GE funded tests[3] are also plotted. Figure 3 shows that as the initial temperature is increased at one power, the maximum temperature approaches the initial temperature. That is, the temperature rise ($T_{max} - T_i$) decreases as the initial temperature increases. This results from increased convection and radiation heat transfer from the hotter rod surfaces.

The SS4N data (Section 4.2.2), at one atmosphere pressure, indicated higher maximum temperatures as shown in Figure 3. The difference can only be partially explained by uncertainties in the tests. The differences between the two test series (still not completely understood) are discussed in more detail in Reference 7.

The SS2N and earlier test data indicated that there is a relatively small effect of spray flow rate on the bundle thermal response. Figure 4 shows the cladding temperature rise as a function of spray rate at three different peak powers with initial temperature as a parameter. There is a small effect of spray flow rate between 0.5 gpm, one fifth the BWR minimum rate, and 5 gpm, twice the minimum. For example, at 250 kW peak power, increasing the rate from 2.5 to 5.0 gpm at an initial temperature of approximately 1350°F results in a reduction from 570°F to 470°F on the cladding temperature increase. Thus, considerable margin is demonstrated and no sudden deterioration in performance is observed as flow is reduced to one-fifth of the design value.

The tests with bottom flooding starting approximately two minutes after the power decay and spray flow was initiated indicated that the temperature rise is terminated almost immediately with the onset of flooding. Thus, there was no evidence of the coolant failing to reach the hottest parts of the test bundle.

Individual rod local heat transfer coefficients during the spray transients were originally calculated at the midplane of the test bundle using the FILMCO computer program.[6] Figure 5A is an example of the coefficients
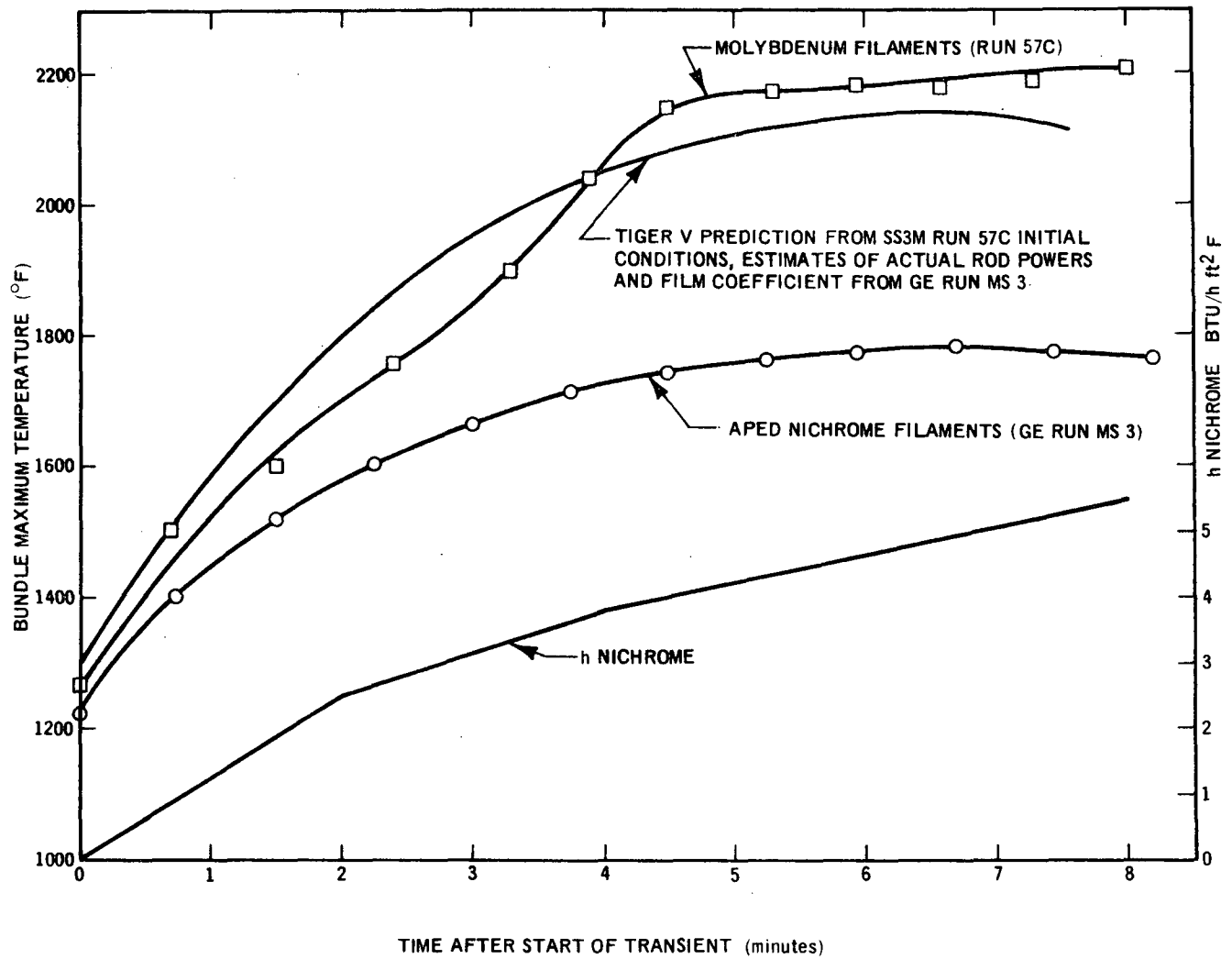
Figure 1   *Effect of Molybdenum Power Shifting on Bundle Maximum Temperature*
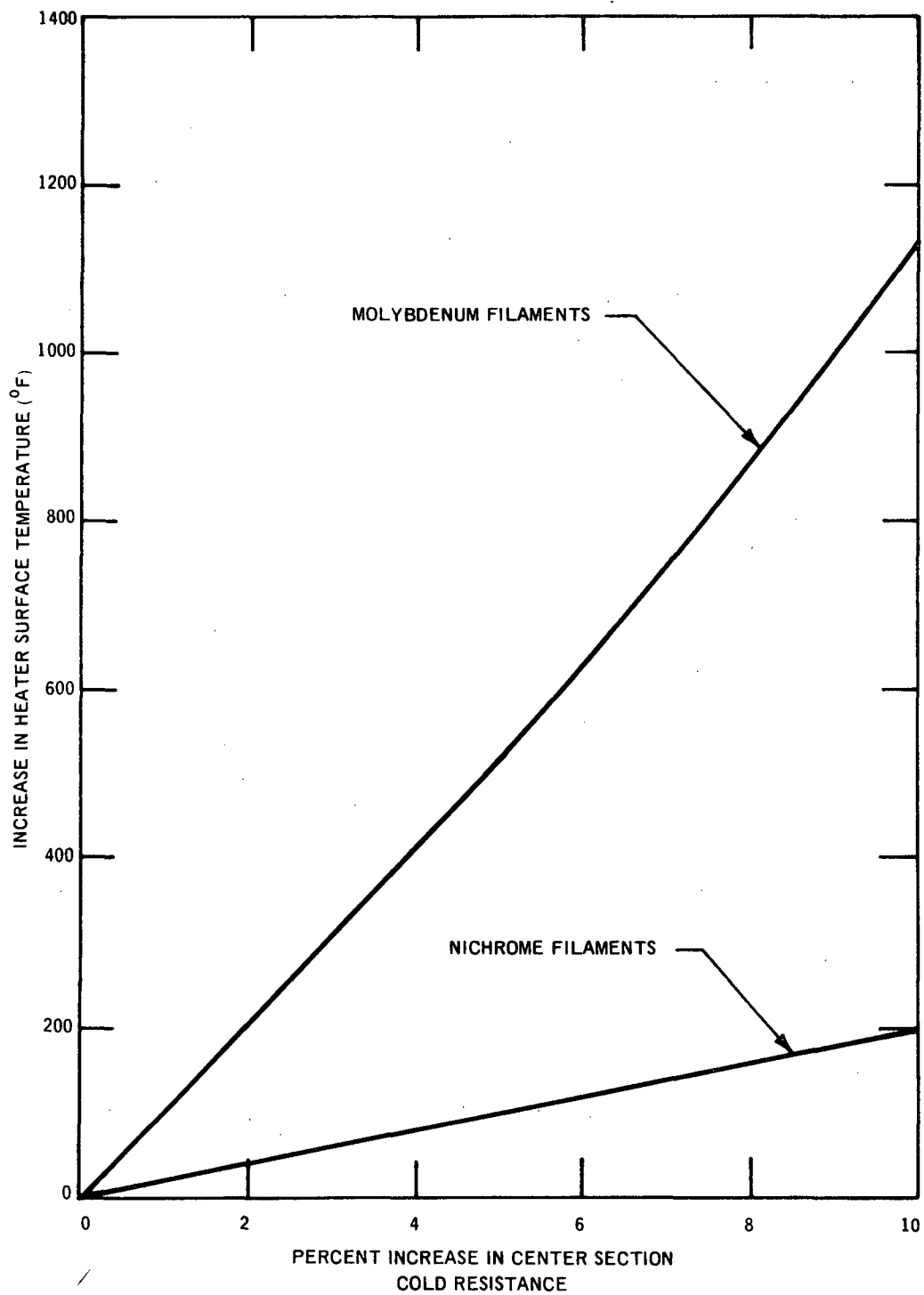
Figure 2   Sensitivity of Molybdenum and Nichrome-Filamented Heater Maximum Surface
Temperature to Center Section Cold Resistance
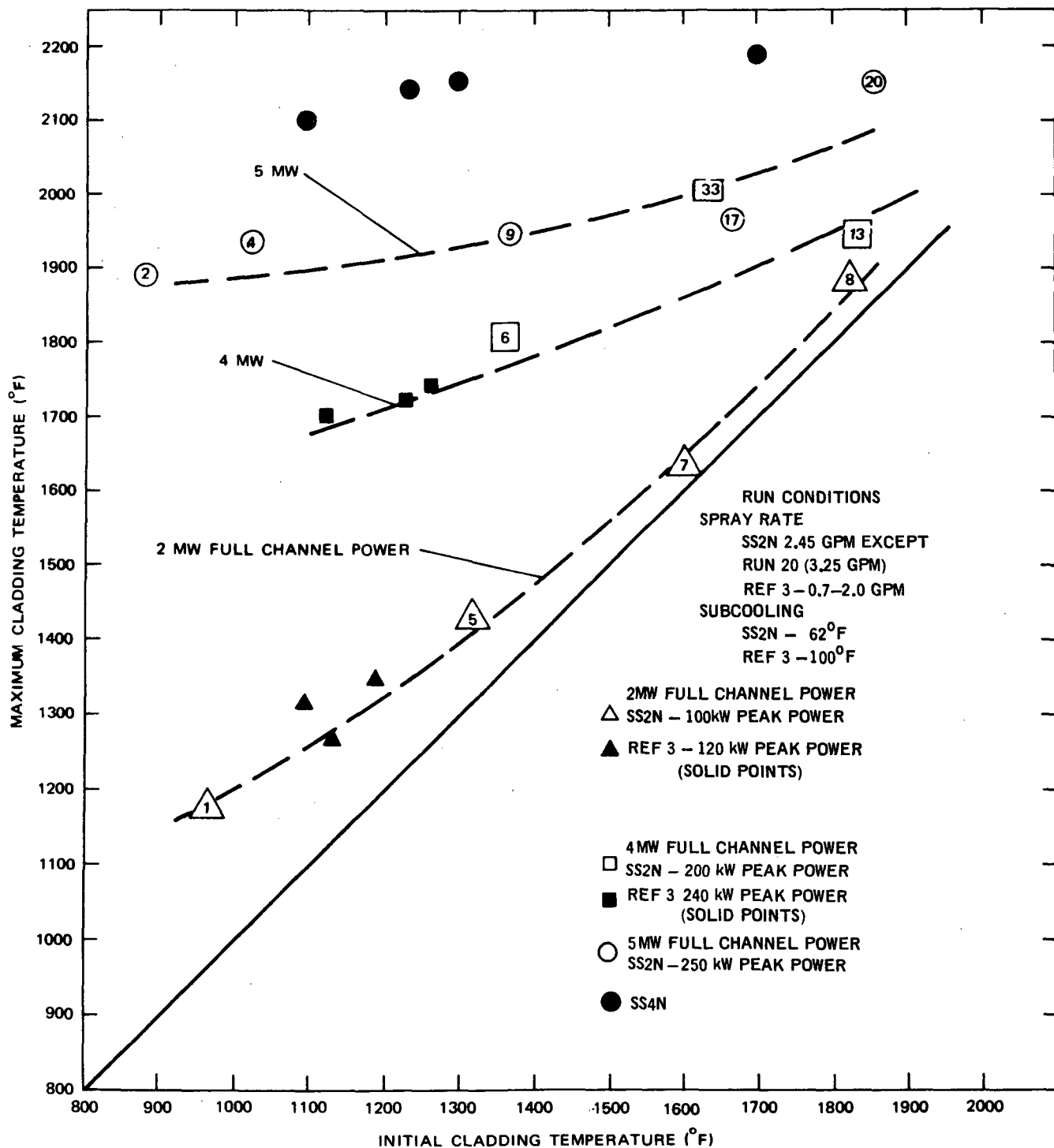
Figure 3 Effect of Initial Cladding Temperature and Bundle Power on Maximum Cladding Temperature; FLECHT Bundle SS2N
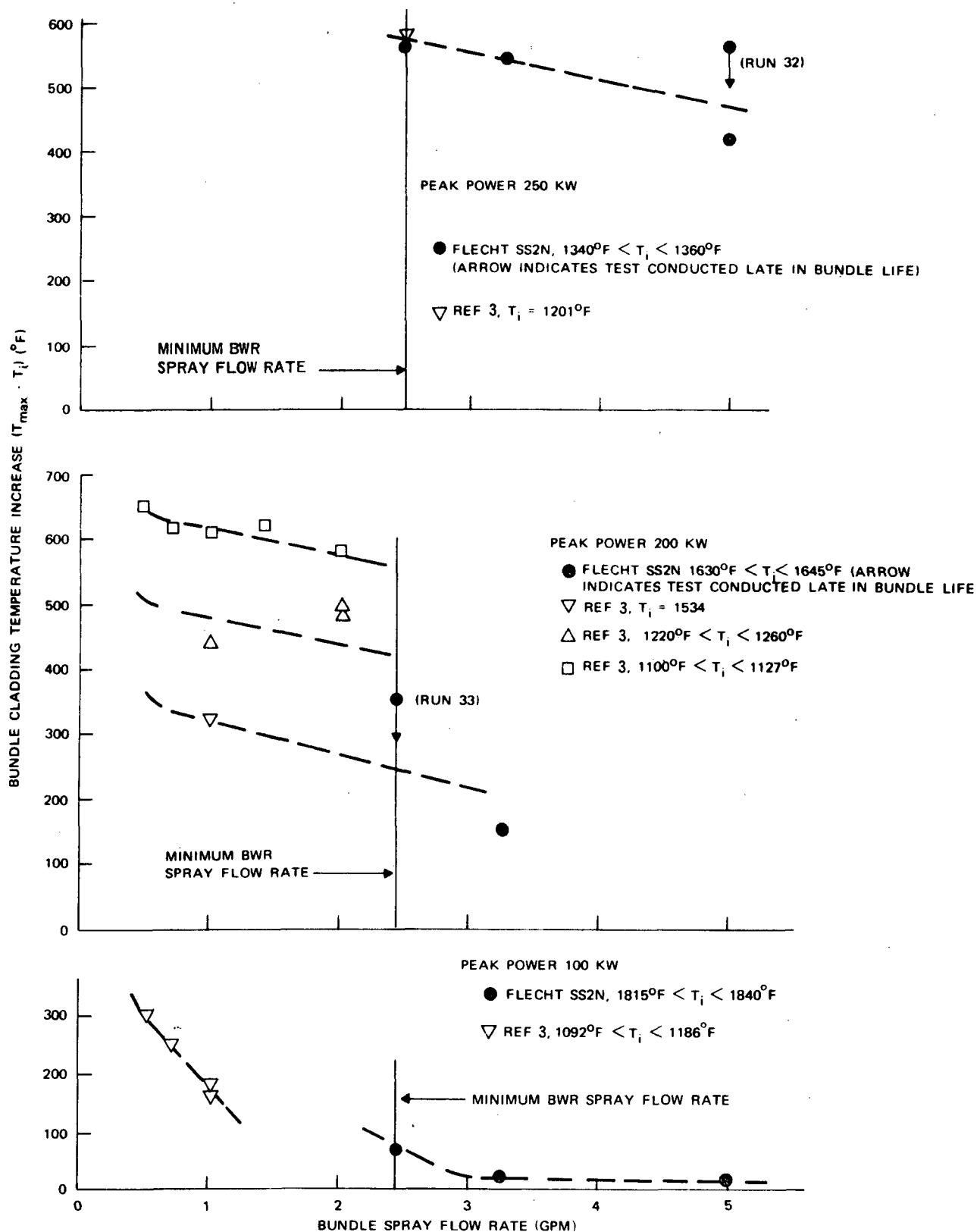
Figure 4   Effect of Spray Flow Rate at 100, 200 and 250 kW Peak Power and
Various Initial Temperatures; FLECHT Stainless Steel-Clad Bundle SS2N
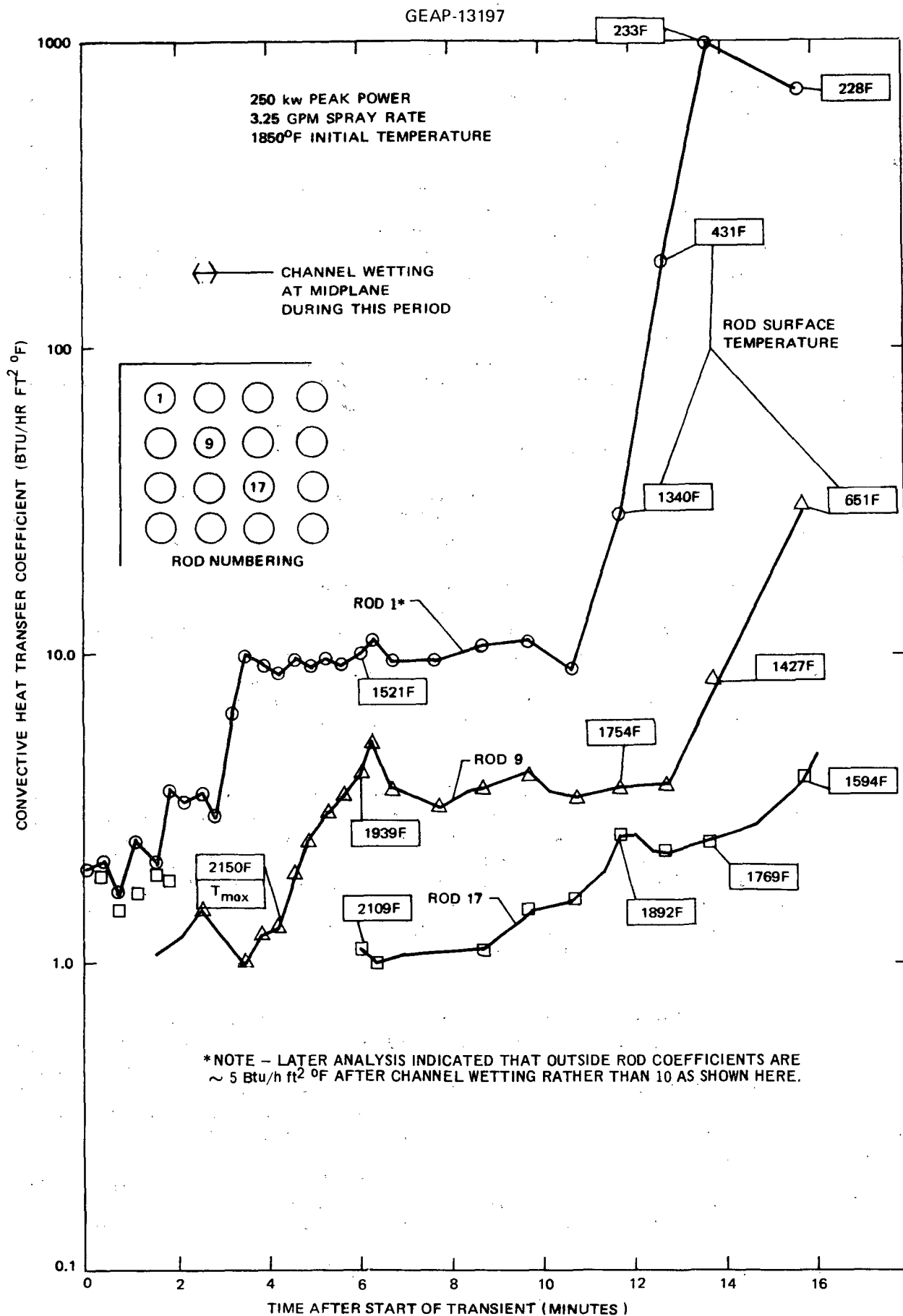
Figure 5A   Film Coefficient Variation with Time and Bundle Position in
High Temperature ($T_{max} = 2150°F$) Spray Cooling Transient in Bundle SS2N

-11-

calculated. The coefficients decreased as distance from the channel increased. This suggests that the coolant is more dense near the channel which enclosed the test bundle. The coefficients on outer rods increased dramatically when the channel was cooled to saturation. Apparently, water drops sputtering off the film front as it advances down the channel, impinge on the outer rods (and to a smaller extent on the inner rods) and cause an increase in local convective heat transfer. The coefficients calculated for the highest temperature spray transient (SS2N run 20) were used to conservatively predict the results of three Zircaloy-clad test bundles.[9,10] The calculation was later refined by improving the FILMCO program. The improved version calculated heat transfer coefficients on a greater number of rods and included a better radiation model (the channel emissivity was changed to that of water at the time of channel wetting). An example of the calculated film coefficients is shown in Figure 5B. The prediction of Zircaloy test results using coefficients determined in this manner is discussed in Sections 6 and 7.

4.2.2 Bundle SS4N (Pressure to 300 psia)

The reactor vessel pressure decay following the postulated loss of coolant is not immediate. A significant time interval (a few minutes) will exist during which the pressure will be well above atmospheric (say from 30 to 200 psia). Consequently, the first series of SS4N tests was conducted with system pressure variable from 15 to 300 psia.

The test results show that increasing the system pressure significantly enhances the effectiveness of the spray cooling mechanism. Figure 6 shows the midplane temperature variation of a central rod with time after spray initiation at several pressures.

Increasing the pressure reduces the maximum temperature and causes the bundle to cool to saturation more quickly. For example, at 15 psia a maximum temperature of 2080°F was recorded and the temperature was still above 1900°F, 28 minutes of the spray initiation; at 200 psia the maximum temperature was 1740°F and the midplane had cooled to below 1200°F after 24 minutes.

More effective spray cooling performance at high pressure appears to result from the fact that the channel and heater rods are more easily wetted (cooled to saturation temperature) as the pressure increases. As the coolant saturation temperature increases, the Leidenfrost temperature (at which the surfaces will wet) increases. Consequently, the liquid film progresses down the channel and the heater rods wet more rapidly as the pressure increases.[7] The coolant density throughout the bundle is thereby increased and more effective cooling results.[7] In addition, with the channel and outer rods wetting more quickly as the pressure increases, the cold sink for radiation heat transfer is closer to the hottest rod (typically one of the nine central rods) and lower temperatures result.

4.3 ZIRCALOY-CLAD BUNDLES

Five Zircaloy-clad bundles were tested under spray cooling conditions during the FLECHT program. Four of the bundles were heated with molybdenum filaments (Zr2K Kanthal was the exception) and many of the molybdenum power shifting problems discussed in Section 4.1 were encountered again. In spite of these problems and other experimental difficulties, a great deal of valuable information relating to the performance of Zircaloy cladding under extremely severe loss-of-coolant conditions was obtained from these tests. In addition, although the thermal response of the molybdenum-heated bundles cannot be considered typical of BWR fuel bundle performance, it was possible to calculate the actual local power densities and to subsequently provide a check of the emergency cooling heat transfer models developed from stainless steel-clad bundle tests (Sections 6 and 7).

4.3.1 Bundle Zr2K (Internal Pressure)

Zircaloy-clad test bundle Zr2K (with constant resistance Kanthal heating elements) was tested with a peak power of 195 kW, spray flow of 2.45 gpm, and an initial temperature of 1800°F. The heater rods were internally pressurized to approximately 150 psig (at a cladding temperature of 1500°F) with argon gas to simulate* the effects of fuel rod internal pressure due to the buildup of fission gases. A maximum cladding temperature of approximately 2250°F was recorded (Figure 7). The electrical failure of ten heater rods (a current surge followed by a complete loss of power) complicated the analysis of the results to some extent but the cladding perforations appeared to have a small effect on the spray cooling performance.

The Zircaloy channel wetting data showed the expected result (Figure 8). The Zircaloy channel with a smaller heat capacity was heated to a higher initial temperature at transient initiation than was the SS2N channel. However, the Zircaloy channel cooled to saturation much more quickly than did the stainless steel channel at the same initial temperature.

---

* The distribution of internal rod pressure was not simulated by the test. A uniform internal pressure was selected to maximize the cladding distortion.[9]
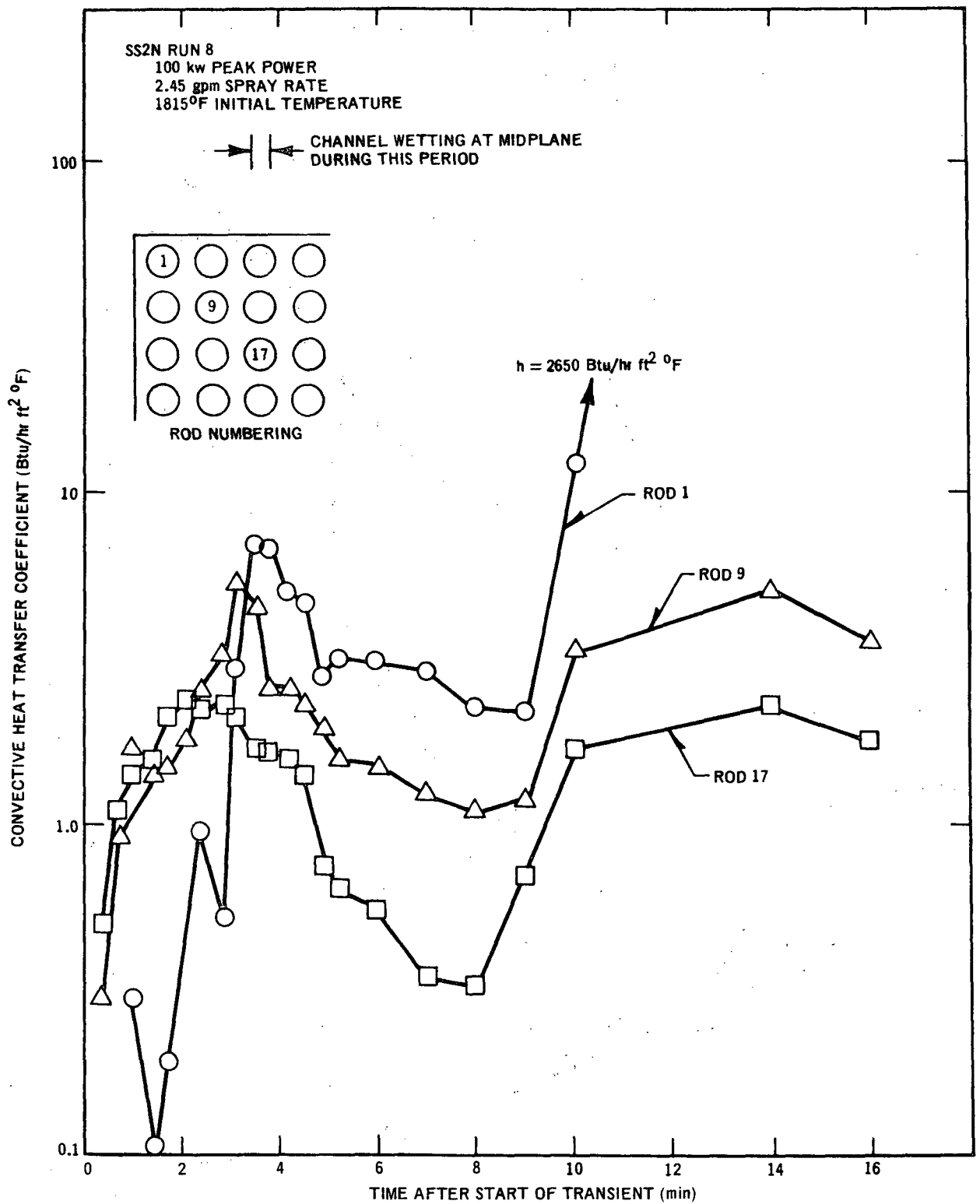
Figure 5B   *Typical Film Coefficient Variation with Time and Bundle Position
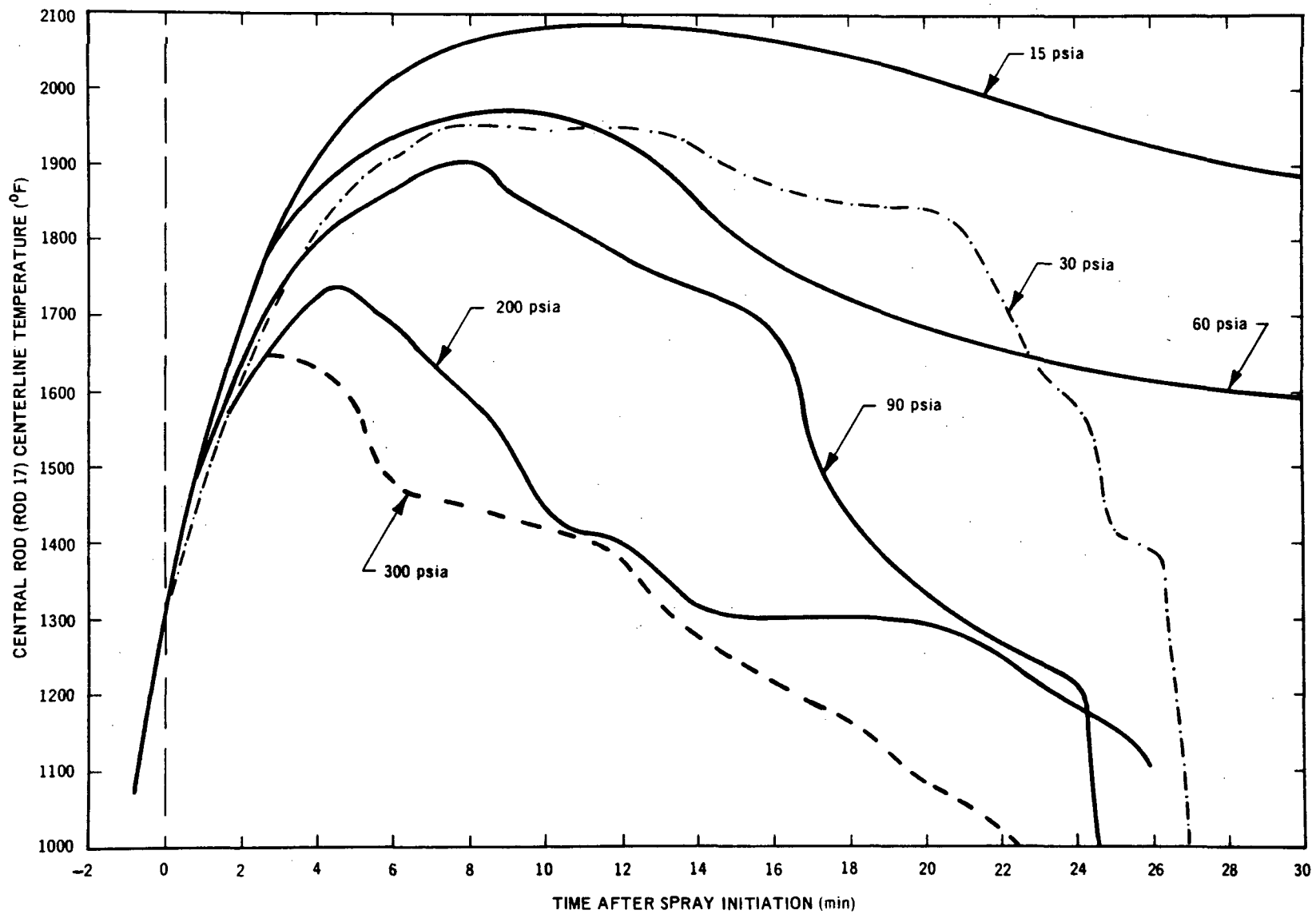(Improved FILMCO Model)*

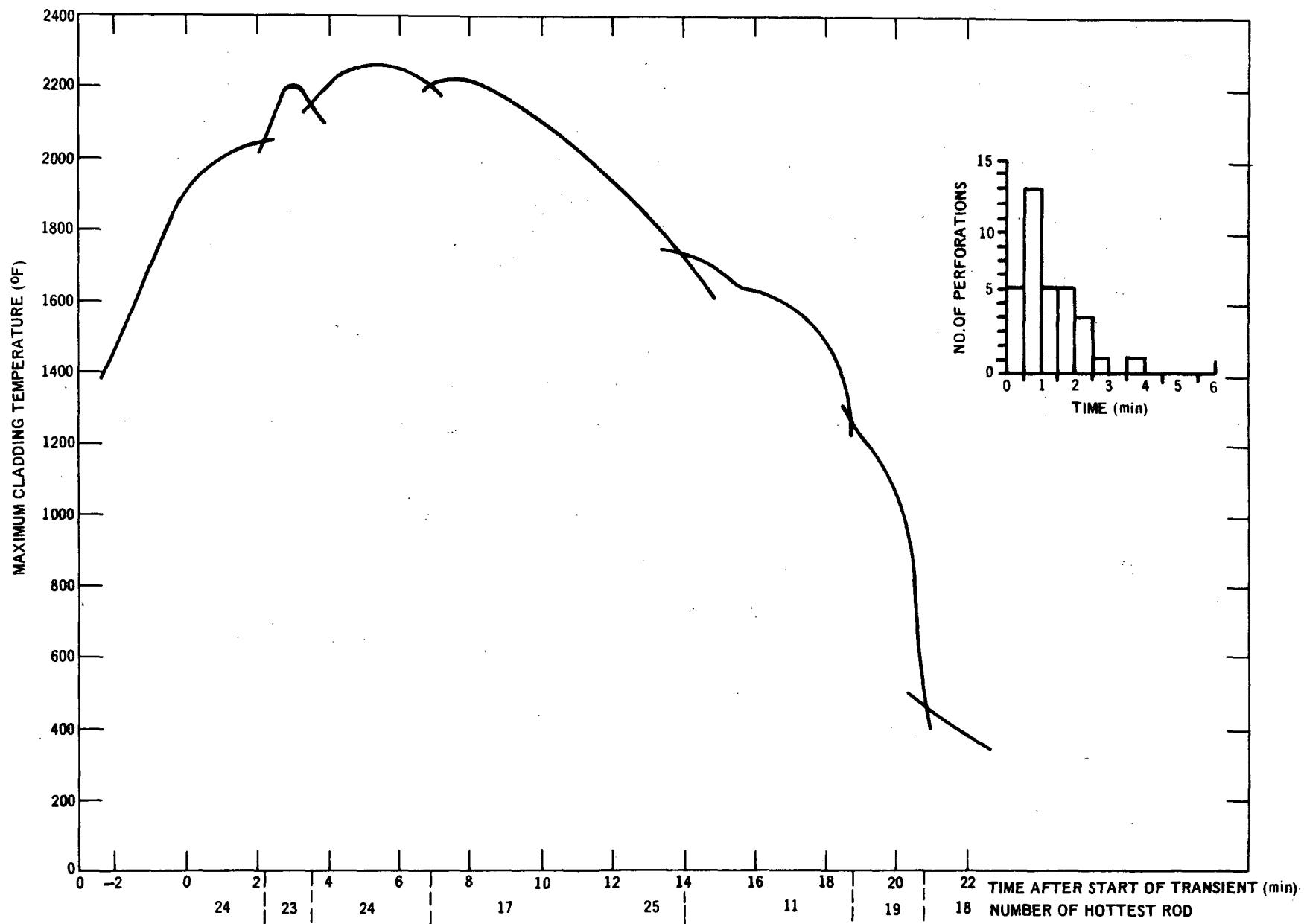*Figure 6   Effect of System Pressure on Spray Cooling Transients*

Figure 7   Maximum Cladding Temperature and Perforation Times in Bundle Zr2K
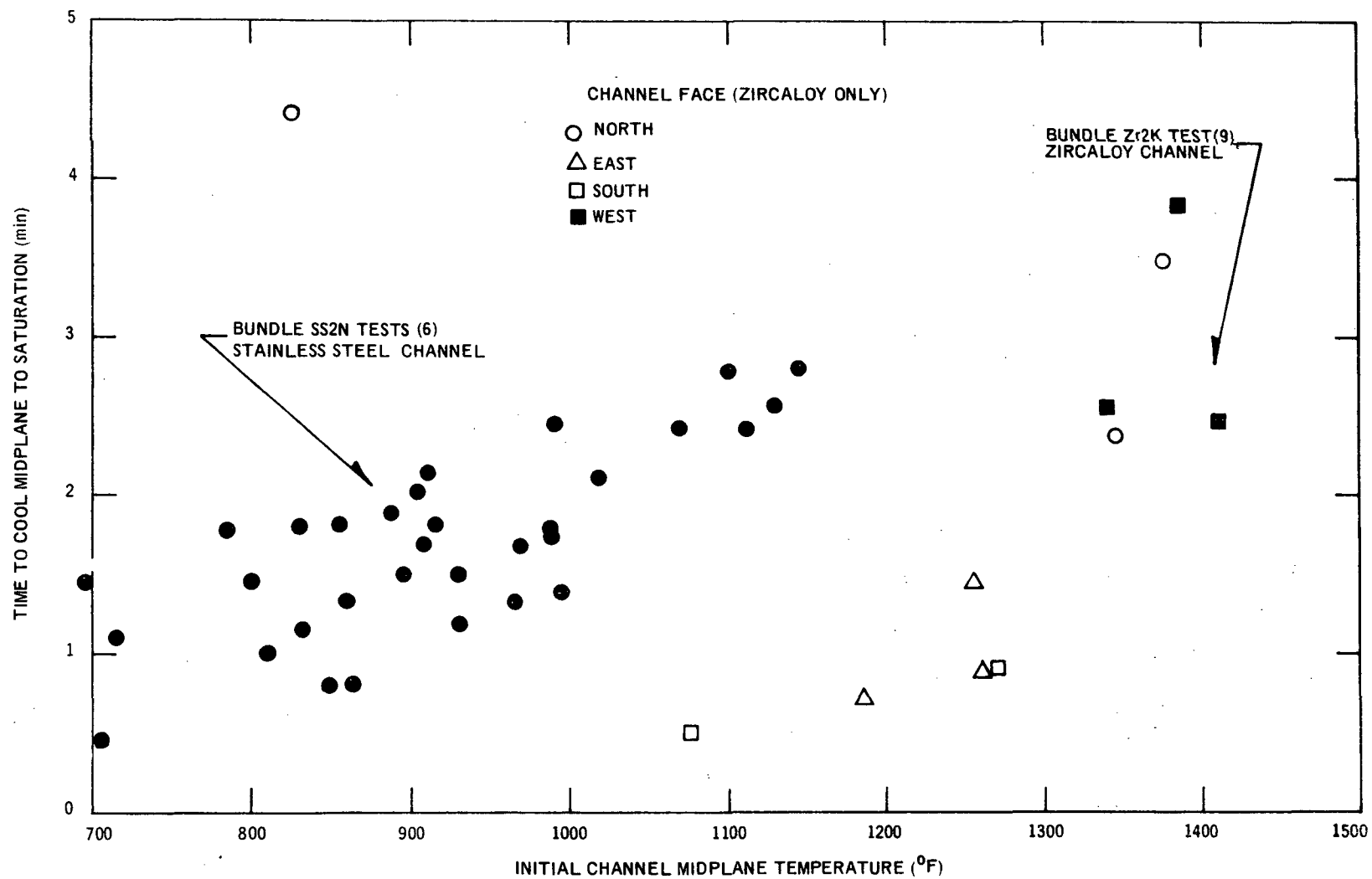
Figure 8   Effect of Initial Channel Temperature on Time to Cool Stainless Steel and
Zircaloy Channels to Saturation

Previous cladding perforation data indicated that the cladding perforates when it is heated to such an extent that the hoop stress exceeds the ultimate tensile strength. Figure 9 shows the Zr2K perforation data and that of several other investigators. The temperatures at the perforation locations were estimated from the elevations instrumented and are not sufficiently accurate to confirm that failure occurs when the ultimate tensile strength is exceeded. The cladding perforations were similar in nature to that observed in earlier GE funded testing,[12] and a recent in-pile test reported by Oak Ridge.[13] A local swelling occurred at or near the plane of maximum rod temperature. The failure was characterized by a small axial slit ~ 1/2-inch long. The swelling was limited to about four inches along the axis. The tubes usually exhibited maximum swelling in the direction of the hottest neighbor. There was no indication that the swelling and perforation on one tube affected the failure on an adjacent tube. A photograph of the bundle in the area of most of the perforations is shown in Figure 10. Thirty-nine of the forty-nine rods perforated. The rods that did not perforate were located on the outside of the test bundle. The test bundle was cast in an epoxy resin and cross-sectioned to determine the coolant flow area reduction resulting from the perforations. Figure 11 shows the cross section in the area of most severe blockage. The minimum cross-sectional rod flow area (the area around a rod) was approximately half that available before the perforations occurred. The area reduction was confined to a relatively short length, with a 10% reduction being typical at 10 inches away from the location of most severe blockage.

4.3.2 Zircaloy-Clad Bundles with Molybdenum Filaments

Although the thermal response of the four test bundles with molybdenum heating elements cannot be considered typical of fuel bundle response during a postulated accident, the effect of the transients on the Zircaloy cladding gives an indication of the cladding performance under extremely severe loss of coolant conditions.

Test bundle Zr1M was spray cooled (2.45 gpm) from an initial temperature of approximately 1790°F and a peak power of 198 kW. The bundle attained a maximum temperature of approximately 2230°F, two minutes after spray initiation. Little rod distortion resulted (one to two diameters of displacement on the central rods at one to two feet above the midplane). Zircaloy oxide thicknesses of less than 0.001 inch resulted from the test. Thus, at a maximum temperature of 2230°F, no significant metal-water reaction was noted.

The last three Zircaloy-clad bundles (Zr3M, Zr4M and Zr5M) were tested under extremely severe loss-of-coolant conditions. The maximum cladding temperature at transient initiation was approximately 2300°F in the three tests. The Zr3M and Zr4M cladding attained maximum midplane temperatures of 2330°F and 2530°F, respectively. The heater rod cladding remained intact at the midplane although severe oxidation did occur. Severe cladding damage (heavy oxidation and fragmentation) occurred in the upper part of bundle Zr3M and in the lower part of bundle Zr4M as a result of the molybdenum power shift and a reaction between the cladding and the aluminum oxide insulation.[10] Figure 12 is an example of the worst damage.

The damaged area was confined to about one foot in Zr3M and to the lower five feet of the test bundle in Zr4M. The damage was confined to the central (and in a few cases, the inside) rods and did not reach the channel which enclosed the test bundles. The maximum recorded cladding temperature in these damaged areas was approximately 2900°F. Thus, it appears that the limiting cladding temperature above which severe cladding damage will result in a simulated loss-of-coolant accident is between 2500°F and 2900°F (assuming a similar "time-at-temperature" to that observed in the tests). The Zr5M test results were difficult to interpret because of many thermocouple failures but maximum temperatures were between 2600°F and 2900°F when flooding was initiated. The bundle cooled to saturation almost immediately after flooding water was introduced.

Cladding oxidation data from the Zircaloy-clad test bundles were correlated against a "time-at-temperature" parameter, $\sqrt{D_\alpha t}$. D_α is the temperature dependent diffusion coefficient of oxygen through alpha Zirconium and t is the time at a particular temperature. The data (Figure 13) are consistent with that obtained by Herzel.[14] They indicate that the oxygen penetration (ZrO_2 plus alpha zirconium thickness) is nearly linear with $\sqrt{D_\alpha t}$. Thus, if the thermal response of the cladding can be predicted, the oxygen penetration, and, therefore, the ability of the cladding to resist "shattering" during the cooldown, can be calculated. A similar plot of the ZrO_2 thickness versus $\sqrt{D_\alpha t}$ (Figure 14) indicates that the observed oxidation rates were generally less than the predicted using the Baker-Just equation.[11] A rate constant of approximately 0.55 times that of Baker gives a good fit of the high temperature Zircaloy-clad bundle oxidation data.
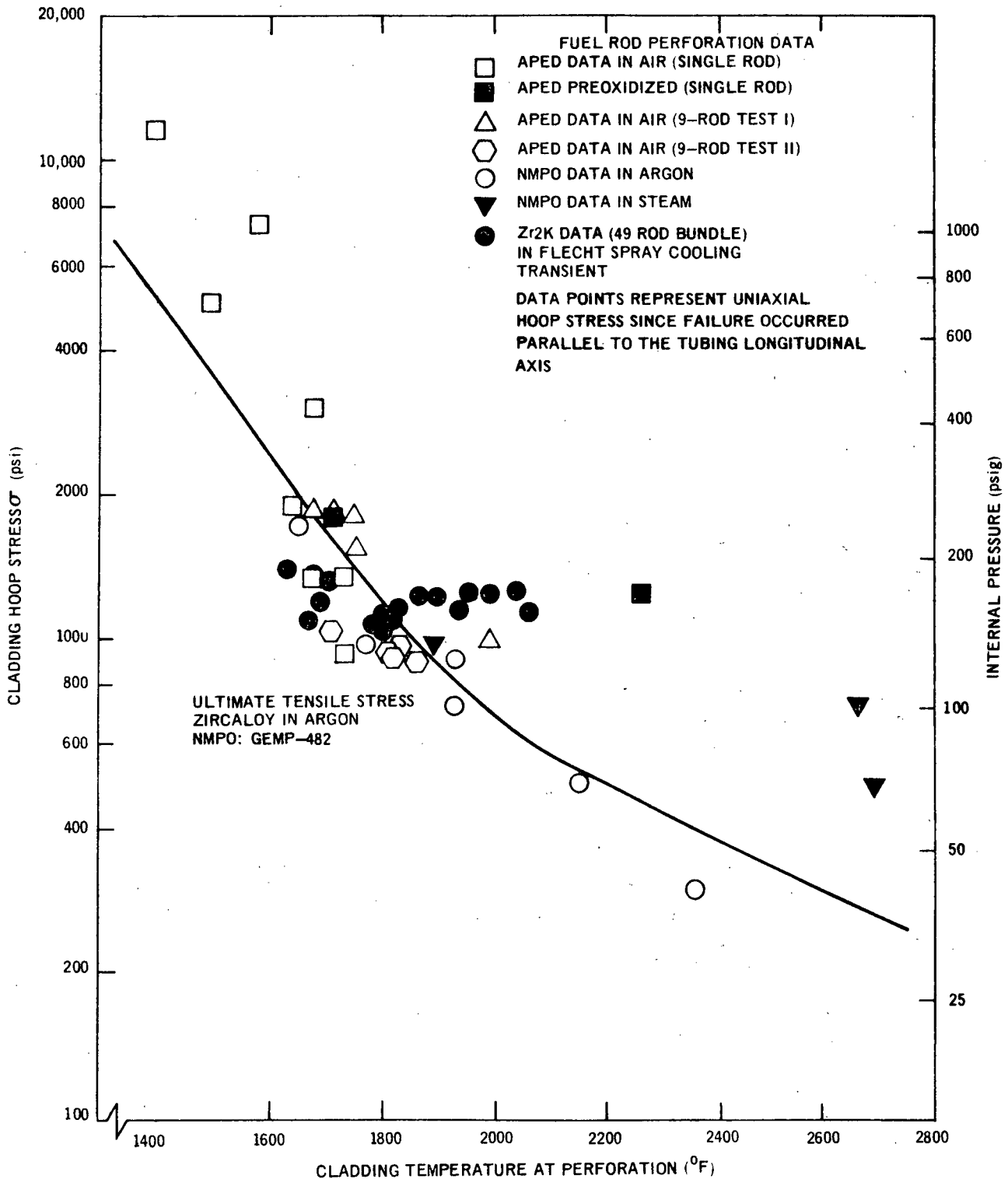
Figure 9   *Cladding Hoop Stress at Failure, Variation with Temperature*
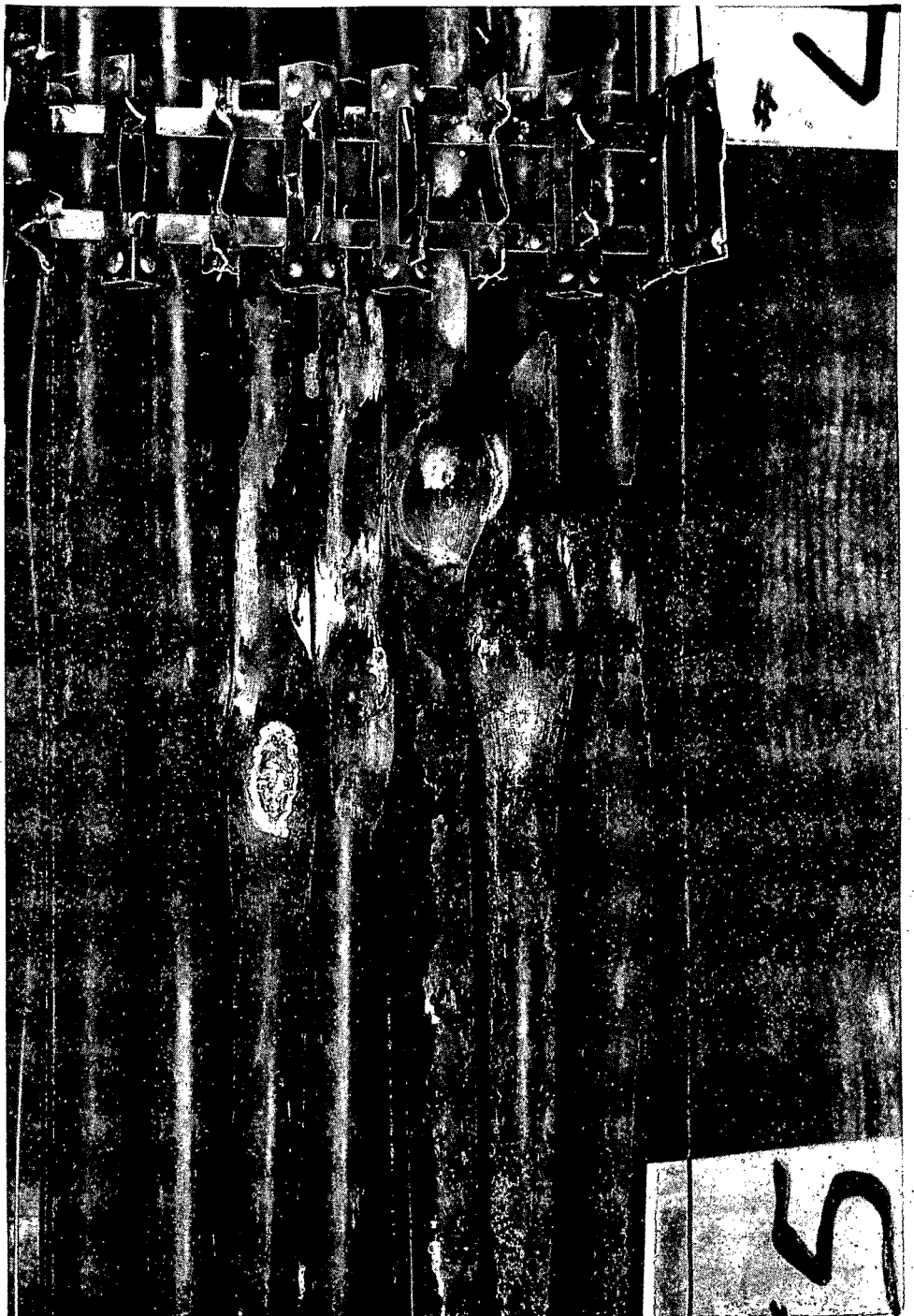
| 35 | 34 | 33 | 32 | 31 | 30 | 29 | ROD NUMBER |

Figure 10   Zircaloy Clad, Internally Pressurized Bundle Perforations in the Area
of Most Severe Flow Blockage
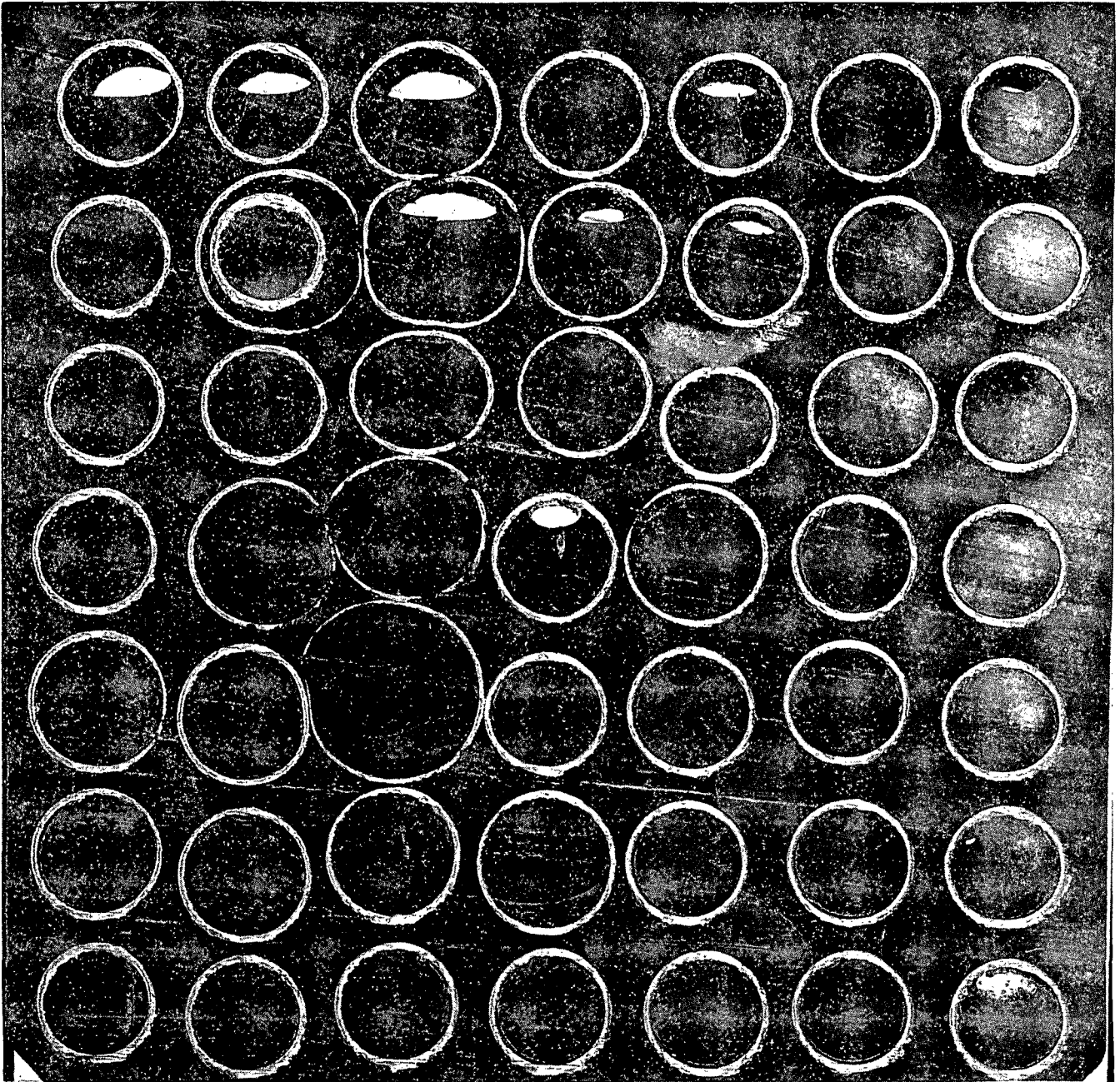
Figure 11   Zircaloy Clad, Internally Pressurized Bundle Cross Section at Five Inches
above the Bundle Center

ROD 28

BOTTOM

TOP

ROD 22

OVERALL VIEW

ROD 22

ROD 28
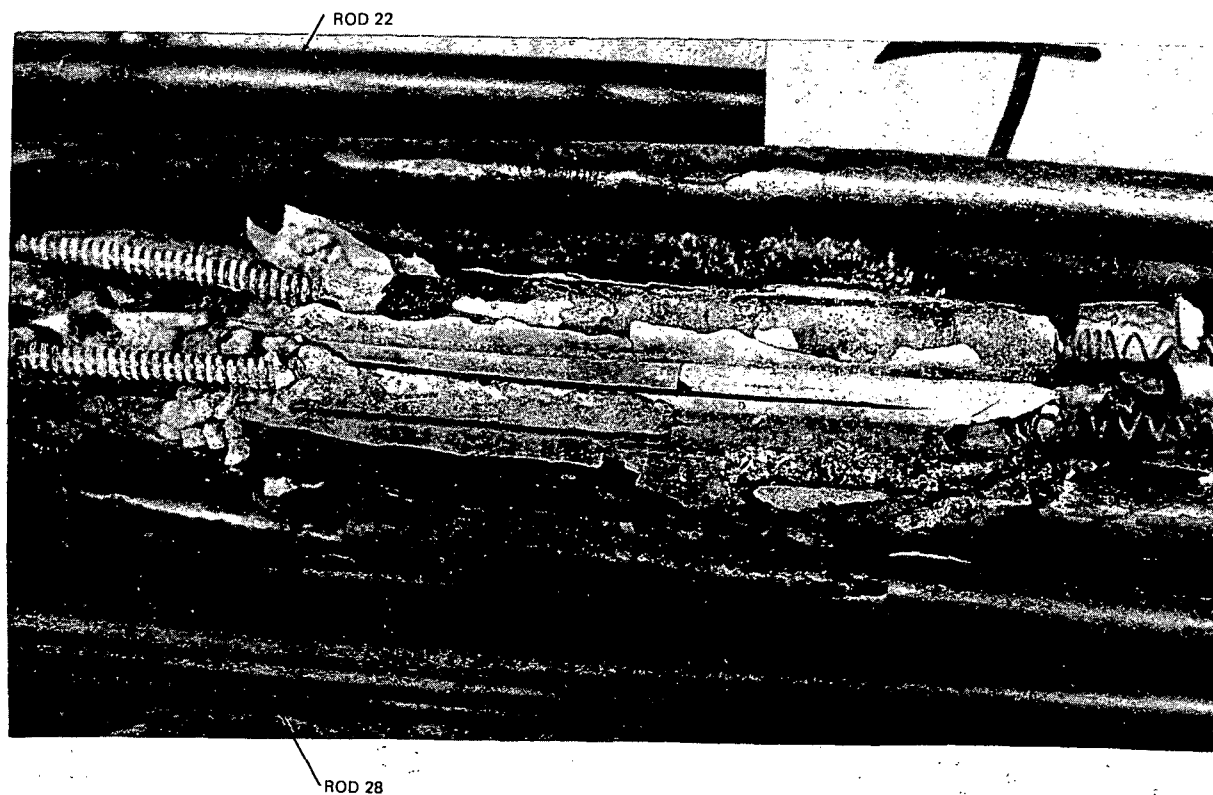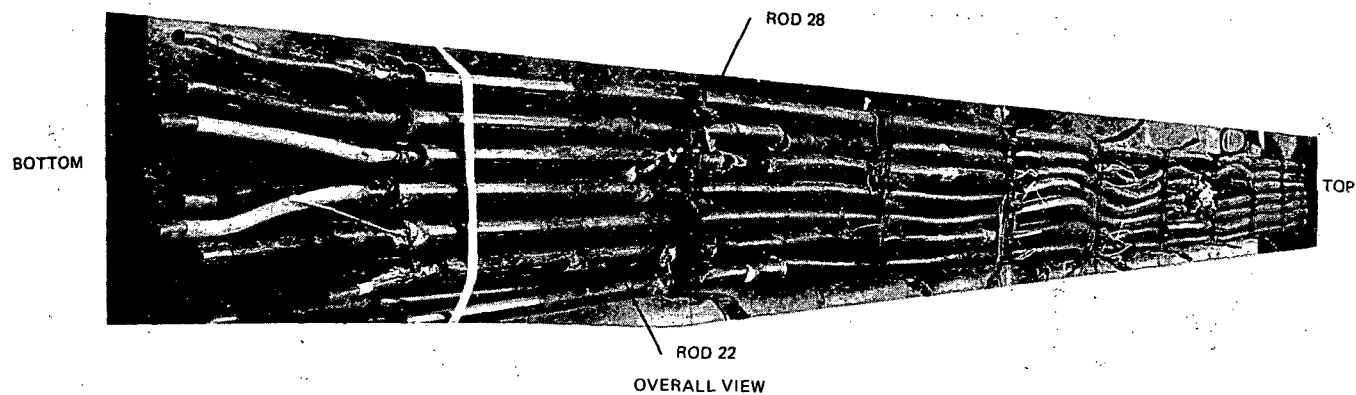
Fourth Row of Rods in Bundle Zr-3 After Testing

Figure 12   Fourth Row of Rods in Bundle Zr-3 After Testing
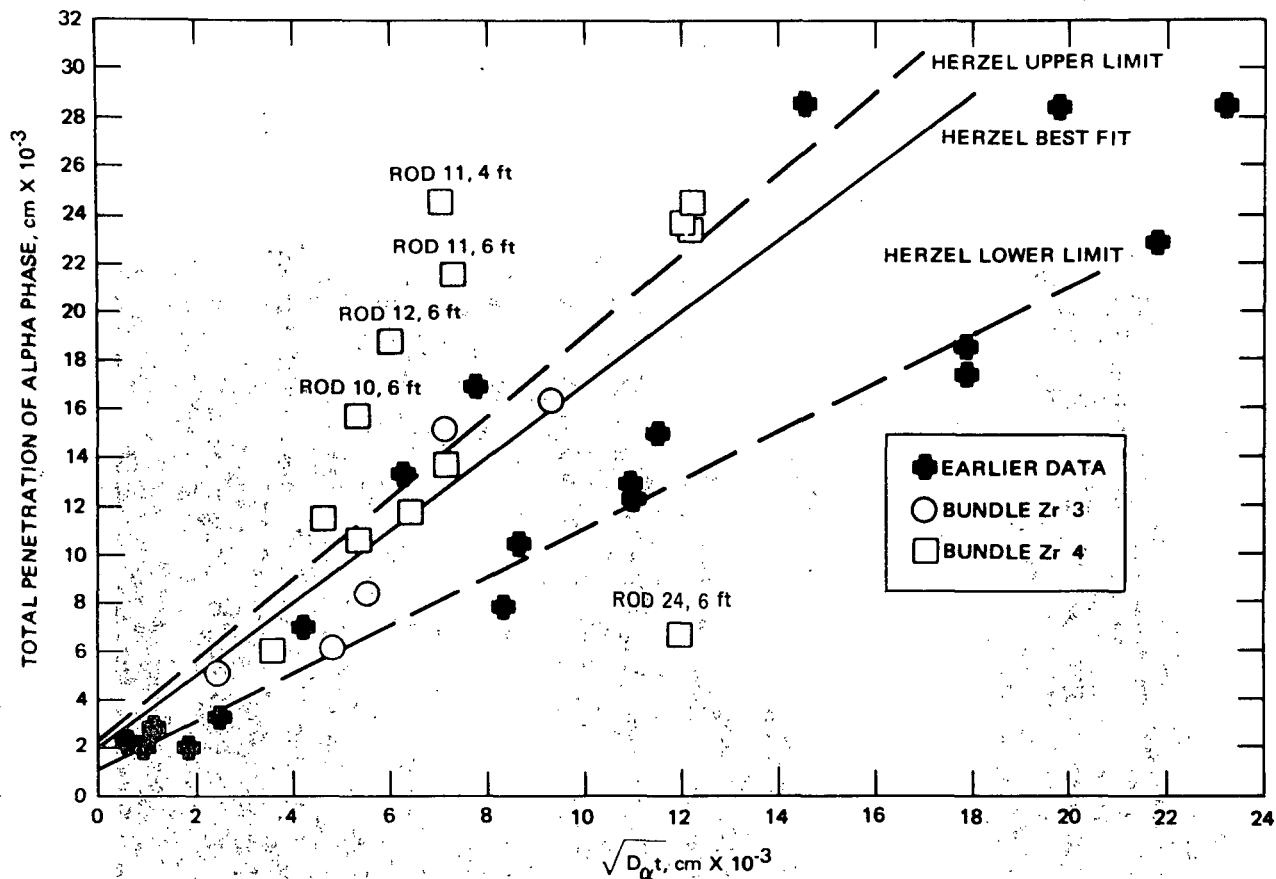
Figure 13   Effect of "Time at Temperature" on Oxygen Penetration

5. FLOODING TEST RESULTS

The results of the FLECHT bottom flooding tests are summarized in this section. Detailed results are available in the following FLECHT documents:

Test Bundles	Document
SS1N (Stainless steel-clad, Nichrome filaments)	GEAP-10117 (reference 15)
SS4N (Stainless steel-clad, Nichrome filaments, high pressure)	GEAP-13190 (reference 7)

The test data and analysis indicate that:

a.   The flooding mechanism is so effective that the bundle temperature rise is terminated almost immediately (less than one minute) after flooding initiation and little improvement results from increasing the flooding rate above approximately three inches per second.

b.   Increasing the system pressure above atmospheric improves the performance of bottom flooding.

5.1 FLOODING TESTS AT ONE ATMOSPHERE (SS1N)

Atmospheric pressure flooding tests were conducted with peak powers from 240 to 390 kW, initial temperature from $1300°F$ to $2150°F$ and with flooding rates from 0.6 to 6.0 inches per second. The largest temperature increase recorded ($T_i = 1400°F$ to $T_{max} = 1550°F$) occurred at the lowest flooding rate tested (0.6 inches per second). All other tests resulted in a temperature increase of less than $100°F$.* The highest temperature recorded during this test series was approximately $2150°FF$* from an initial temperature of approximately $2150°F$, with a peak power of

* Slightly higher increases could have occurred. The data acquisition sweep time (45 seconds) was not sufficient to accurately record the bundle maximum temperatures.

Figure 14   *Effect of "Time at Temperature" on ZrO_2 Thickness*

300 kW and a flooding rate of 3.7 inches per second. A small effect of initial temperature was noted. The higher the temperature, the smaller the temperature rise.

Perhaps the most significant result of this test series was the small effect of flooding rate above 3 inches per second. Figure 15 shows the maximum cladding temperature in 5 transient tests at flooding rates from 0.6 to 6 inches per second. A r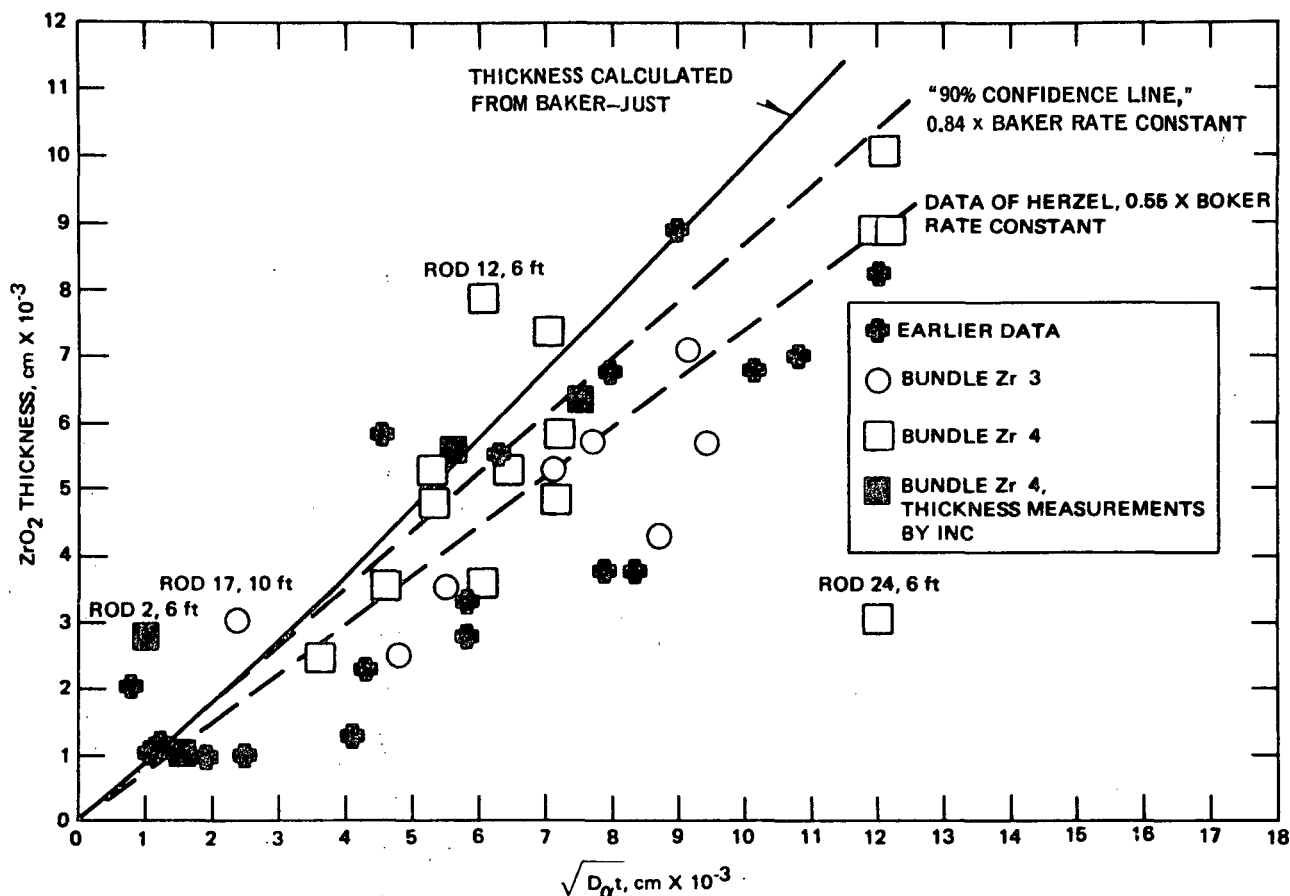elatively large temperature increase ($\sim 150°F$) and slow turnover (T_{max} at $\sim$ 2.5 minutes) results from a flooding rate of 0.6 inches per second. Doubling the flooding rate to 1.3 inches per second roughly halved the temperature increase ($\sim 70°F$) and the time to maximum temperature, ($\sim$ 1 minute). Increasing the flooding rate to 3.7 (which is typical of General Electric BWR's resulted in a further improvement in flooding effectiveness: a 20°F temperature increase in approximately 0.5 minutes. Further increases in the flooding rate resulted in very little improvement, although the bundle did cool to saturation somewhat more quickly. Thus, increasing the flooding rate above about 3 inches per second provides a negligible improvement in the effectiveness (i.e., a negligible reduction in the maximum temperature) of the flooding mechanism in GE BWR's.

5.2 FLOODING TESTS UP TO 300 PSIA (SS4N)

Tests were conducted with bundle SS4N with system pressure variable up to 300 psia. Most of the tests were conducted from an initial temperature of approximately 1300°F, a peak power of 250 kW and a flooding rate of 3 inches per second.

Test results at one atmosphere agreed well with the SS1N results. Tests at 60 psia showed the same effects as those noted at 15 psia with bundle SS1N: a small improvement in flooding effectiveness as initial temperature is increased and a small improvement (reduction in maximum temperature) as flooding rate is increased above 3 inches per second.

Increasing the system pressure above one atmosphere caused a significant improvement in the effectiveness of bottom flooding heat transfer. Figure 16 shows a central rod midplane temperature response at several pressures. Note that as the pressure is increased, the temperature increase ($T_{max} - T_i$) is reduced and the thermocouple cools to saturation much more quickly. For example, at 15 psia this position reaches saturation at 140 seconds, and at 100 psia
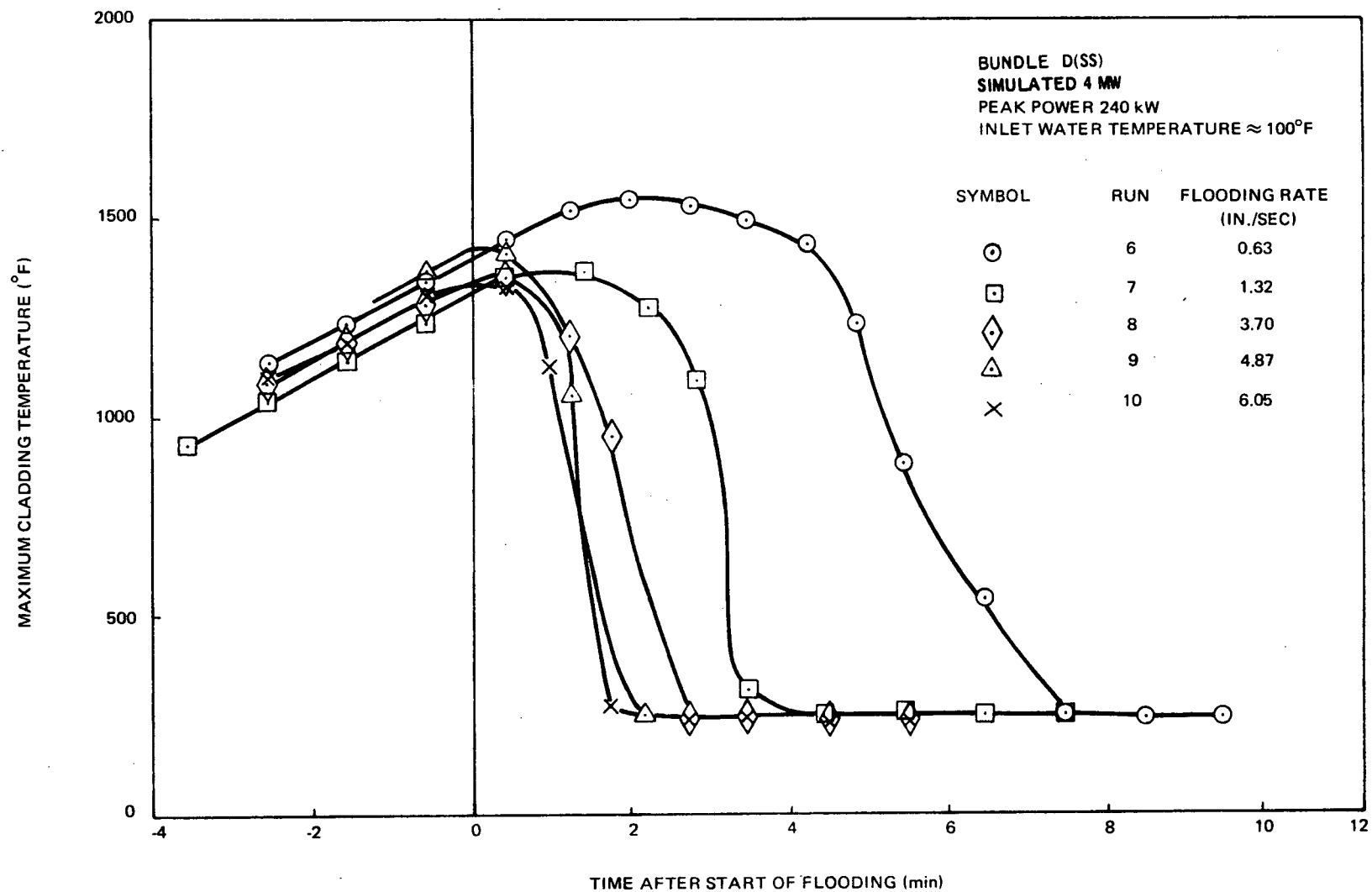
Figure 15   Effect of Flooding Rate in Transient Flooding at 240 kW Peak Power,
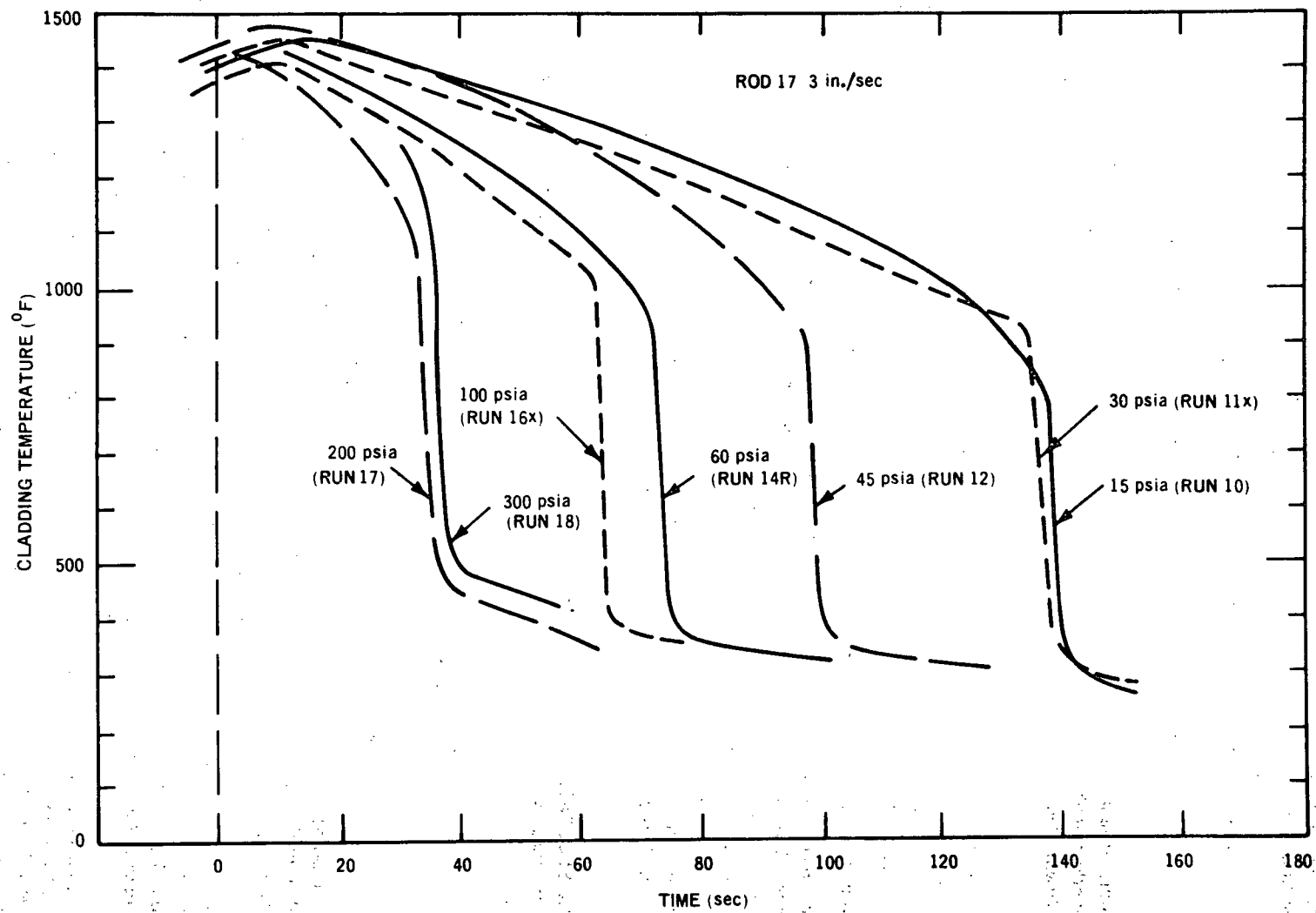FLECHT Bundle SS1N

Figure 16   Effect of Pressure on Central Rod Midplane Response

the quench time is reduced to 65 seconds. The increased flooding effectiveness as pressure increases appears to result from two separate effects. More liquid drops are carried away with the vapor at high pressures.[7] This results in better heat transfer during the early stages of the transient (i.e., up to and a little past the maximum temperature). Thus, a smaller temperature increase is observed at high pressures. In addition, the Liedenfrost temperature (at which the surfaces will quench) increases with increasing pressure. Therefore, the rods wet more easily (i.e., from a higher surface temperature). Thus, a shorter period to quench to saturation is observed at high pressure.

6. SPRAY COOLING HEAT TRANSFER MODEL

The current General Electric spray cooling heat transfer model was developed from bundle SS2N test data.[16] This section briefly describes the method of calculating local convective heat transfer coefficients from the test data. The model is shown (Section 7) to be a reasonably good representation of the spray cooling process in a loss-of-coolant accident.

6.1 HEAT TRANSFER CALCULATION MODEL

Local coefficients were calculated using an improved version of the FILMCO[6,7] program. The calculational model is briefly as follows: Radiation in the axial direction and conduction are neglected and an energy balance is written at the midplane of each instrumented heater rod,

Energy rate in = energy storage rate + convection out + radiation out.

The energy rate in term is determined from the total bundle power and the local and axial power peaking factors for the rod concerned. The storage term is calculated from the measured slope of the thermocouple response. The radiation term is calculated by assuming diffuse grey body radiation from the rod to the other rods in the bundle and to the channel enclosing the bundle. The heater rod emissivity is taken as 0.7* and that of a wet body is taken as 0.96. The convection term is then determined from the energy balance. The local convective heat transfer coefficient is then calculated assuming heat transfer to the coolant at saturation temperature. The coefficient calculated therefore represents all heat transfer (convection and radiation) to the coolant except radiation to the coolant on wetted bodies.

6.2 GENERAL ELECTRIC CORE SPRAY MODEL

The current model was developed from the SS2N data.** Analysis of data from the early[†] SS2N runs suggested a constant film coefficient for each rod type[16]:

Corner rod (Group 1)	— 3.0 Btu/h ft² °F
Side rod (Group 2)	— 3.5 Btu/h ft² °F
Inside rod (Group 3)	— 1.5 Btu/h ft² °F
Central rod (Group 4)	— 1.5 Btu/h ft² °F
Channel	20 until wetting
	1000 after wetting

It will be recalled[6,7] that channel wetting causes a dramatic increase in the local coefficients on the outside rods. An understanding of this phenomena contributes to the understanding of the complete spray cooling process. However, this effect of wetting is of relatively short duration, and it may be neglected in calculations intended to calculate maximum cladding temperatures. The only significance of channel wetting in the model is that the channel emissivity is changed to that of water (0.96) when the channel wets. Channel wetting time can be determined from Figure 17.

When applied to reactor analyses the model assumes that the metal-water reaction proceeds at the rate predicted by Baker (100% MWR). When calculating test temperatures a 50% MWR assumption is usually made[10] to be consistent with the rates observed in the tests.

---

* The possible errors resulting from these and other assumptions are discussed in detail in reference 7. The effect of assuming an emissivity of 0.7 (the emissivity could possibly be as high as 0.9) deserves some mention here. With an emissivity of 0.9, outside rod coefficients would be about 0.2 to 0.5 Btu/h-ft² °F lower, inside rod coefficients about 0.3 to 0.4 lower, and central rod coefficients about 0.2 to 0.4 higher. These differences are relatively small compared to the estimated calculation sensitivity of 1.0 Btu/h-ft² °F.

** Coefficients were also calculated from bundle SS4N data at 15 psia. See reference 7.

† Since a significant amount of distortion occurred in bundle SS2N, early runs were selected to give a minimum distortion effect on the calculated coefficients.
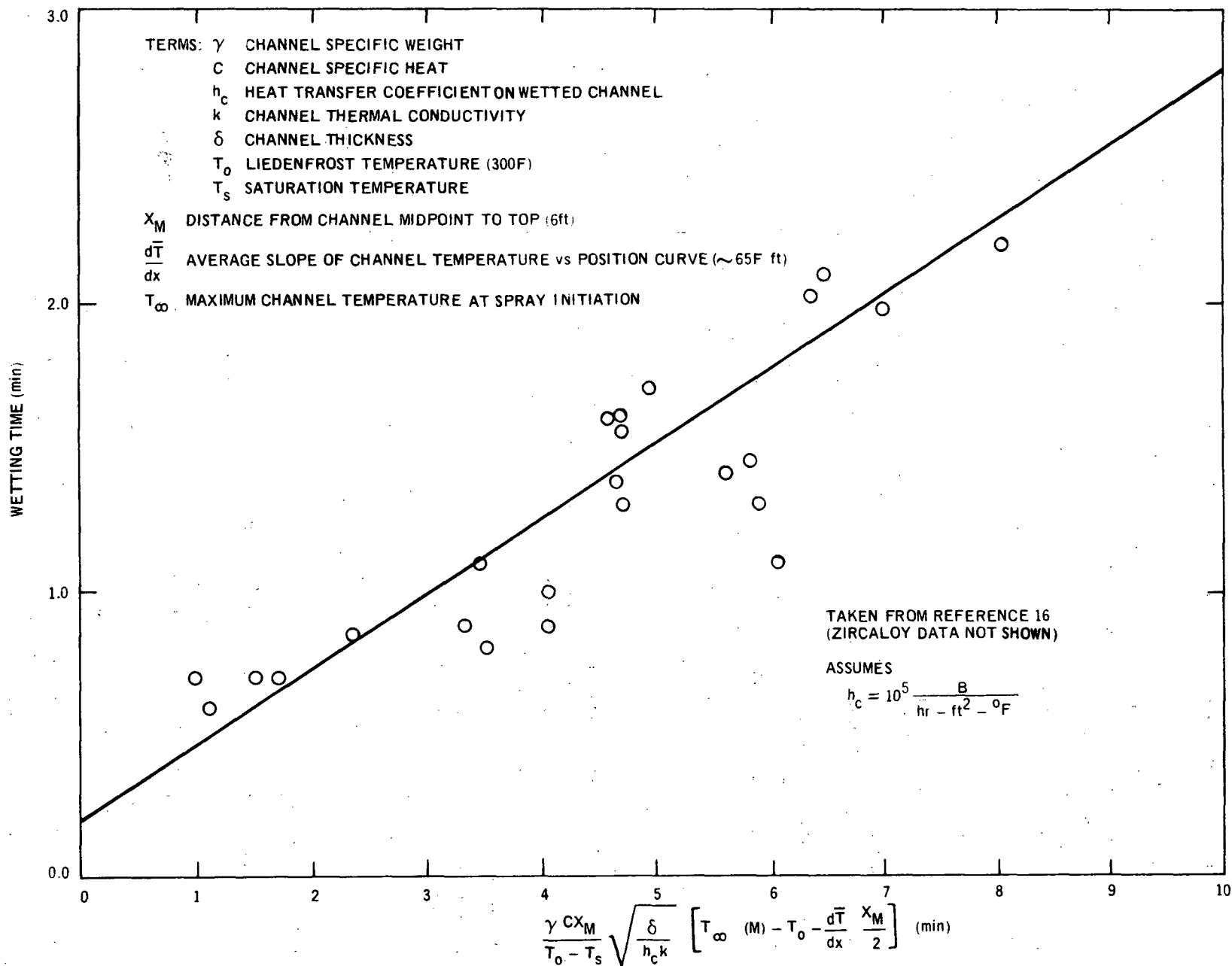
Figure 17   Channel Wetting Correlation

7. ZIRCALOY-CLAD BUNDLE THERMAL RESPONSE PREDICTIONS

The midplane thermal response of three Zircaloy-clad bundles tested under the FLECHT program (Zr2K, Zr3M and Zr4M) has been calculated using the current General Electric model. Since the FLECHT data indicates that a metal-water reaction of approximately one-half that of Baker (50% MWR) is more appropriate in full scale loss-of-coolant simulations, calculations were made assuming 50% and 100% MWR. Diffuse grey body radiation with a Zircaloy emissivity of 0.67 was assumed. The channel emissivity was taken at 0.96 after wetting.

All the heater rods were not instrumented at the midplane and several heater rod electrical failures occurred in two of the tests (Zr2K and Zr3M) before the midplane maximum temperature had occurred. Consequently, a different rod grouping for the radiation calculation was used for each of the three bundles. The rod grouping is shown in Figures 18, 19 and 20.

Bundle Zr2K Grouping (Figure 18)
Single groups of one rod represent most of the rods instrumented at the six foot elevation. Group 5 represents the 20 uninstrumented outside rods. Group 18 represents nine of the uninstrumented inside rods. Group 19 represents the three heaters (12, 19 and 32) which failed electrically before transient initiation.

Bundle Zr3M Grouping (Figure 19)
Because of the significant molybdenum power shifting which occurred in bundle Zr3M, it was necessary to calculate individual rod local peaking factors as a function of time. In the interests of economy, the relatively coarse grouping shown in the figure was selected. Group 2 represents several outside rods. For comparison with the test data, separate calculations were made using the initial temperature and power variation of Rod 2 and Rod 4. The Group 6 calculations were similarly compared to the Rod 24 and 26 response. Group 10 represents the group of heaters which lost power early in the transient.

Bundle Zr4M Grouping (Figure 20)
Bundle Zr4M was well instrumented at the midplane and temperatures as high as $2,500°F$ were recorded. To provide as many comparisons as possible, the relatively fine grouping shown on the figure was selected. Group 7 represents one set of outside rods in one SCR power group and Group 20 represents another set in another power group. Groups 21 and 22 represent inside rods in two different power groups. Most of the other groups represent single instrumented rods.

7.1 COMPARISON OF PREDICTIONS WITH TEST DATA
The predictions given by the model at 50 and 100% metal-water reaction are compared to the test data in the following three subsections. A summary of the predictions is presented in Tables 2, 3, and 4. These tables show the observed and predicted maximum temperatures and times of maximum temperature for each operable* midplane thermocouple. Each of the following three subsections includes a comparison of the predicted temperature with the test data for several rods in each test bundle. All of the predictions are compared with the test data in Appendix A.

7.2 BUNDLE ZR2K PREDICTIONS
Figure 21 shows the Rod 2 predictions compared with the test data. The prediction is reasonably good. The calculated temperatures are never more than $100°F$ from the data until the thermocouple indicated unexplained low readings at five minutes after spray initiation. Note that there is very little difference in the calculations at 50 or 100% MWR at this relatively low temperature ($\sim 1900°F$). Other outside rod predictions (Table 2) ranged from $30°F$ to $190°F$ over the observed maximum temperature at 50% MWR and from $50°F$ to $230°F$ over the observed value at 100% MWR.

The rod 30 comparison is shown on Figure 22. The calculation at 50% MWR is quite good (within $50°F$ of the data for eight minutes). Note that the MWR is somewhat more significant ($50°F$ difference between 50% and 100% MWR) at this temperature ($\sim 2100°F$). Only one inside rod calculation resulted in an underprediction of the maximum temperature. The thermocouple on this rod (Rod 23, see Figure A-8) was quite erratic and the actual maximum temperature is not known accurately. Other inside rod calculations overpredicted the maximum temperature by about $45°F$ with 50% MWR and by about $80°F$ with 100% MWR (Table 2).

* Several thermocouples in bundle Zr2K gave erratic readings. Some are included in Table 1.
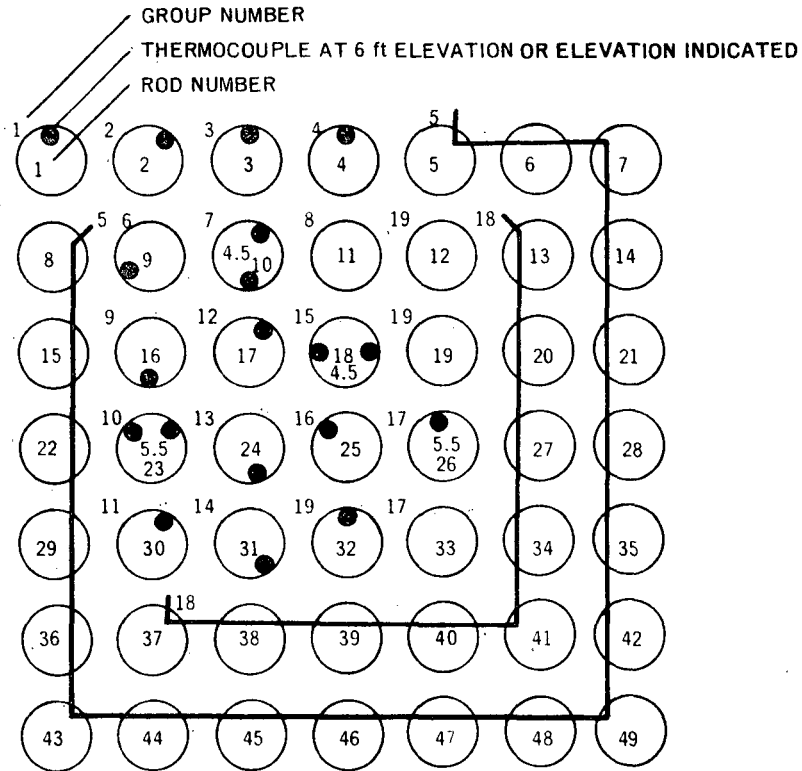
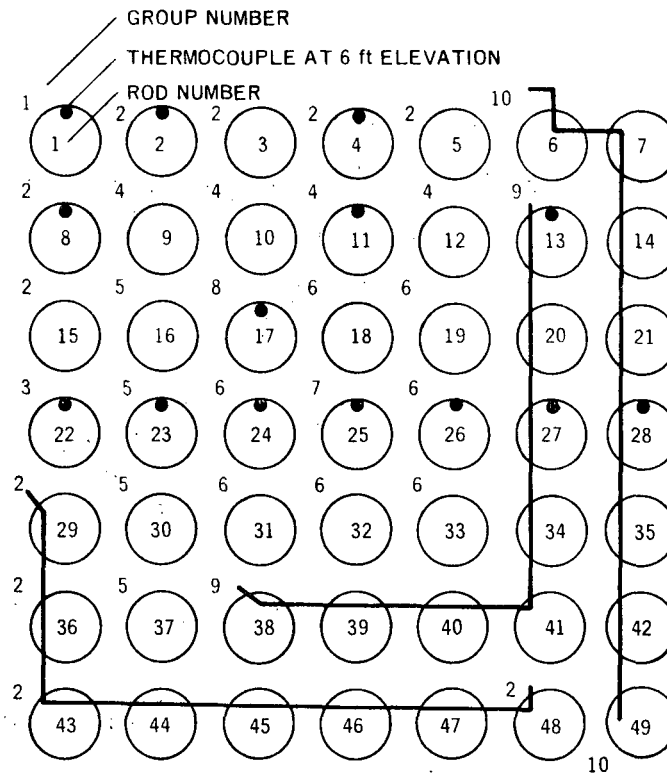Figure 18   Bundle Zr2K 19 Group Model
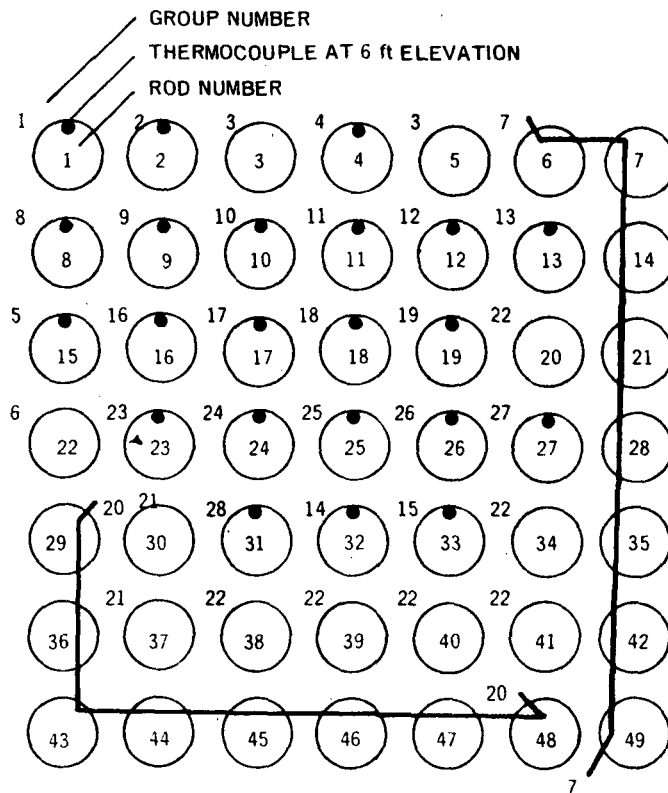

Figure 19   Bundle Zr3M 10 Group Model

Figure 20   Bundle Zr4M 28 Group Model

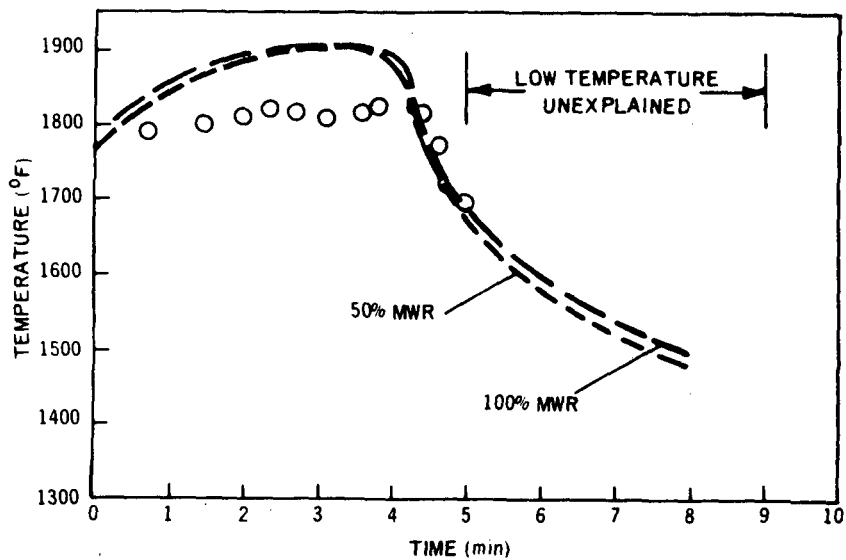Figure 21   Bundle Zr2K Rod 2 Midplane Thermal Response Prediction

Table 2
Zr2K PREDICTION SUMMARY

| | Maximum Temperature (°F) | | | | | Time of Maximum Temperature (min) | | | | |
| | Observed | Predicted MWR | | Error[1] MWR | | Observed | Predicted MWR | | Error[2] MWR | |
Rod		50%	100%	50%	100%		50%	100%	50%	100%
1	1780	1810	1830	+30	+50	3.5	2.8	3.0	−0.7	−0.5
2	1830	1890	1920	+60	+90	4.2	3.0	3.0	−1.2	−1.2
3	1700	1890	1930	+190	+230	0.3	3.0	3.0	+2.7	+2.7
4	1740[3]	1910	1940	+170	+200	1.2[3]	3.5	3.8	+2.3	+2.6
9	1990	2030	2060	+40	+70	3.8	3.0	3.0	−0.8	−0.8
10 (4.5)[4]	1940	2040	2070	+100	+130	4.0	3.0	3.5	−1.0	−0.5
23	2180[3]	2070	2120	−110	−60	3.4	3.5	4.0	+0.1	+0.6
30	2010	2060	2100	+50	+90	3.4	4.0	4.0	+0.6	+0.6
17	2180[3]	2120	2180	−60	~0	7.0	4.0	4.0	−3.0	−3.0
24	2240[3]	2130[5]	2170[5]	−110	−70	5.1	4.0	4.0	−1.1	−1.1
31	1930	2080	2130	+150	+200	3.7	4.0	4.0	+0.3	+0.3
18(4.5)[4]	2060	2120	2160	+60	+100	7.2	3.8	4.0	−3.4	−3.2
26(5.5)[4]	1920	2060	2110	+140	+190	8.1	3.8	4.0	−4.3	−4.1
32(5.5)[4]	1970	1950	2010	−20	+40	8.3	3.8	4.0	−4.5	−4.3

NOTES

1   Maximum temperature error = predicted minus observed.
   Thus, + indicates overprediction of maximum temperature.
2   Time of maximum temperature error = predicted minus observed.
   Thus, + indicates maximum predicted temperature occurred later than the data indicated.
3   Erratic thermocouple.
4   Observed temperatures are from thermocouples at elevations noted.
5   A current increase may have increased the local power at the midplane of rod 24.
   Calculations which include such a local power increase result in maximum temperature
   predicting approximately 100°F higher than those shown here.

Only one central rod thermocouple at the six foot elevation performed well during the Zr2K transient. The prediction for this rod (31) is shown in Figure 23. Both calculations are quite conservative: the actual maximum temperature (1930°F) is overpredicted by from 150 to 200°F with 50% to 100% MWR. Other predictions were compared to thermocouples at 4.5 and 5.5 feet above the bottom of the heated length. These predictions were also conservative (except for Rod 32 where the maximum temperature was underpredicted by 20°F with 50% MWR).

Thus, the current model with 50% MWR assumption performs well in predicting the Zr2K data and the 100% MWR assumption makes the predictions very conservative. Unfortunately however, the thermocouples performed quite poorly in this test and there were only a few reliable inside and central rods on which the temperature was accurately known.

7.3 BUNDLE ZR3M PREDICTIONS

Figure 24 shows that Rod 22 predictions are within 100°F of the data for the first five minutes of the transient. The outside rod predictions ranged from 90°F under to 60°F over the observed maximum temperature with 50% MWR and from 90°F under to 100°F over the observed value with 100% MWR (Table 2).

Only two inside rods were instrumented at the midplane. The prediction of the hotter (Rod 23) is shown in Figure 25. Both calculations underpredict the maximum temperature (2140°F observed, 2020°F calculated with
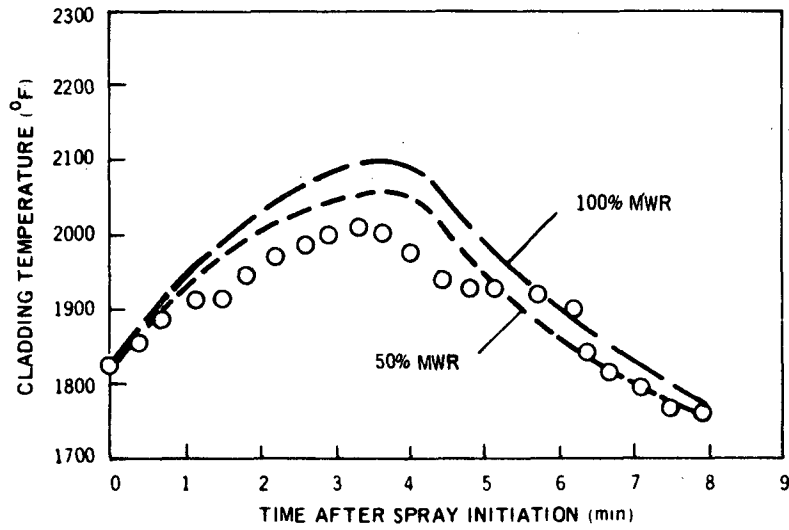
Figure 22   Bundle Zr2K Rod 30 Midplane Thermal Response Prediction
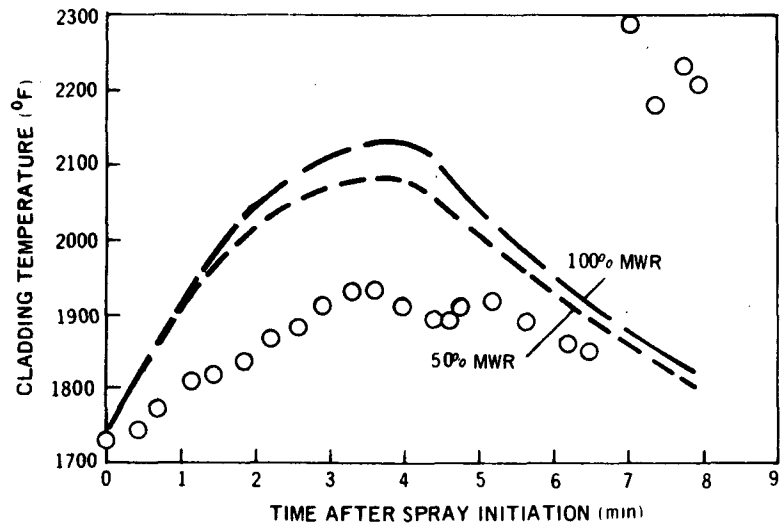

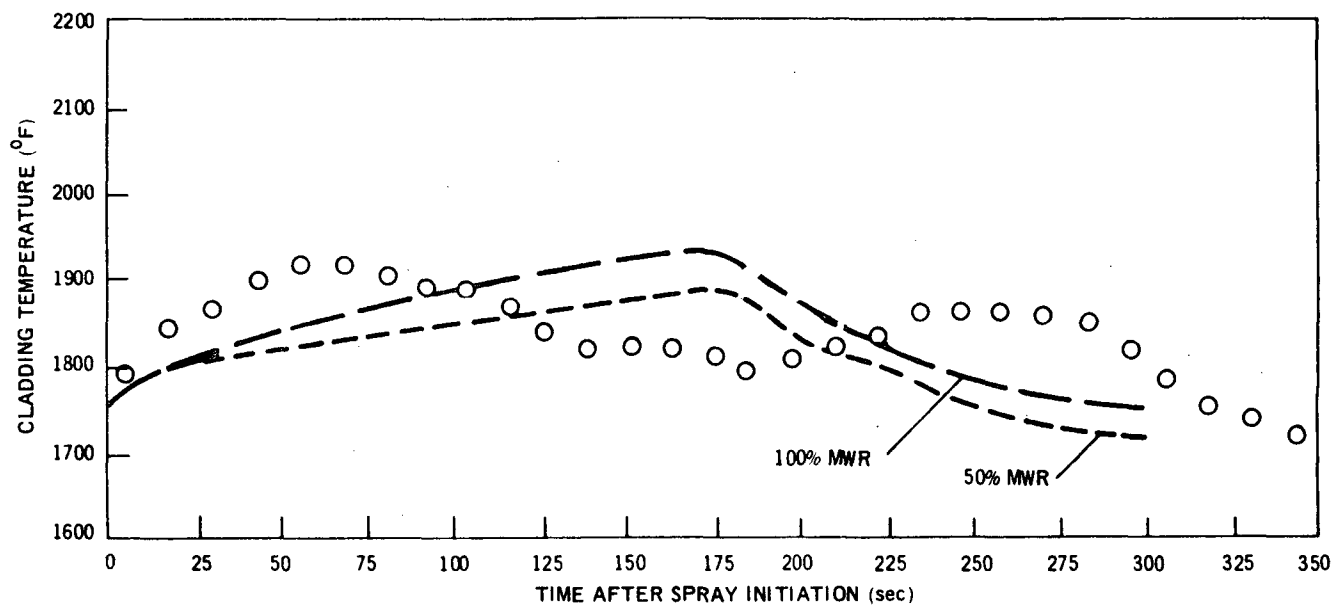Figure 23   Bundle Zr2K Rod 31 Midplane Thermal Response Prediction

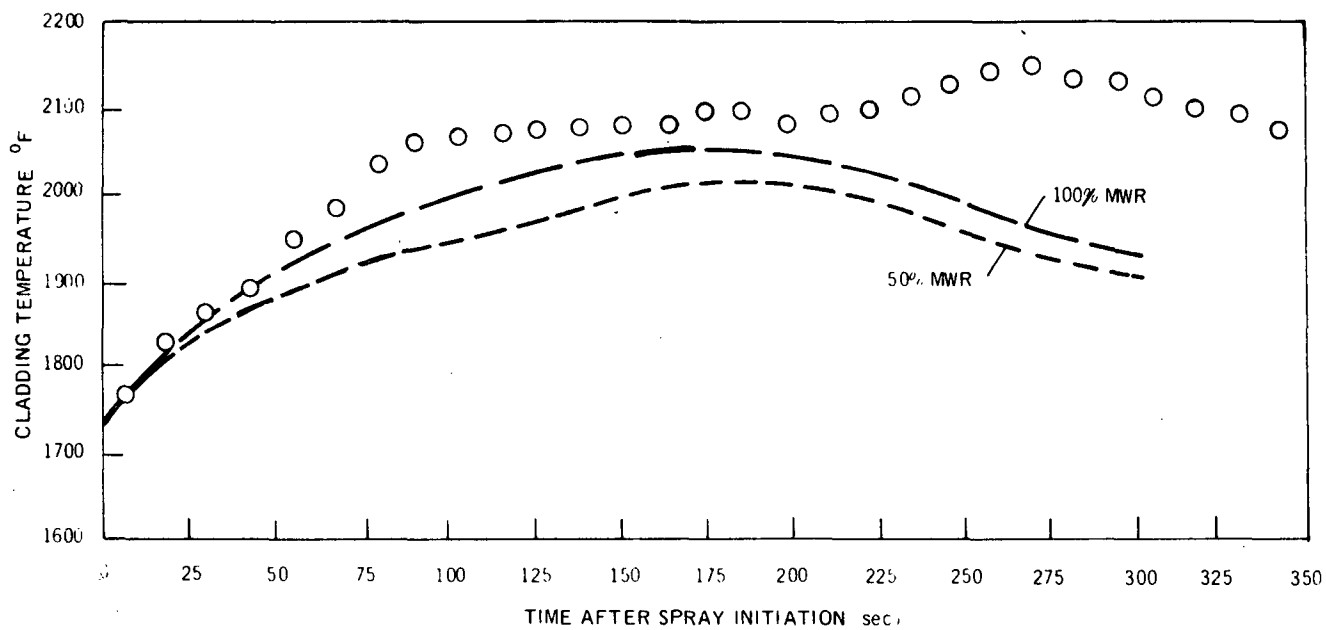Figure 24   Bundle Zr3M Rod 22 Midplane Thermal Response Prediction

Figure 25   Bundle Zr3M Rod 23 Midplane Thermal Response Prediction

Table 3
Zr3M PREDICTION SUMMARY

Rod	Maximum Temperature (°F)					Time of Maximum Temperature (sec)				
	Observed	Predicted MWR		Error[1] MWR		Observed	Predicted MWR		Error[2] MWR	
		50%	100%	50%	100%		50%	100%	50%	100%
1	1760	1670	1670	−90	−90	90	150	150	+60	+60
2	1880	1780	1830	−100	−50	80	170	170	+90	+90
4	1740	1800	1840	+60	+100	90	175	175	+85	+85
22	1920	1880	1930	−40	+10	70	175	175	+105	+105
11	2090	2040	2090	−50	~0	200	180	180	−20	−20
23	2140	2020	2060	−120	−80	270	180	180	−90	−90
17	2200	2270	2330	+70	+130	190	200	200	+10	+10
24	2300	2180	2230	−120	−70	230	200	200	−30	−30
25	Probable TC Malfunction									
26	2330	2220	2280	−110	−50	250	200	200	−50	−50

NOTES

1   Maximum temperature error = predicted minus observed.

   Thus, + indicates overprediction of maximum temperature.

2   Time of maximum temperature error = predicted minus observed.

   Thus, + indicates maximum predicted temperature occurred later than data indicated.

50% MWR and 2060°F with 100% MWR). Rod 11 calculations were somewhat more accurate, with the 100% MWR calculation predicting the maximum temperature almost exactly.

The Rod 26 calculations are compared with the test data in Figure 26. The calculations are quite good (within 50°F of the data) up to about 2.5 minutes but the maximum temperature is underpredicted (2330°F observed, 2220°F calculated with 50% MWR and 2280°F with 100% MWR). The Rod 24 calculations were similar. The Rod 17 calculations resulted in a 70°F overprediction with 50% MWR and a 130°F overprediction with 100% MWR.

In making these calculations it was necessary to assume the local power on all the uninstrumented rods.* The power which was thought to be the most reasonable was used. In a few cases (five rods) the power may have been somewhat higher than that assumed. Calculations were also made assuming these higher powers. The predicted temperatures were 50 to 100°F higher when higher powers were assumed on the uninstrumented rods.

Thus, the model performs reasonably well in predicting the Zr3M data. With 100% MWR (which is used in reactor calculations), the predicted maximum temperatures of the hottest rods ranged from 70°F under to 130°F over the observed value. These differences are reasonable and should be expected considering the uncertainties involved (Appendix B) in predicting maximum temperatures in these tests.

7.4 BUNDLE ZR4M PREDICTIONS

The Zr4M outside rod temperatures were overpredicted[10] by several hundred degrees. The reason for the large overpredictions is not completely understood but a large part of the error has been attributed[10] to the fact that outside rod local power was not accurately calculated and that some water accumulated in the bottom of the test bundle after spray initiation. Consequently, outside rod predictions were not attempted as part of the present comparisons. Instead, outside rod powers were arbitrarily reduced to one-half that estimated in order to bring the predicted temperature closer to the test data. Thus, outside rod calculated temperatures in the present predictions have no significance except to provide a more reasonable radiation boundary condition for inside and central rods. This technique assumes that whatever caused the low temperatures in the outside rods did not effect inside and central rod temperatures.

* The power is calculated from the recorded cladding temperature (required because of the molybdenum power shift), the heater rod current and the heater rod resistance. Thus, if the cladding temperature is not recorded, the power can not be calculated.
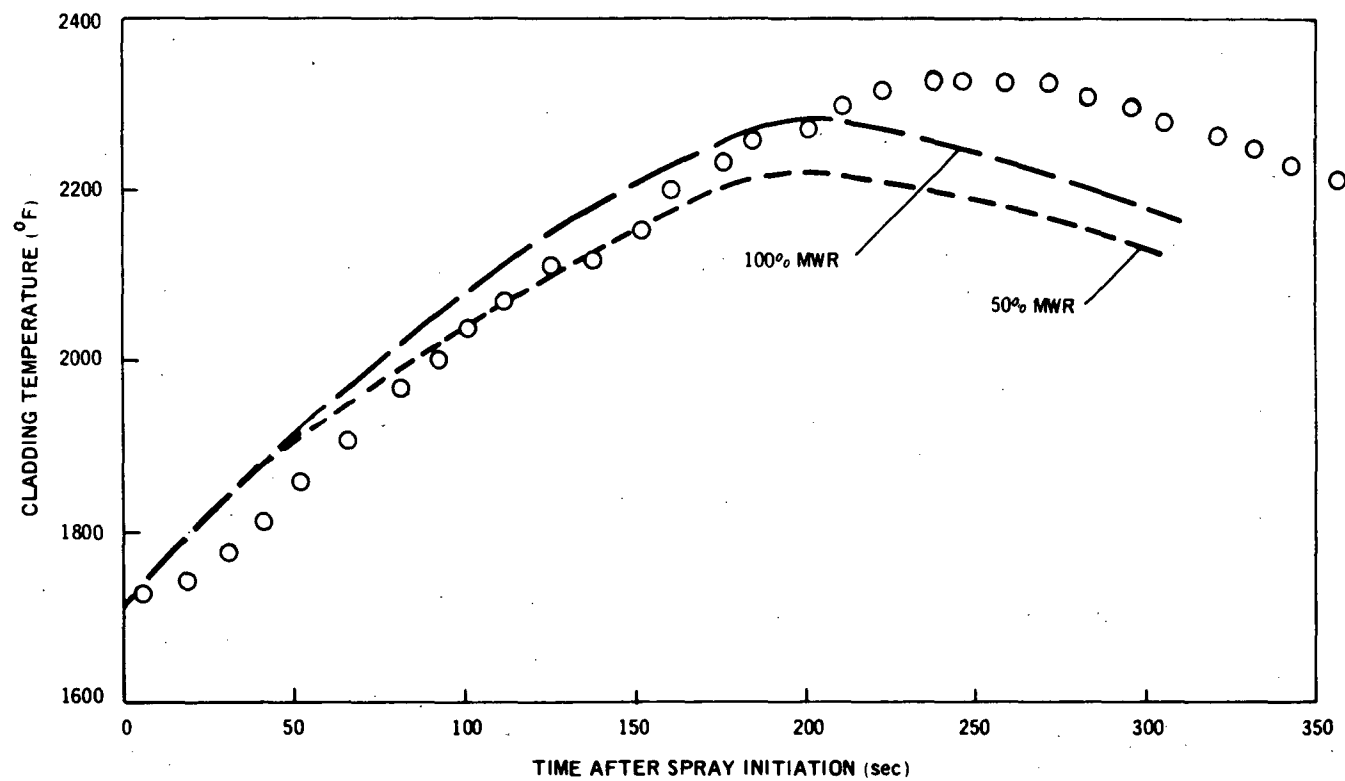
Figure 26   Bundle Zr3M Rod 26 Midplane Thermal Response Prediction

Table 4
Zr4M PREDICTION SUMMARY

Rod	Maximum Temperature (°F)					Time of Maximum Temperature (sec)				
	Observed	Predicted MWR		Error[1] MWR		Observed	Predicted MWR		Error[2] MWR	
		50%	100%	50%	100%		50%	100%	50%	100%
9	2180	2240	2340	+60	+160	15	125	125	+110	+110
10	2190[3]	2330	2440	+140	+250	50-100[3]	120	120	–	–
11	2310	2350	2470	+40	+160	105	120	120	+15	+15
12	2240	2310	2430	+70	+190	105	120	120	+15	+15
13	1970	2180	2290	+210	+330	60	120	120	+60	+60
16	2320	2330	2440	+10	+120	80	120	120	+40	+40
23	2230	2350	2470	+120	+240	40	120	120	+80	+80
27	2110[3]	2280	2420	+170	+310	120[3]	125	125	+5	+5
17	2530	2440	2560	–90	+30	110	120	120	+10	+10
18	2530	2450	2590	–80	+60	155	120	120	–35	–35
19	2300	2400	2540	+100	+240	140	120	120	–20	–20
24	2530	2450	2580	–80	+50	120	120	120	~0	~0
25	2530	2470	2630	–60	+100	125	125	125	~0	~0
26	Probable TC Malfunction									
31	2240	2410	2530	+170	+290	110	120	120	+10	+10
32	2250	2430	2570	+180	+220	140[3]	125	125	–15	–15
33	2100[3]	2400	2530	+300	+430	140[3]	125	125	–15	–15

NOTES

1   Maximum temperature error = predicted minus observed.
      Thus, + indicates overprediction of maximum temperature.
2   Time of maximum temperature error = predicted minus observed.
      Thus, + indicates maximum predicted temperature occurred later than data indicated.
3   Erratic thermocouple
4   Outside rod power was reduced by 50% in these calculations (see Section 7.4).

      Figure 27 compares the Rod 16 predictions with the test data. The 50% MWR calculation is quite accurate for the first 1.5 minutes (within 50°F of the data and about 100°F above the data after 1.5 minutes). The maximum temperature is predicted very well (~ 10°F over the observed value of 2320°F). The 100% MWR prediction is about 100°F above the 50% prediction. All other inside rod maximum temperatures were predicted more conservatively. The predictions ranged from 10°F to 210°F over the observed maximum temperature with 50% MWR and from 120°F to 330°F over with 100% MWR.

      Figure 28 compares the predictions with the Rod 24 data. The maximum temperature is underpredicted by about 80°F with 50% MWR and overpredicted by about 50°F with 100% MWR. The Rod 24 predictions are typical of the other three hottest rods in the Zr4M transient (Rods 17, 18, 24 and 25 all had maximum temperatures of approximately 2530°F). The predictions of the other central rod temperatures ranged from 100°F to 300°F over the observed maximum temperature with 50% MWR and from 240°F to 430°F over the observed value at 100% MWR. Note that the value of the MWR rate constant is quite important at these high temperatures.
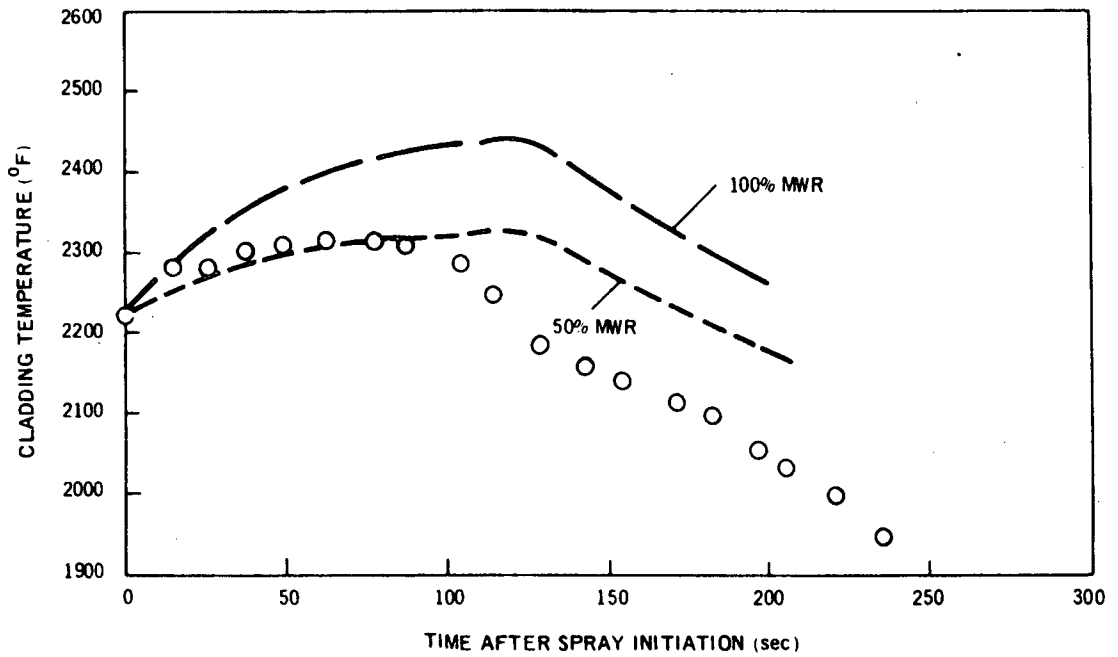
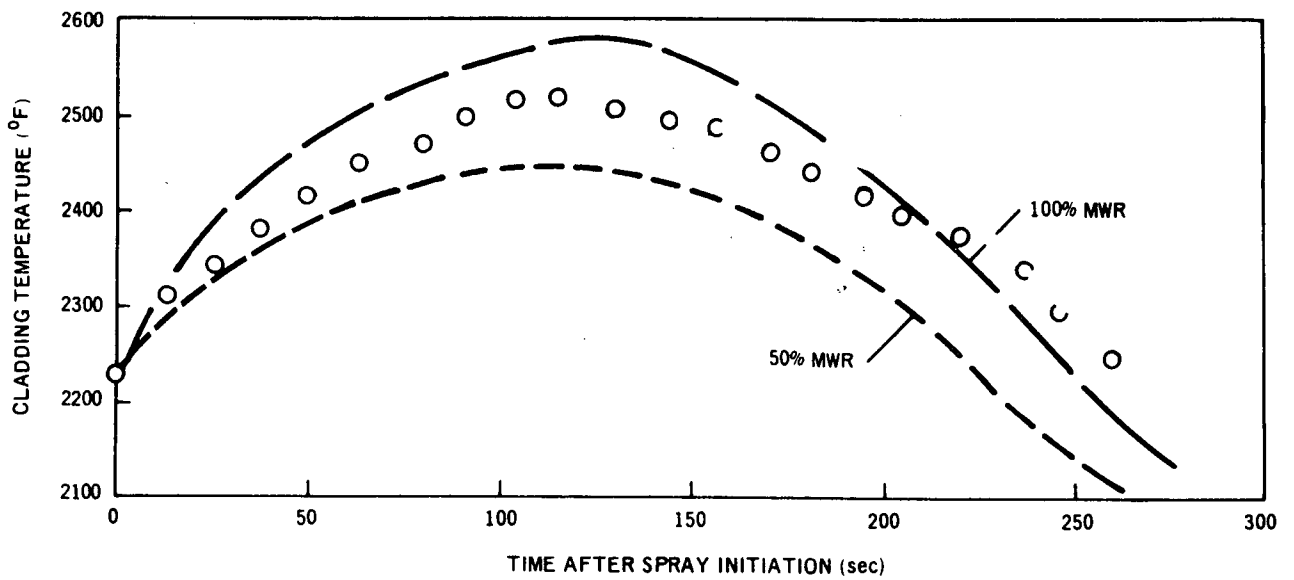Figure 27   Bundle Zr4M Rod 16 Midplane Thermal Response Prediction

Figure 28   Bundle Zr4M Rod 24 Midplane Thermal Response Prediction

Thus, the model performs well in predicting the hottest Zr4M temperatures. Outside rod temperature predictions were not accurate but were very conservative. Had the outside rod calculated temperatures not been forced to be closer to the data by arbitrarily reducing the outside rod power, the calculated inside and central rod temperatures would have been approximately 100 to 200°F higher, and all test temperatures would have been overpredicted.

7.5 INTERPRETATION OF PREDICTIONS

The accuracy of the predictions discussed in this section must be considered in light of the uncertainties involved in predicting individual rod maximum temperatures in these tests. The uncertainties are estimated in Appendix B with the following assumptions:

a. Local power is uncertain to ~ 10%. The principal reason for this uncertainty arises from the difficulty of calculating the local power density when a "molybdenum power-shift" is occurring (see Reference 5 and Section 4.1).

b. The metal-water reaction rate constant is equal to 0.5 ± 0.5 times that of Baker.*

c. The local convection coefficient is equal to 1.0 ± 0.5 Btu/h ft² °F.

d. The local radiation grey body factor is accurate to 10%. An uncertainty in this term results from the distortion which occurs in the tests.

The resulting uncertainty in a calculated central rod maximum temperature is shown in Figure B-4. Since the energy addition and energy removal rates are temperature dependent, the uncertainty in the calculated maximum temperature depends on the temperature which is calculated. For example (Figure B-4), if a maximum central rod test temperature is calculated to be 2100°F, the uncertainty is estimated at ~ ± 200°F at about 10:1 odds.

The "error" in maximum temperature ("error" = calculated minus observed temperature) is plotted against the calculated temperature and compared to the estimated uncertainty in Figures 29 and 30. Figure 29 indicates that all 14 inside rod maximum temperature "errors" fall within the uncertainty band. Figure 30 indicates that 16 of the 17 central rod "errors" fall within the uncertainty band. The single point which does not fall within the band is a 300°F overprediction of a central rod maximum temperature in the Zr4M test.

Other presentations of the errors are given in Appendix A ("prediction maps" in which the maximum temperature error is plotted against the error in the time of maximum temperature and a statistical representation of the errors) which also indicates that maximum individual rod test temperatures calculated, using heat transfer coefficients from the current model (Section 6.2) and assuming 50% MWR, will be uncertain by about 200°F.

It should be noted that the above comments apply only to a calculation of test temperatures. Calculations of maximum temperatures in the reactor case should be biased to the conservative side for several reasons:

a. Conservative assumptions are made concerning the local power density.

b. A conservative 100% metal-water reaction is assumed.

c. Heat transfer coefficients calculated from tests at one atmosphere pressure are assumed to apply throughout the accident. All loss-of-coolant accidents result in pressures greater than one atmosphere and, depending on the specific accident postulated, the pressure may be considerably higher than one atmosphere. The bundle SS4N data indicates a significant increase in heat transfer coefficients as the pressure increases to ~ 200 psia.

It is estimated that the combined effect of these conservative assumptions and of other assumptions during the blowdown phase** of the postulated accident results in calculated reactor maximum temperatures being from 100°F to 400°F higher than the temperatures which would occur in an actual accident.

It is therefore concluded that the current General Electric core spray heat transfer model can be used to conservatively predict maximum temperature in a postulated BWR loss-of-ccolant accident when 100% metal-water reaction is assumed.

8. CONCLUSIONS AND RECOMMENDATIONS

8.1 CONCLUSIONS

Only the most important conclusions resulting from the BWR-FLECHT test program are summarized here. Others, of somewhat less general importance are included in Sections 4 and 5.

1. Use of the current General Electric core spray heat transfer model developed from the BWR-FLECHT data should provide conservative predictions of maximum cladding temperatures when 100% metal-water reaction is assumed (Section 7).

---

* This range was selected to facilitate the present calculation (a normal distribution of uncertainties is assumed) and is not intended to imply that zero metal-water reaction is possible.

** Although the blowdown phase of the accident was not studied under the FLECHT program, it is of interest to note an estimate of the effect of the conservative assumptions in the entire accident.
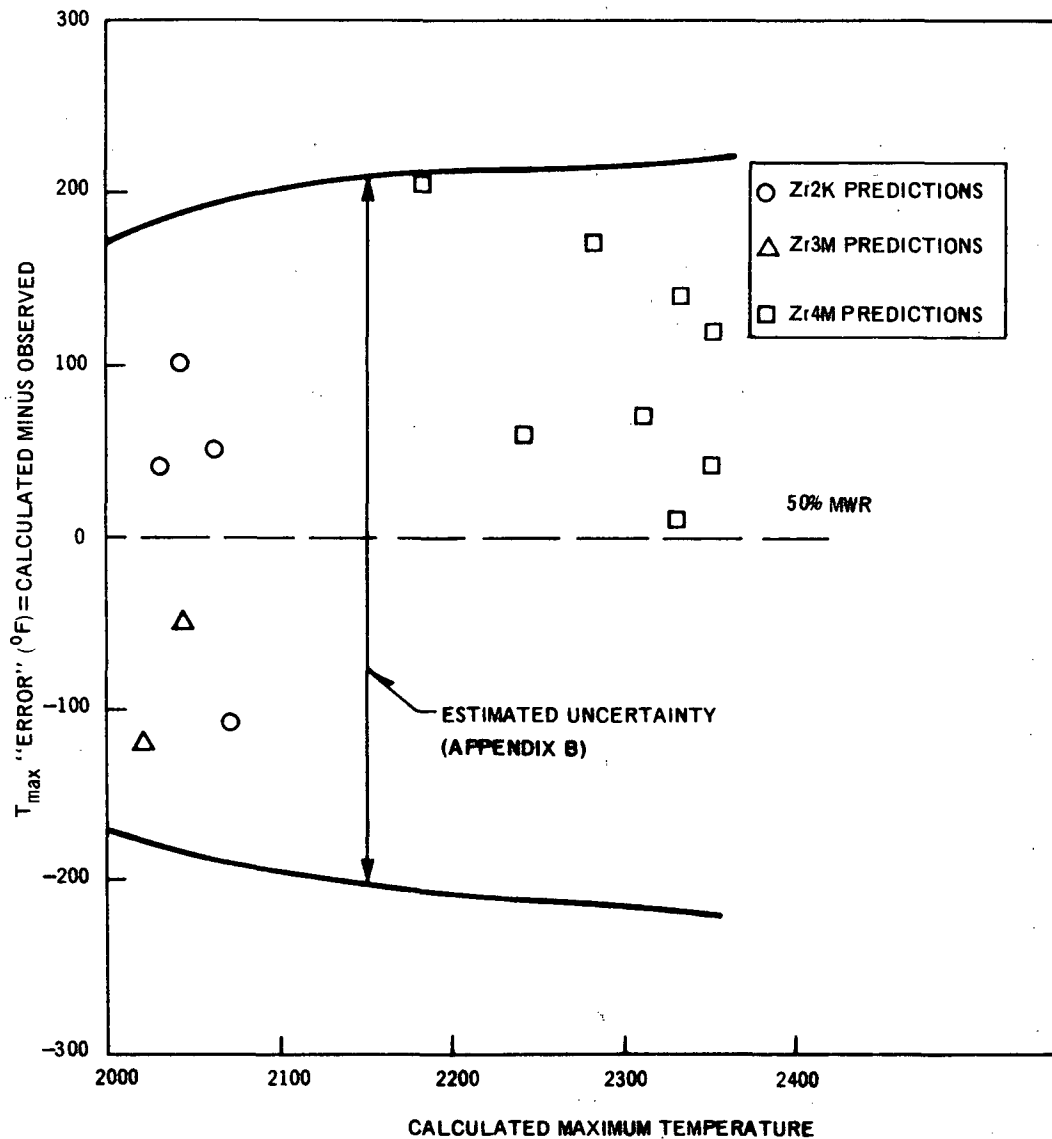
Figure 29   Inside Rod Maximum Temperature Error

2.   Increasing system pressure above one atmosphere significantly enhances the effectiveness of both the top-spray and bottom-flooding modes of emergency cooling (Sections 4 and 5).

3.   No cladding fragmentation can be expected if maximum temperatures are less than 2500°F. Severe fragmentation can be expected if temperatures reach 2900°F and if the "time-at-temperature" is similar to that which occurred in the FLECHT tests (Section 4).

4.   Even under extremely severe conditions (where cladding temperatures exceeded 2900°F), cladding damage was confined within the fuel channels in the FLECHT tests. It is therefore probable that damage would also be confined within the channels under very severe BWR loss-of-coolant conditions (Section 4).

5.   The bottom-flooding mode of emergency cooling is so effective that increasing flooding rates above the design value provides a negligible improvement in its effectiveness (Section 5).

8.2 RECOMMENDATIONS

1.   The analysis of the FLECHT data presented here demonstrates that Zircaloy-clad test temperatures can be predicted with reasonable accuracy considering the uncertainties involved in the predictions. Much of the uncertainty in the predictions can be attributed to the heater rod and thermocouple failures which occurred in

the last four Zircaloy-clad tests and the molybdenum power shifting in the last three tests. Many of these problems resulted because the heaters were tested under much more severe conditions than their design anticipated. These problems can be avoided by minor heater design improvements and by selecting more appropriate test conditions. A lower temperature (initial temperature $\sim 1300^{\circ}$F), constant resistance heated Zircaloy-clad bundle test would allow a significant reduction in test uncertainties. In addition, such a test could more nearly be considered as a direct demonstration" of the ability of the core spray system to limit cladding temperature increases following a loss-of-coolant accident.

Therefore, it is recommended that another Zircaloy-clad test be conducted using improved heater rods and more representative initial conditions.

2. The cooling capability of core spray at elevated pressures should be investigated further so that advantage can be taken of the increased effectiveness with no compromise to reactor safety.
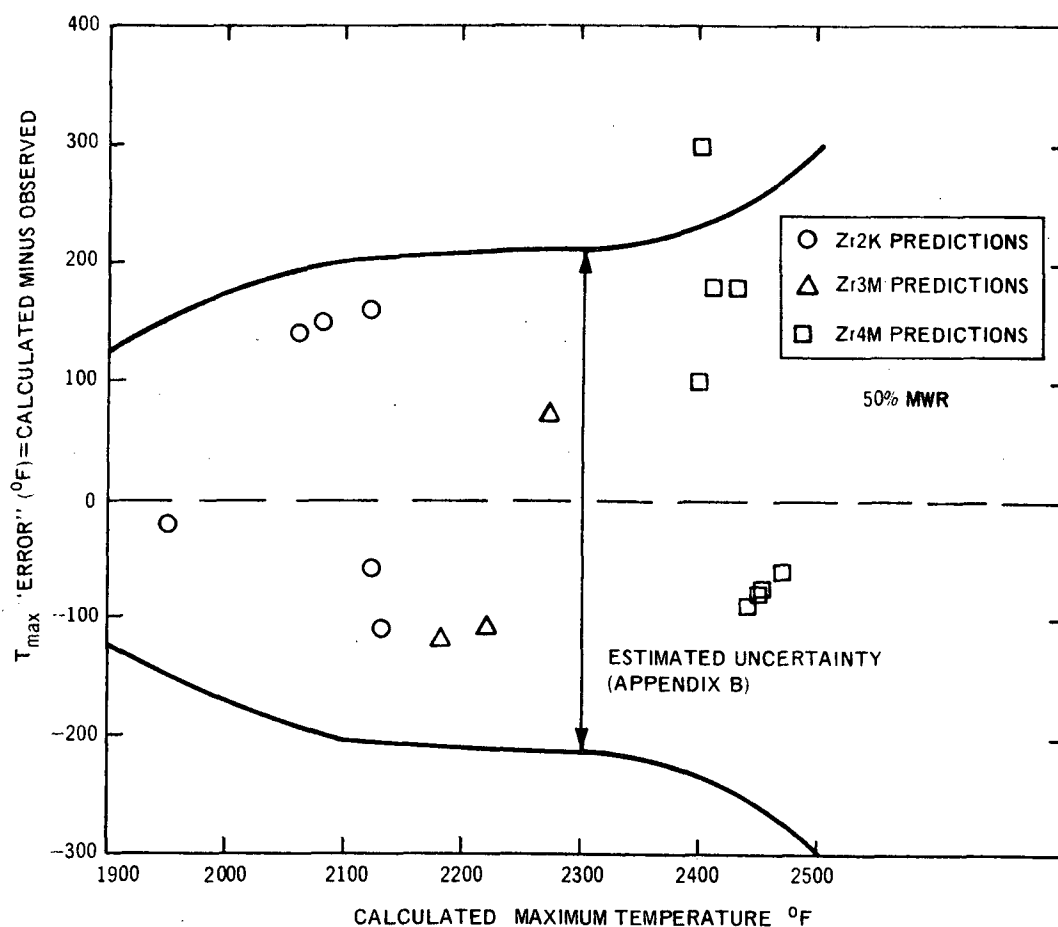
Figure 30   Central Rod Maximum Temperature Error
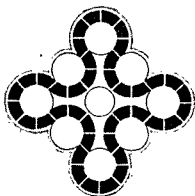
Aerojet Nuclear Company

January 14, 1971
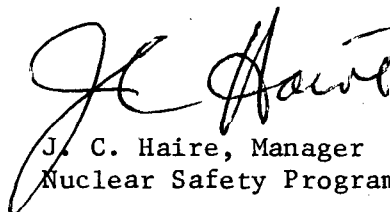
Dr. C. W. Bills, Director
Nuclear Technology Division
Idaho Operations Office
U. S. Atomic Energy Commission
Idaho Falls, Idaho   83401

TRANSMITTAL OF GEAP-13197 - Hai-11-72

This letter is to implement distribution of the General Electric Company
BWR-FLECHT final report (GEAP-13197). Preparation of this document
completes the scope of work General Electric Company performed under
subcontract to Aerojet Nuclear Company* on emergency core cooling.
Aerojet Nuclear Company believes that this document effectively summarizes
the project activities and presents a "state-of-the-art" summary of
General Electric Company's emergency core cooling analysis capability.

Acting in its capacity as project technical director, Aerojet Nuclear
Company is in the process of preparing its own final report which is
to be published at the end of the fiscal year.

Patent clearance on the enclosed document has been received.

J. C. Haire, Manager
Nuclear Safety Program Division

lk

Encs.

cc: Director, DRDT
     Assistant Director for Nuclear Safety, DRDT - 4
     Assistant Director for Project Management, DRDT
     LOFT Project Manager, DRDT
     LOFT Program Manager, DRDT

---

*Aerojet Nuclear Company succeeded Idaho Nuclear Corporation on
 July 1, 1971.

cc: (Contd.)
    Chief, Thermal Reactor Safety Branch, DRDT
    Assistant Director for Army Reactors, DRDT
    Assistant Director for Plant Engineering, DRDT
    Assistant Director for Program Analysis, DRDT
    Assistant Director for Reactor Technology, DRDT
    Assistant Director for Reactor Engineering, DRDT
    Assistant Director for Engineering Standards, DRDT
    Director, Division of Reactor Standards - 11
    Chief, Systems and Performance Branch, DRS
    Division of Compliance
    Division of Compliance, Region IV
    Division of Naval Reactors - 2
    Division of Reactor Licensing
    Chicago Operations Office, AEC
    Oak Ridge Operations Office, AEC
    Richland Operations Office, AEC
    San Francisco Operations Office, AEC
    Director, LOFT Project Division, ID
    C. M. Rice, ANC
    Manager, WRSPO
    R. Blanco, ORNL
    R. G. Bock, GE (wo/enc.)
    A. P. Bray, GE (wo/enc.)
    G. M. Brown, SNE
    J. Buchanan, Nuclear Safety Information Center
    W. A. Carbiener, BMI
    M. W. Carbon, Univ. of Wisconsin
    D. F. Cope, ORNL
    W. B. Cottrell, ORNL - 4
    H. K. Fauske, Argonne
    G. Fischer, Argonne
    R. F. Fraley, Exec. Sec., ACRS - 17
    H. A. Johnson, Uni. of Inst. of Eng. Research, Berkeley
    B. LaMar, Argonne
    J. Marchaterre, Argonne
    J. D. McAdoo, Westinghouse
    D. W. Montgomery, B&W
    J. B. Moore, SCE
    D. L. Morrison, BMI
    C. Muehlhause, National Bureau of Standards
    C. Parks, B&W
    J. W. Riches, Douglas United Nuclear
    P. L. Rittenhouse, ORNL
    T. Rockwell, MPR Associates
    S. Rosen, CE
    R. Sevy, Argonne
    V. E. Schrock, Uni. of Inst. of Eng. Research, Berkeley
    F. J. Climent, Aerojet General

cc: (Contd.)
    P. Shewmon, Argonne
    M. Siegler, GE (wo/enc.)
    W. Simmons, Argonne
    W. A. Sutherland, GE (wo/enc.)
    G. E. Wade, GE (wo/enc.)
    R. Wascher, B&W
    R. A. Wiesemann, Westinghouse
    M. F. Valerino, CE
    S. Vandenberg, GE (wo/enc.)
    R. Vogel, Argonne
    DTIE, ORNL - 2
    NRTS Tech. Lib. - 3
    Nuclear Fuel Services

REFERENCES

1. Levy, S. and Hodde, J. A., *Spray Cooling of a Multirod Fuel Assembly,* January 1960 (GEAP-3318).

2. Janssen, E., et al., *Core Spray Test Program, Browns Ferry Nuclear Power Station Design and Analysis Report,* Appendix E, 1965.

3. Schraub, F. A., and Leonard, J. E., *Core Spray and Core Flooding Heat Transfer Effectiveness in a Full-Scale Boiling Water Reactor Bundle,* June 1968, (APED-5529).

4. Bock, R. G., *Full Length Emergency Cooling Heat Transfer Program Test Plan,* August 1968 (GEAP-5676).

5. Duncan, J. D. and Bock, R. G., *The Performance of Molybdenum Filaments in BWR Emergency Cooling Heat Transfer Tests,* November 1969 (GEAP-10092).

6. Duncan, J. D. and Leonard, J. E., *Heat Transfer in a Simulated BWR Fuel Bundle Cooled by Spray Under Loss-of-Coolant Conditions,* June 1970 (GEAP-13086).

7. Duncan, J. D. and Leonard, J. E., *BWR Standby Cooling Heat Transfer Under Simulated Loss-of-Coolant Conditions Between 15 and 300 psia,* May 1971 (GEAP-13190).

8. Leonard, J. E. and Duncan, J. D., *Preliminary Results of the BWR-FLECHT Internally Pressurized, Zircaloy-Clad Bundle, Spray Cooling Test,* January 1970 (NEDG-13064).

9. Duncan, J. D. and Leonard, J. E., *Thermal Response and Cladding Performance of an Internally Pressurized, Zircaloy-Clad, Simulated BWR Fuel Bundle Cooled by Spray Under Loss-of-Coolant Conditions,* September 1970, (GEAP-13112).

10. Duncan, J. D. and Leonard, J. E., *Thermal Response and Cladding Performance of Zircaloy-Clad Simulated Fuel Bundles Under High Temperature Loss-of-Coolant Conditions,* May 1971 (GEAP-13174).

11. Lemmon, A. W., *Studies Relating to the Reaction Between Zirconium and Water at High Temperatures,* January 3, 1957 (BMI-1154).

12. Schraub, F. A., and Bock, R. B., *Fuel Rod Failures During Simulated Loss-of-Coolant Conditions,* March 1968 (APED-5479).

13. Lorenz, R. A., Parker, G. W., and Hobson, D. O., *Preliminary Evaluation of the First Fuel Rod Failure Transient Test of a Zircaloy-Clad Fuel Rod Cluster in TREAT,* November 26, 1969 (ORNL-TM-2774).

14. Herzel, R., and Meservey, R. H., *The Brittle Behavior of Zircaloy Under Emergency Cooling Conditions,* Oral presentation at the Fifteenth Annual Conference of the American Nuclear Society, June 19, 1969, Seattle, Washington.

15. Duncan, J. D., and Leonard, J. E., *Response of a Simulated BWR Fuel Bundle Cooled by Flooding Under Loss-of-Coolant Conditions,* December 1969, (GEAP-10117).

16. Rogers, A. E., and Leonard, J. E., *An Analytical Model of the Transient Core Spray Cooling Process,* to be distributed at the December 1971 A.I.ChE Meeting Symposium on "Heat Transfer in Water Cooled Nuclear Reactor Systems."

17. Kline, J. S., and McClintock, F. A., *Describing Uncertainties in Single Sample Experiments,* Mechanical Engineering, January 1953.

APPENDIX A
ZIRCALOY-CLAD BUNDLE THERMAL RESPONSE PREDICTIONS

The predicted response of all operable midplane thermocouples in bundles Zr2K, Zr3M, and Zr4M are presented in this appendix. Two predictions are compared with the data in Figures A-1 to A-47:

a.   The prediction obtained by using the heat transfer coefficients of the current General Electric model (from bundle SS2N, see Section 6.2 and Reference 16) and assuming 50% metal-water reaction. This prediction is labelled 50% MWR.

b.   The prediction obtained by using the current model heat transfer coefficients and 100% metal-water reaction. This prediction is labeled 100% MWR.

It should be noted that assuming 50 and 100% MWR in these calculations is not exactly equivalent to the same assumptions in a reactor calculation since the present calculations start at elevated temperatures (the test initial conditions) and the reactor calculations start at operating temperatures (the reactor initial conditions).

As an aid in interpretating the predictions of the individual thermocouple responses in the three bundle transients, a "prediction map" presentation[10] has been found useful. The error in maximum temperature (predicted minus observed) is plotted against the error in the time of maximum temperature (predicted minus observed) for outside rods, inside rods, and central rods. Prediction maps (with 50% metal-water reaction assumed) for the three groups of rods are presented in Figures A-48 to A-50. Points falling above the horizontal line indicate an overprediction of the maximum temperature. Points falling to the right of the vertical line indicate that the predicted maximum temperature occurred later than the data indicated. Five of the eight outside rod predictions (Figure A-48) were conservative (overprediction of the maximum temperature). The least conservative (predictions of Rods 1 and 2 in the Zr3M transient) were 100°F below the data. All but 2 of the predictions were correct to within two minutes of the observed maximum temperature. Most (8 of 13) of the inside rod predictions (Figure A-49) were conservative and only two (predictions of Rod 23 in the Zr2K and Zr3M transients) were more than 50°F below the data. The largest error in the time of maximum temperature occurred in the predictions of Rod 9 in the Zr4M transient (1.8 minutes late). Most of the calculations predicted the time of maximum temperature to within one minute. Half (7 of 15) of the central rod predictions (Figure A-50) were conservative. Only three of the eight underpredictions gave maximum temperatures more than 100°F below the test data. Only four of the predictions (Bundle Zr2K) were more than one minute off in predicting the time of maximum temperature. Thus, most of the predictions are conservative, several by as much as 200°F. Those which are not conservative underpredict the test maximum temperature by less than 125°F. It is shown in Appendix B that the errors in predicting the maximum temperatures are quite reasonable considering the uncertainties involved in the predictions. Further, most of the calculations result in an accurate (± 1 minute) prediction of the time of maximum temperature.

As a further aid in interpreting the predictions, it is appropriate to examine the maximum temperature prediction errors statistically. The bar graphs in Figure A-51 show the number of times a particular error in maximum temperature occurred for the three rod groups (outside, inside and central). Figure A-52 shows that calculations using the current model heat transfer coefficients and assuming 50% metal-water reaction perform reasonably well in predicting individual rod maximum temperatures. The predictions tend to be slightly conservative as noted below:

a.   Of eight outside rod predictions, four were more than 50°F over the observed maximum temperature and two were more than 50°F under the observed value. Bundle Zr4M outside rod predictions were quite conservative (Section 7.4) and are not included on Figure A-52.

b.   Of thirteen inside rod predictions, six were more than 50°F above the observed maximum temperature and three were more than 50°F below the observed value.

c.   Of fifteen central rod predictions, seven were more than 50°F above the observed maximum temperature and eight were more than 50°F below the observed value. The uncertainty analysis presented in Appendix B indicates that the errors in predicting maximum temperatures are quite reasonable considering the uncertainties in the variables used to predict the temperatures. That is, the local heater rod power, the metal-water reaction rate, the radiation view factors and the convection coefficient are not known exactly. Thus, these "errors" in predicting the maximum test temperatures can be expected.
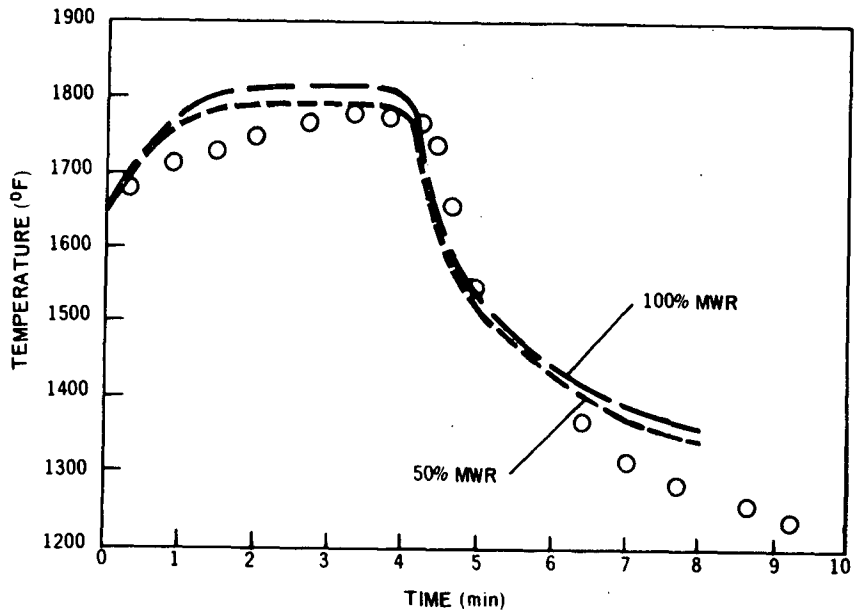
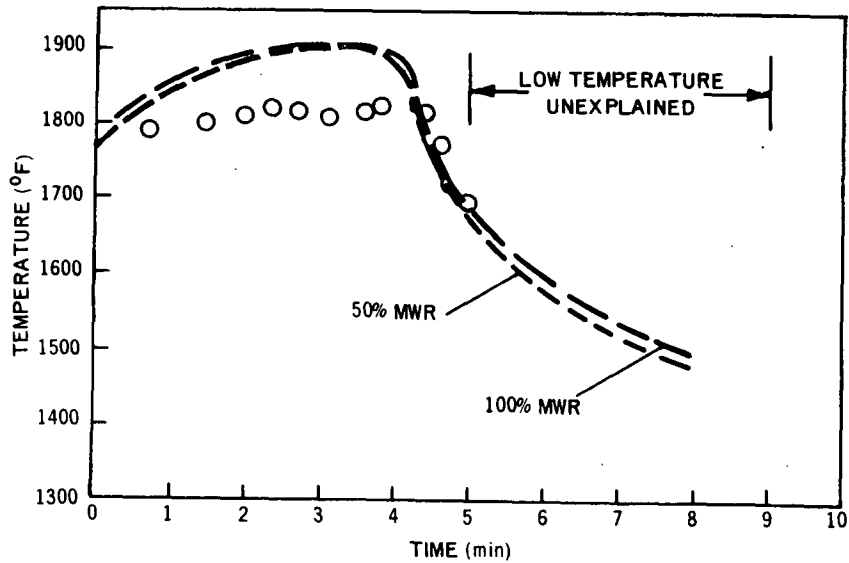Figure A-1   Bundle Zr2K Rod 1 Midplane Thermal Response Prediction

Figure A-2   Bundle Zr2K Rod 2 Midplane Thermal Response Prediction
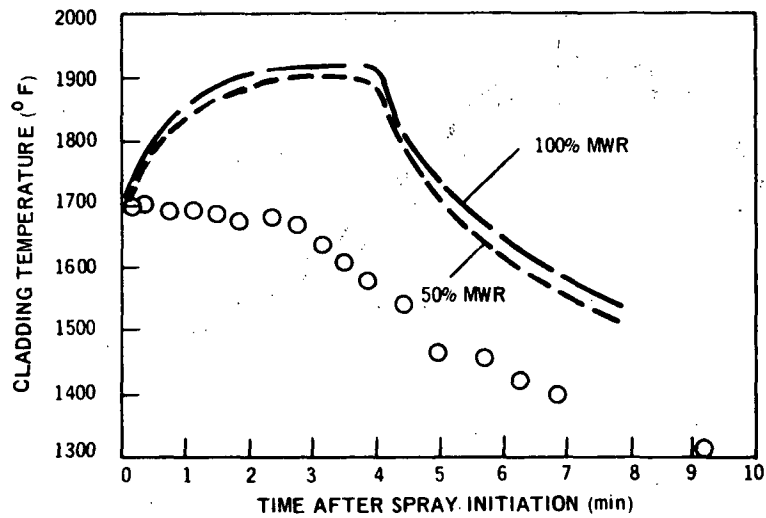
Figure A-3   Bundle Zr2K Rod 3 Midplane Thermal Response Prediction
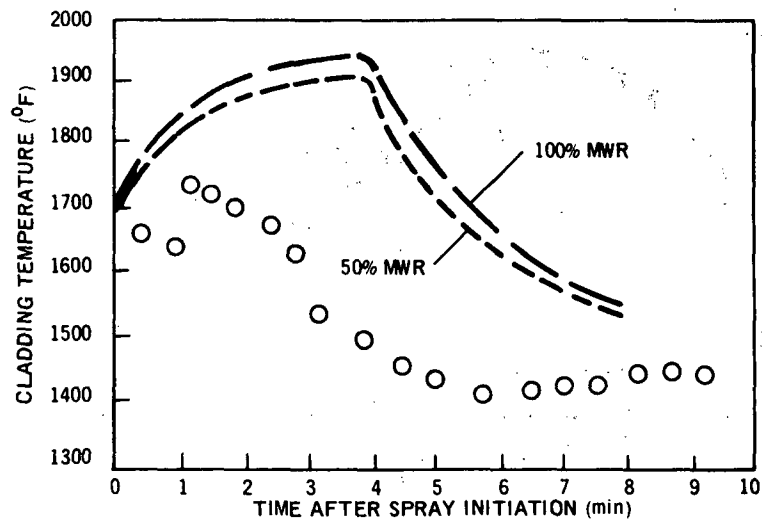

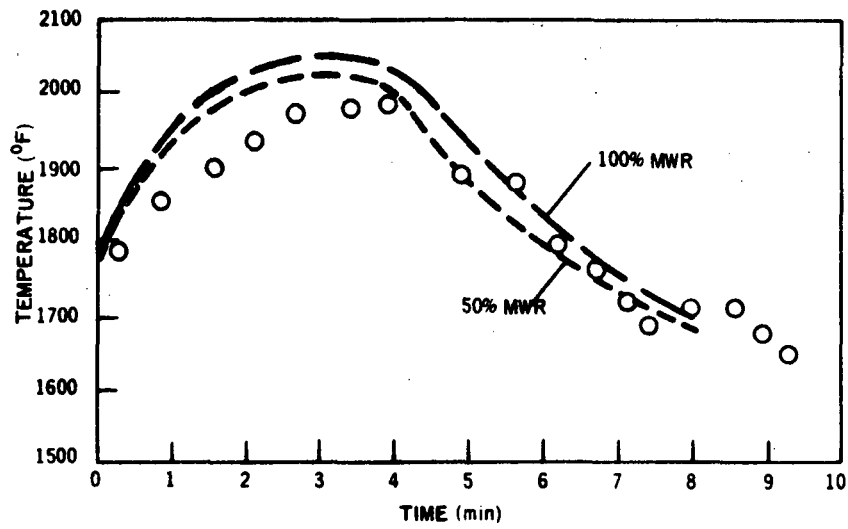Figure A-4   Bundle Zr2K Rod 4 Midplane Thermal Response Prediction

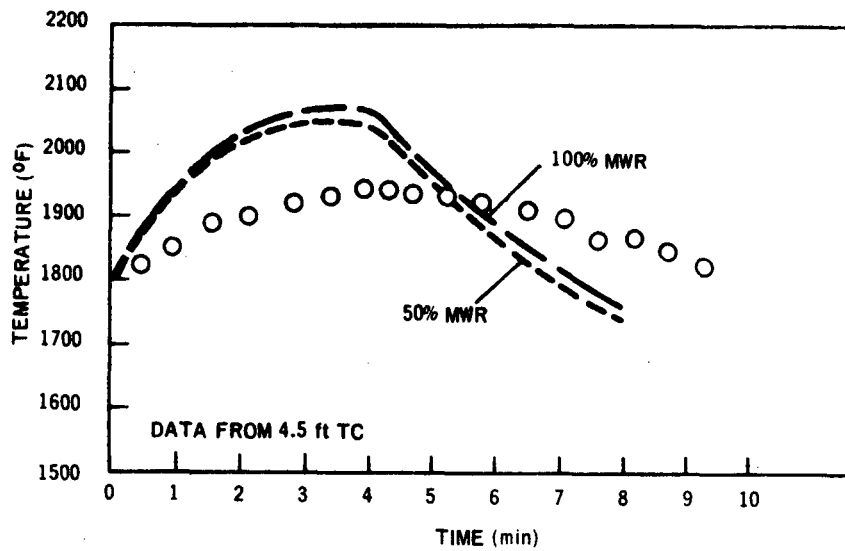Figure A-5   Bundle Zr2K Rod 9 Midplane Thermal Response Prediction

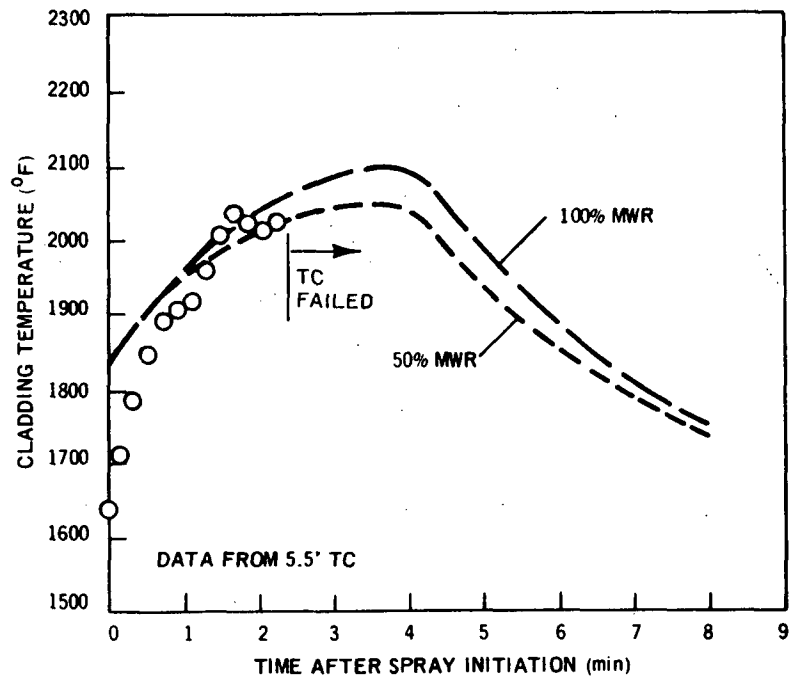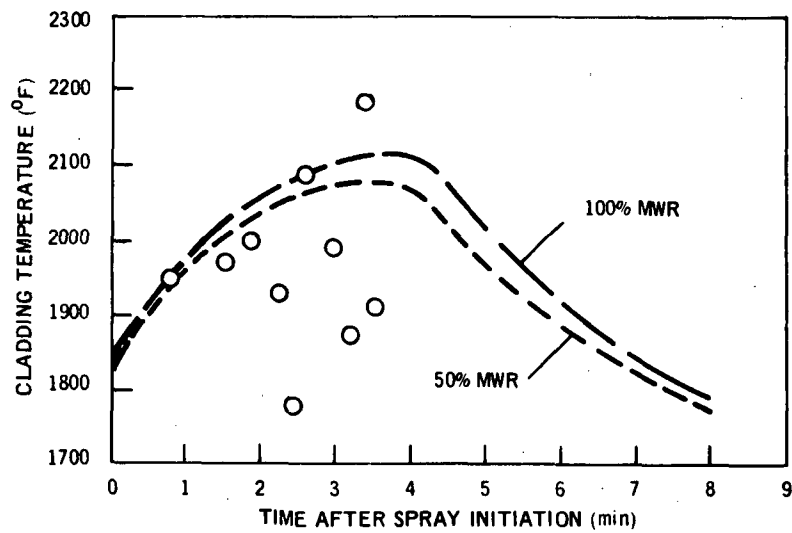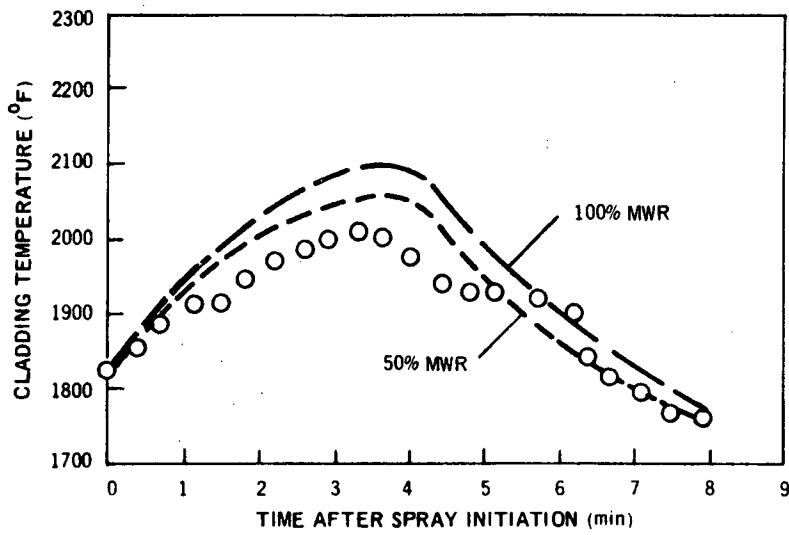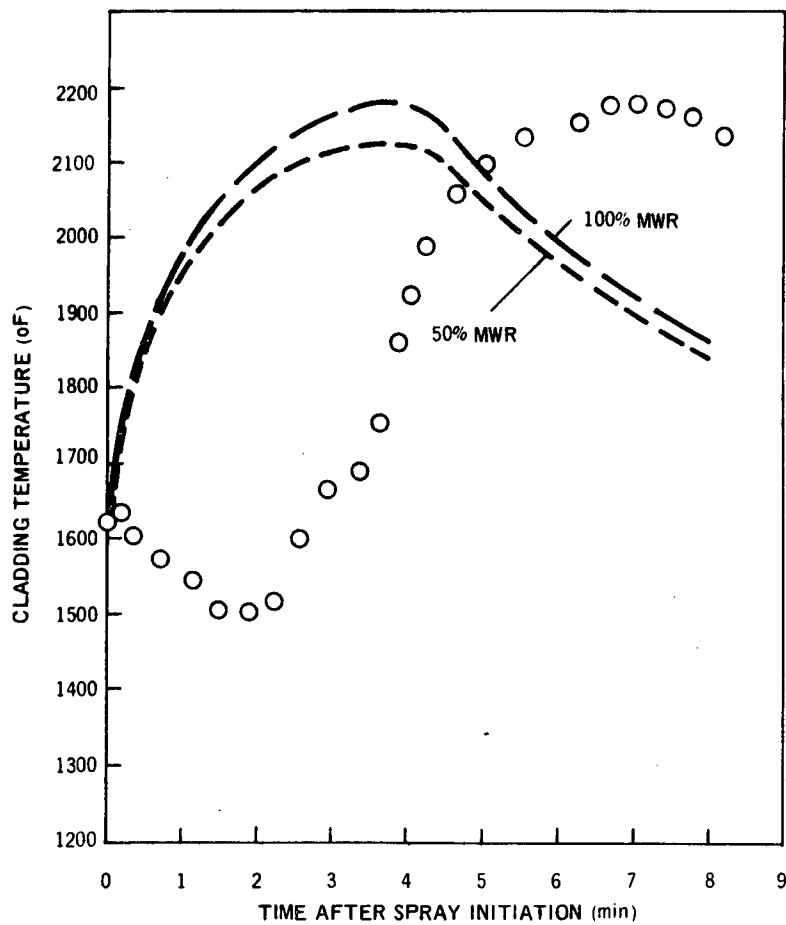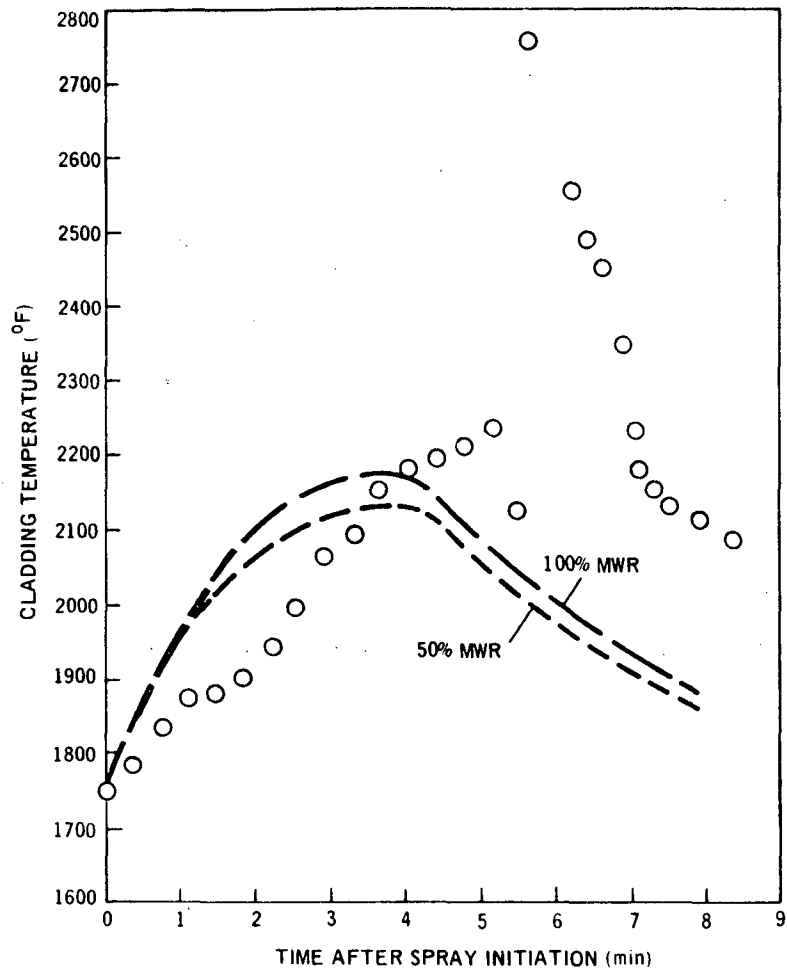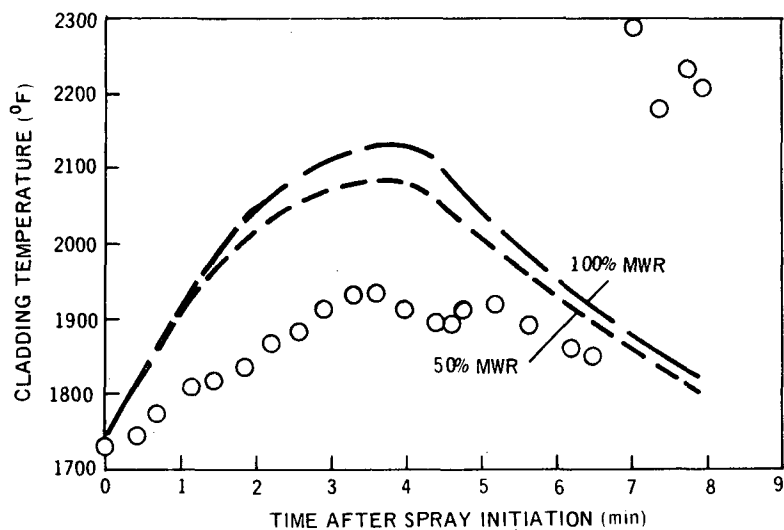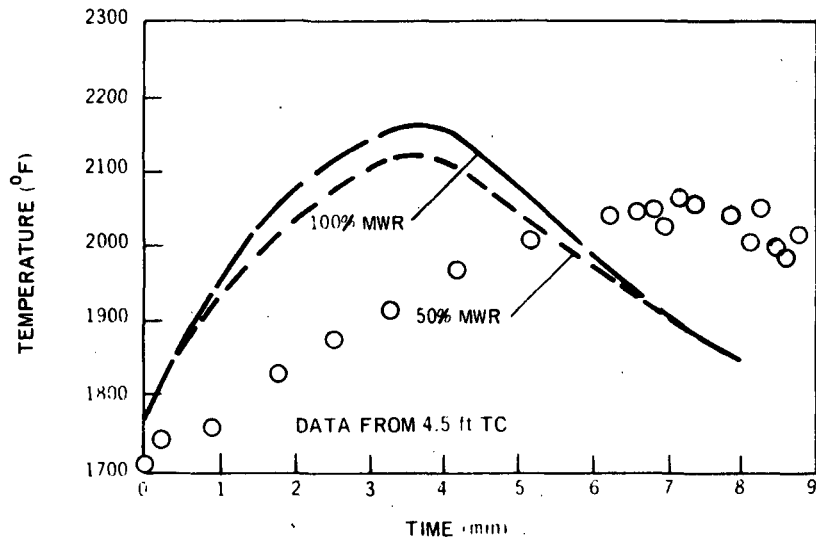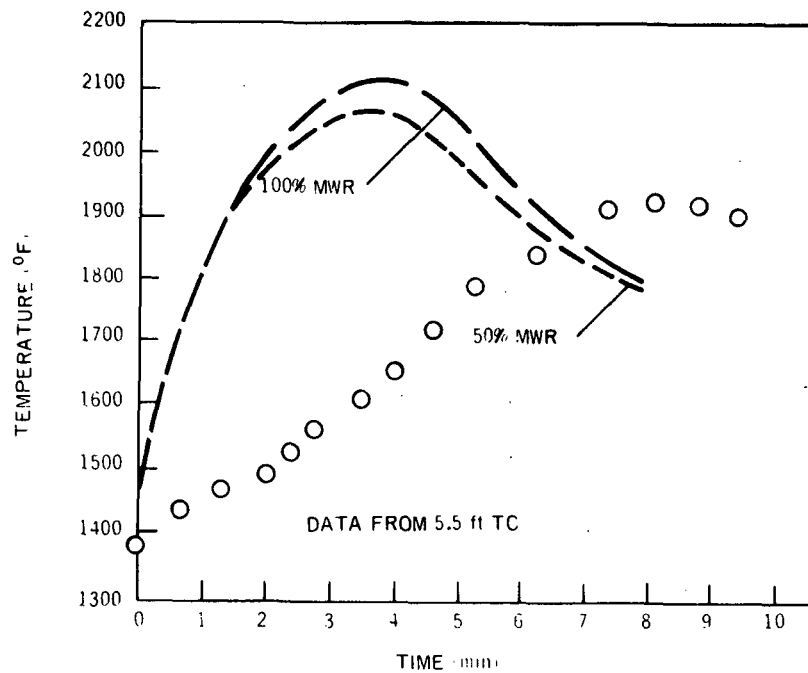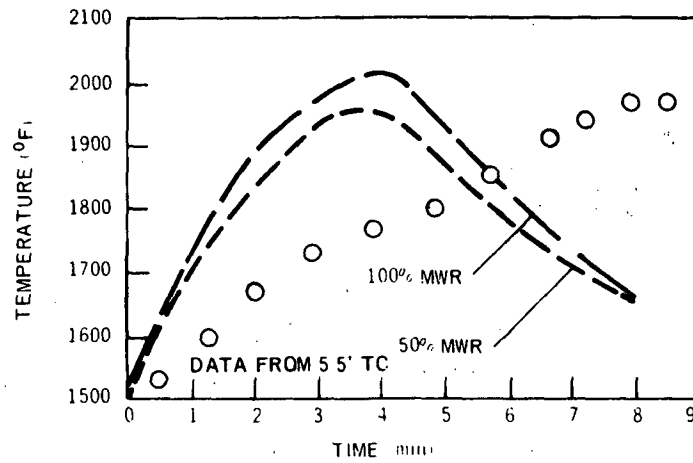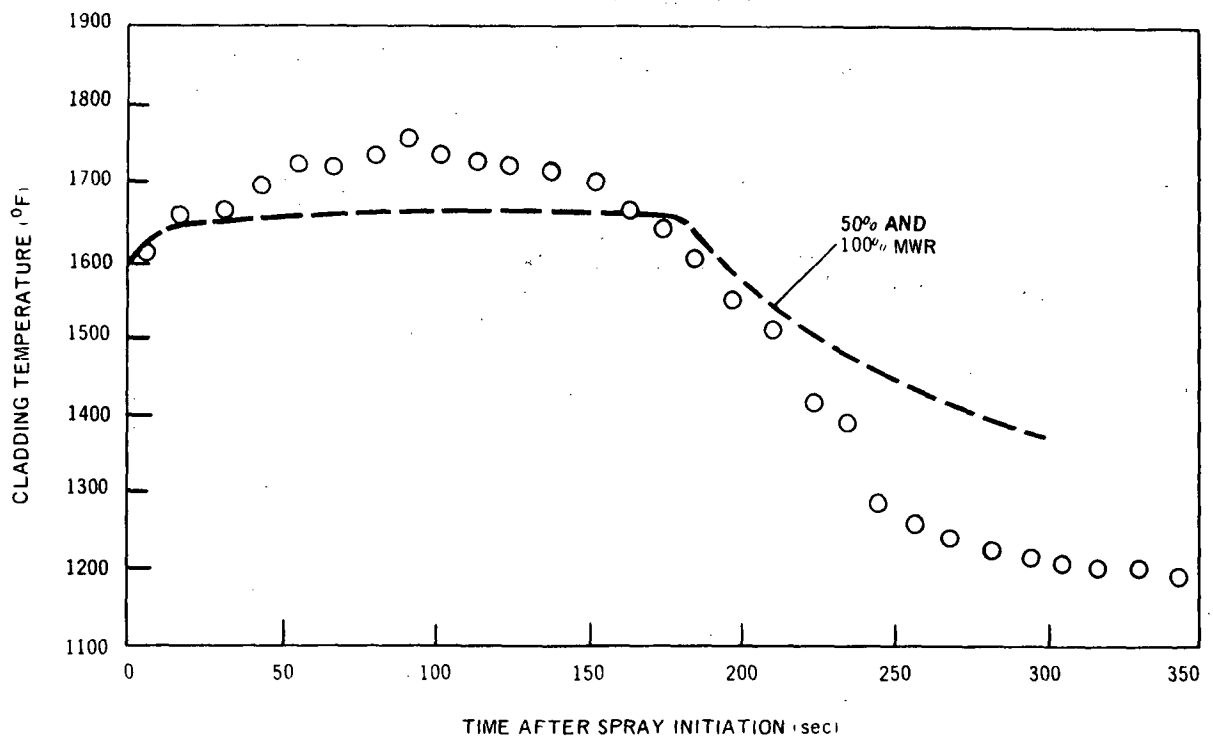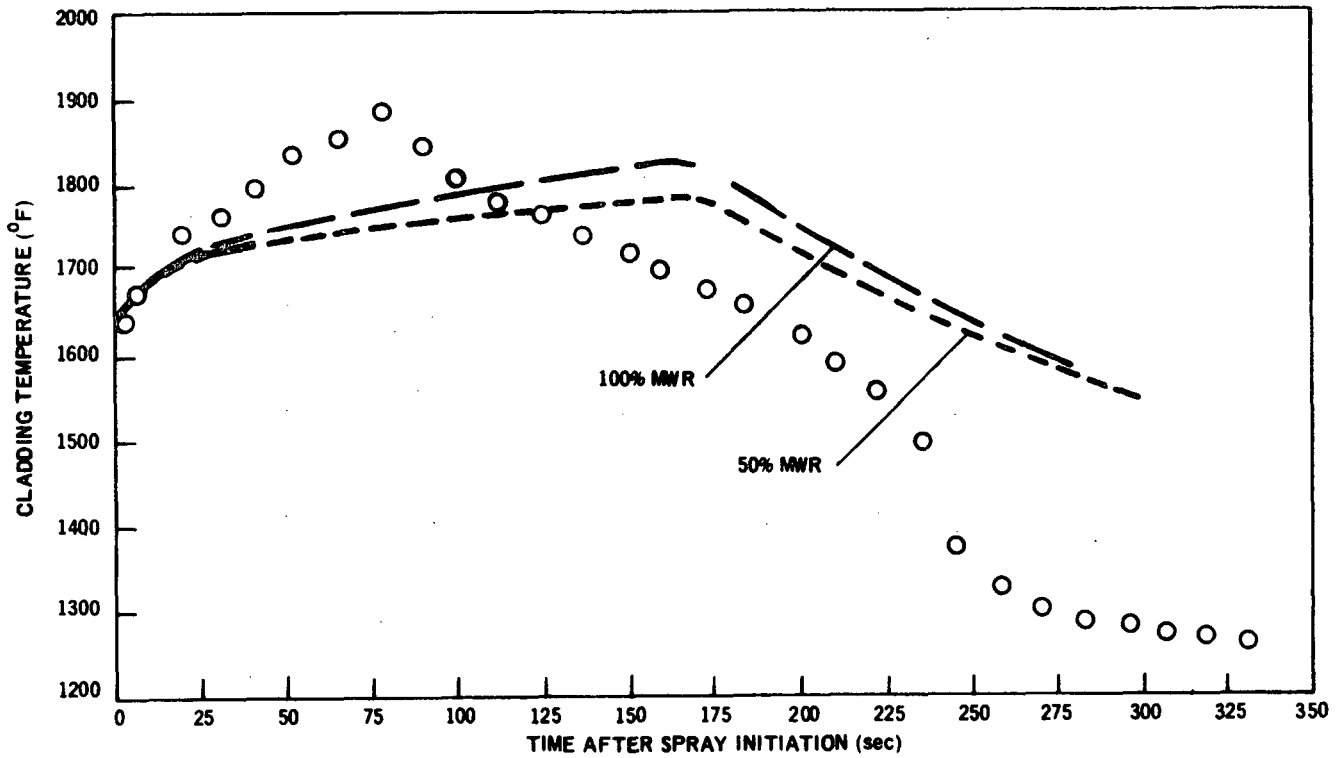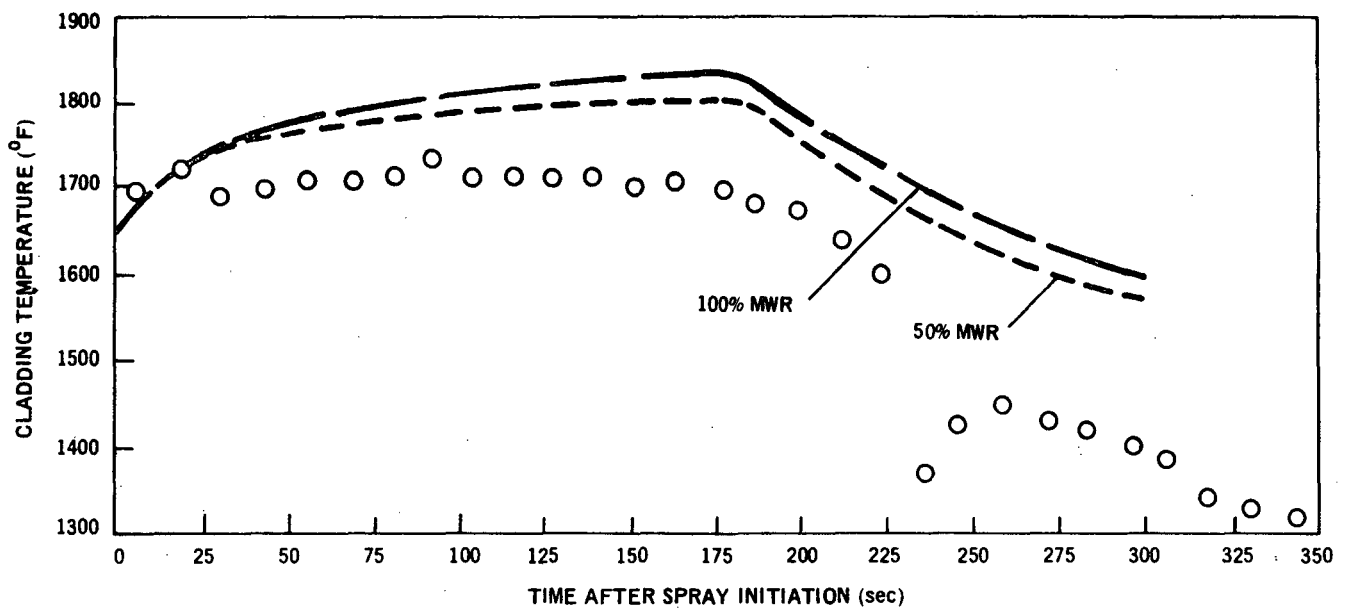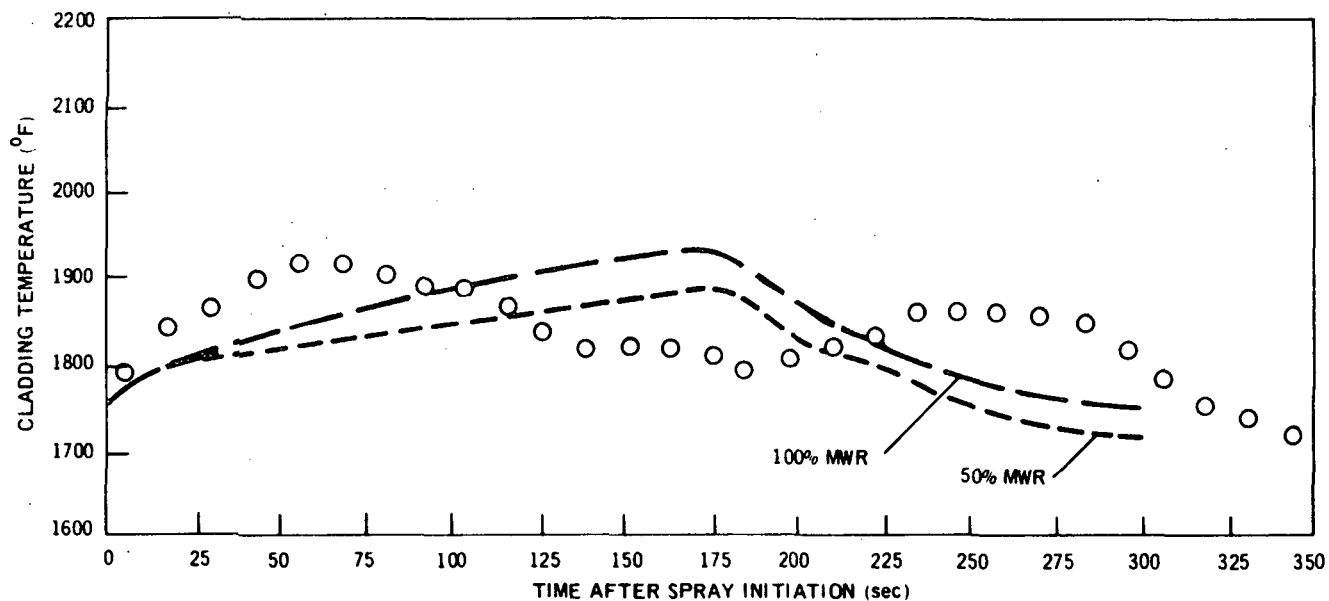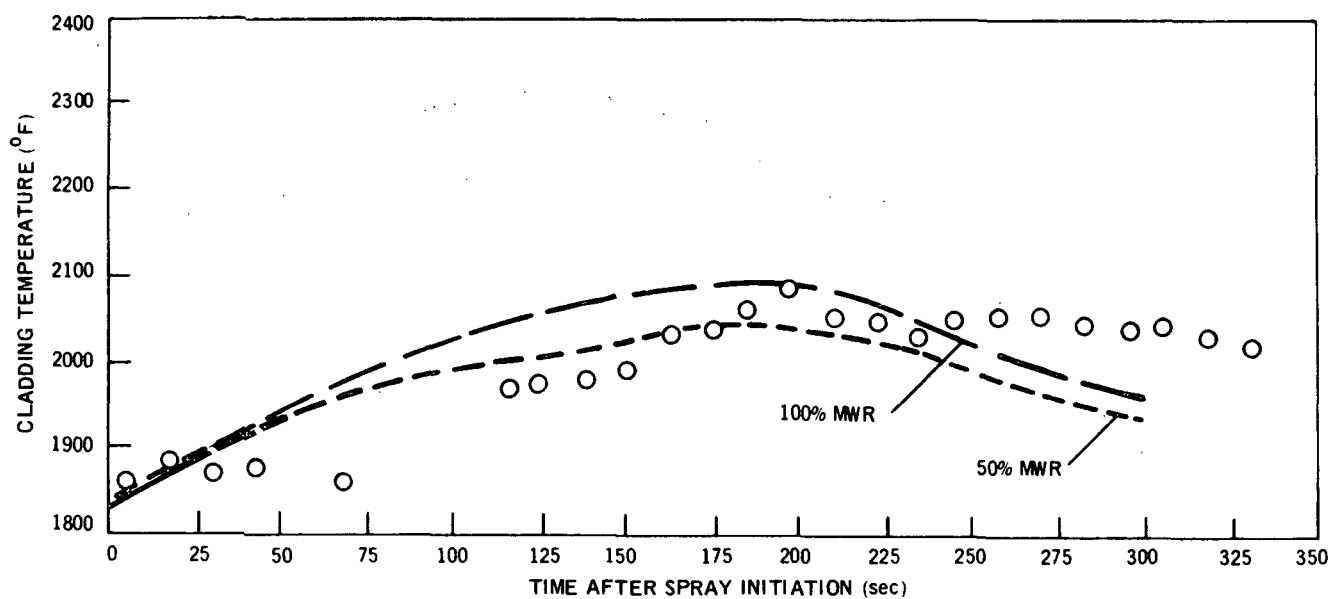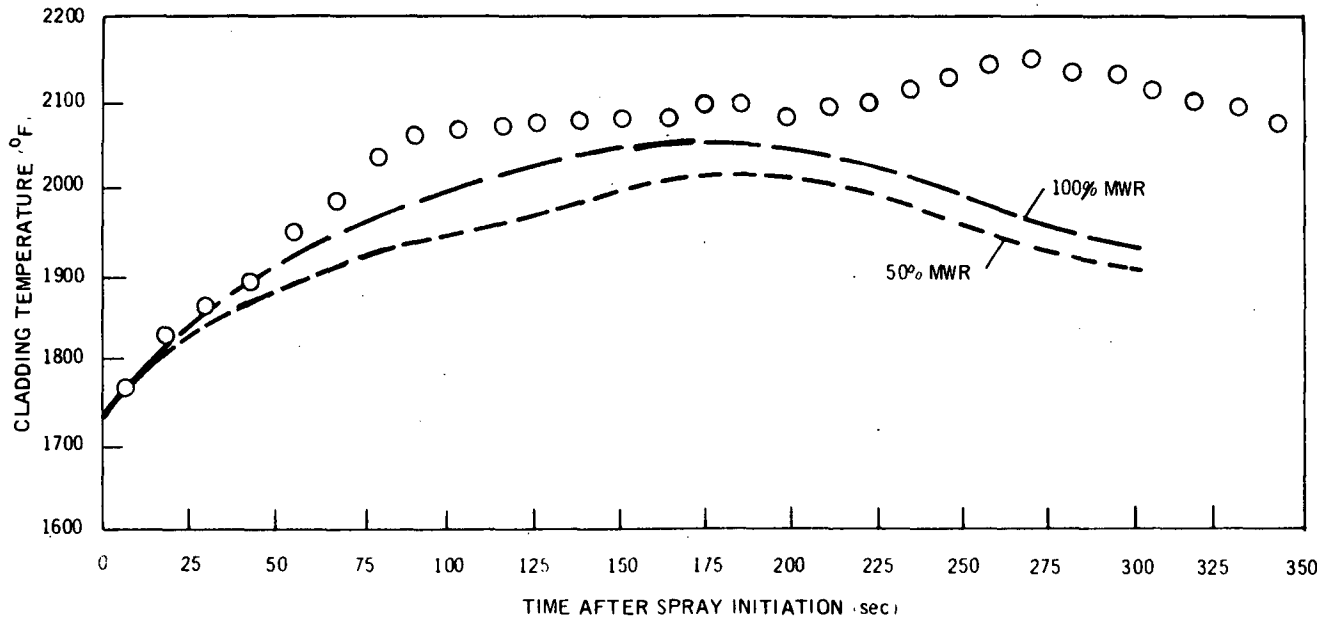Figure A-6   Bundle Zr2K Rod 10 Midplane Thermal Response Prediction

Figure A-7   Bundle Zr2K Rod 16 Midplane Thermal Response Prediction

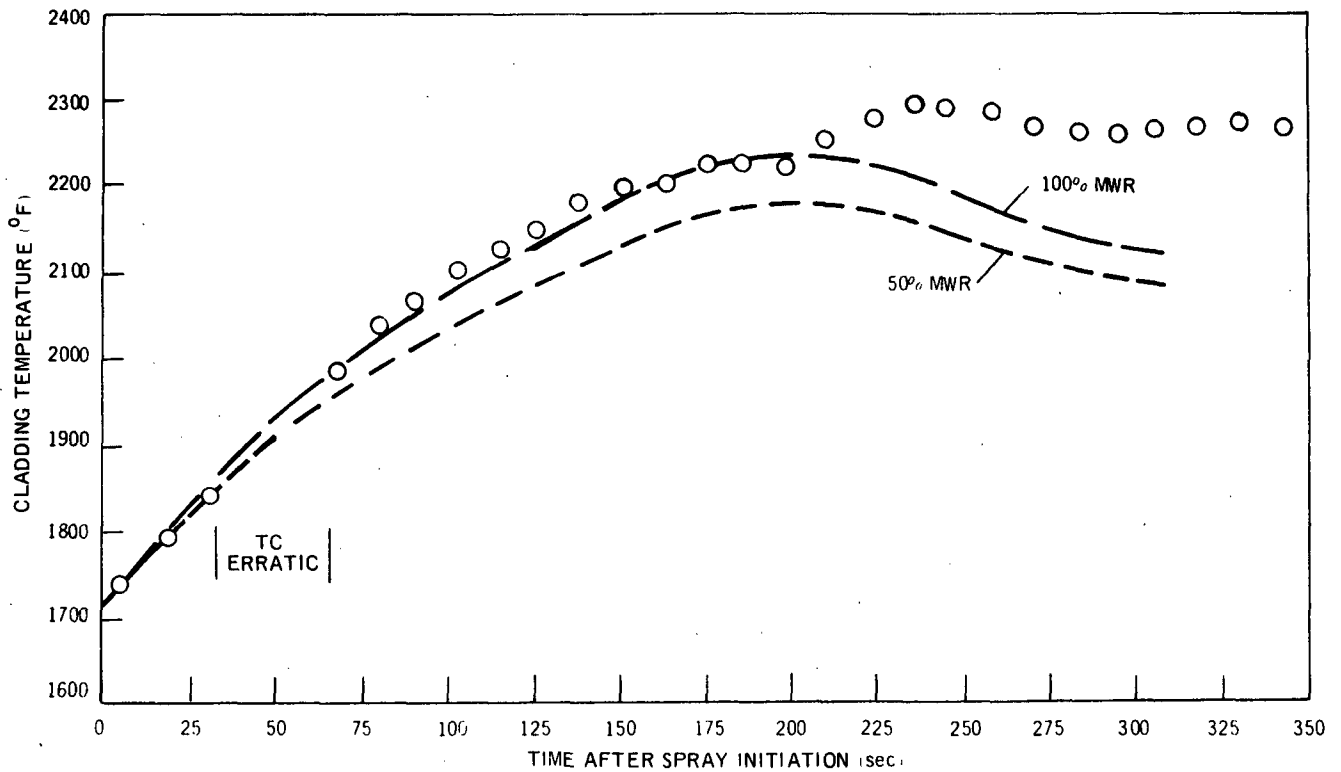Figure A-8   Bundle Zr2K Rod 23 Midplane Thermal Response Prediction

Figure A-9   Bundle Zr2K Rod 30 Midplane Thermal Response Prediction

Figure A-10   Bundle Zr2K Rod 17 Midplane Thermal Response Prediction

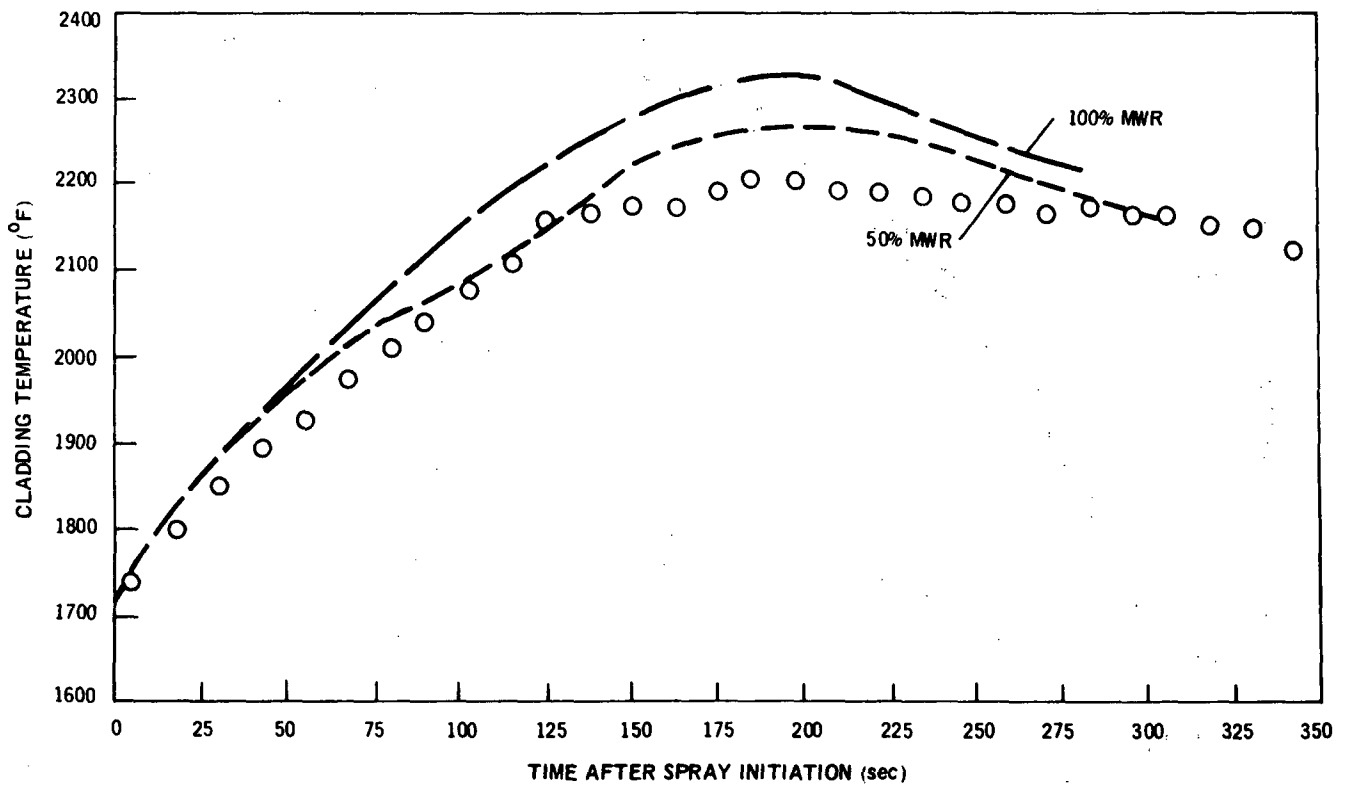Figure A-11   Bundle Zr2K Rod 24 Midplane Thermal Response Prediction

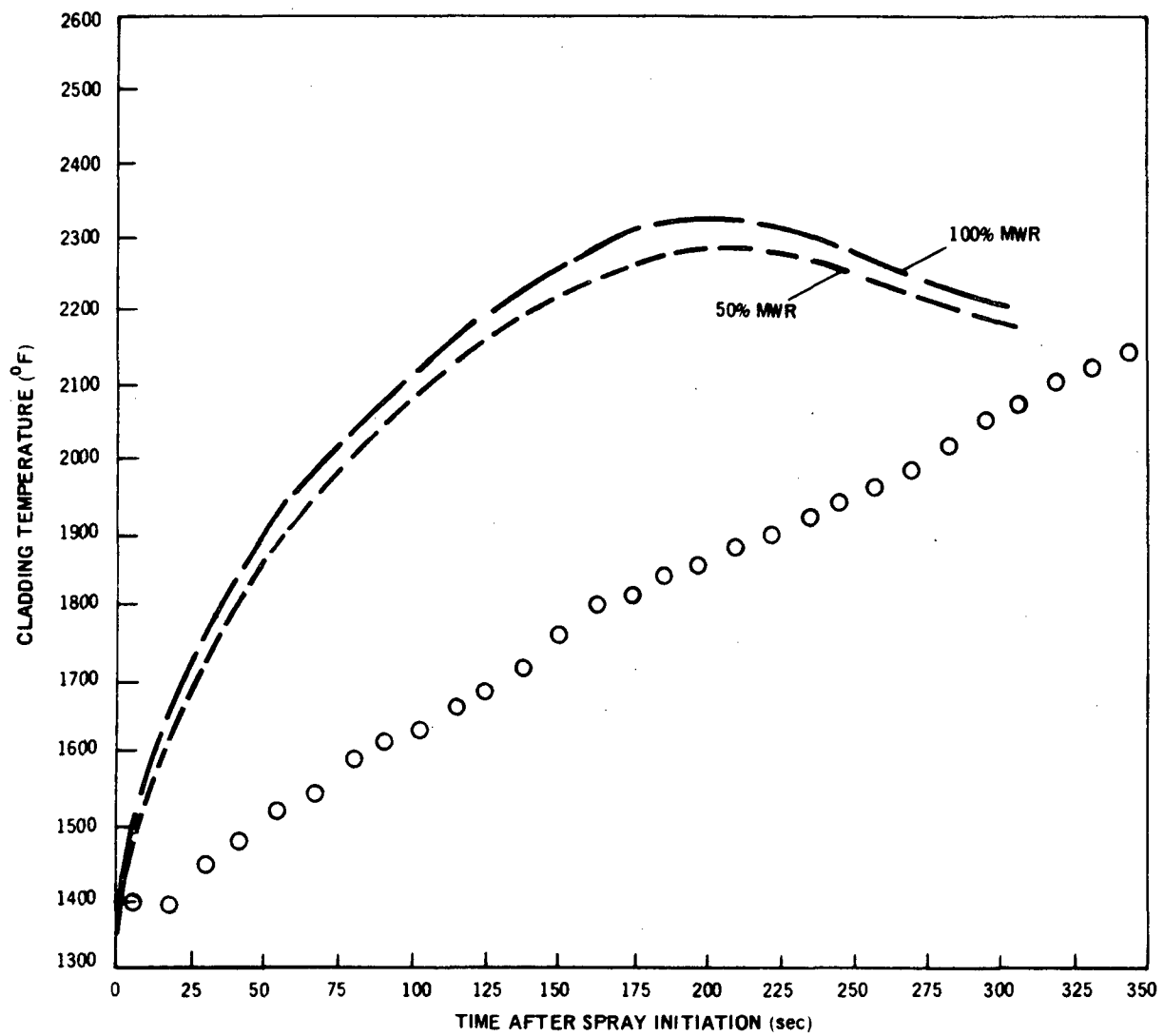Figure A-12   Bundle Zr2K Rod 31 Midplane Thermal Response Prediction

Figure A-13   *Bundle Zr2K Rod 18 Midplane Thermal Response Prediction*

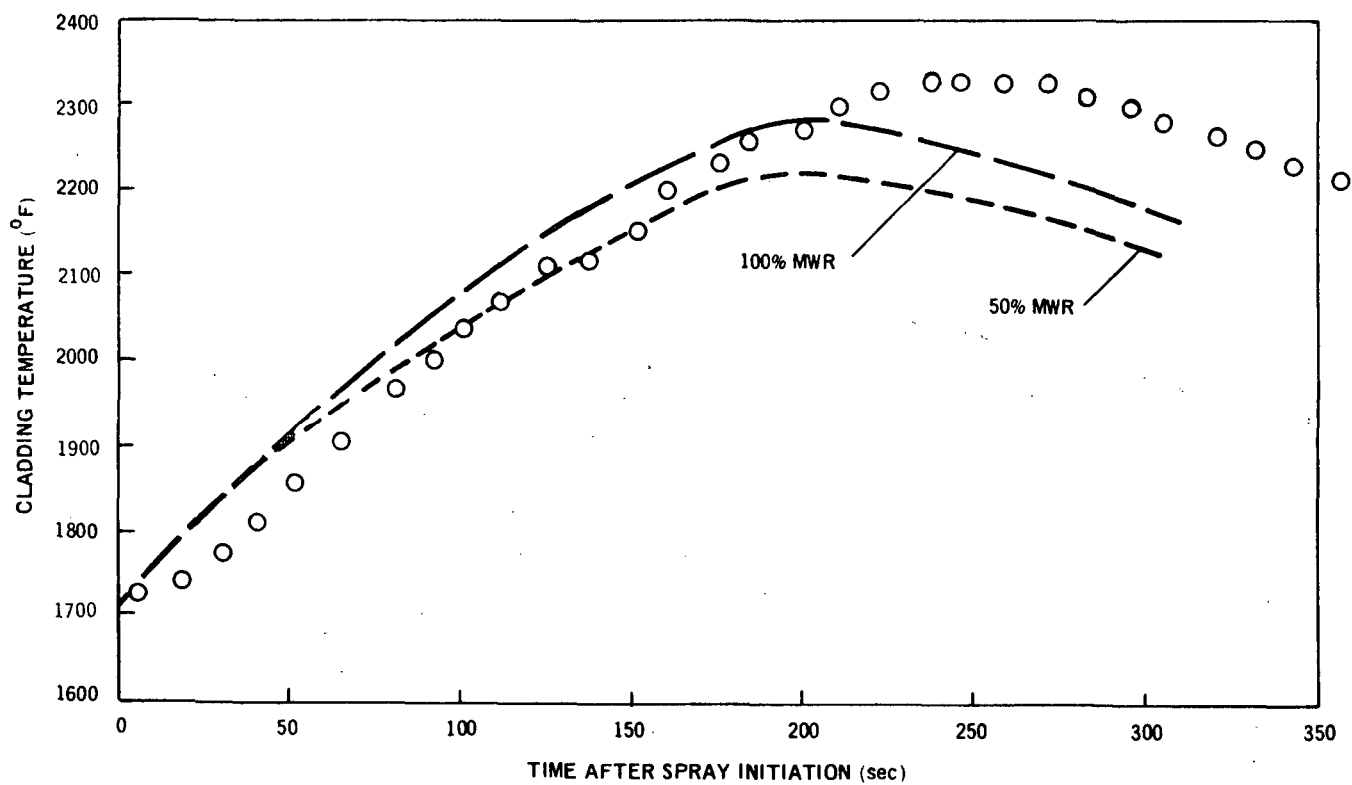Figure A-14   *Bundle Zr2K Rod 26 Midplane Thermal Response Prediction*

Figure A-15   Bundle Zr2K Rod 32 Midplane Thermal Response Prediction
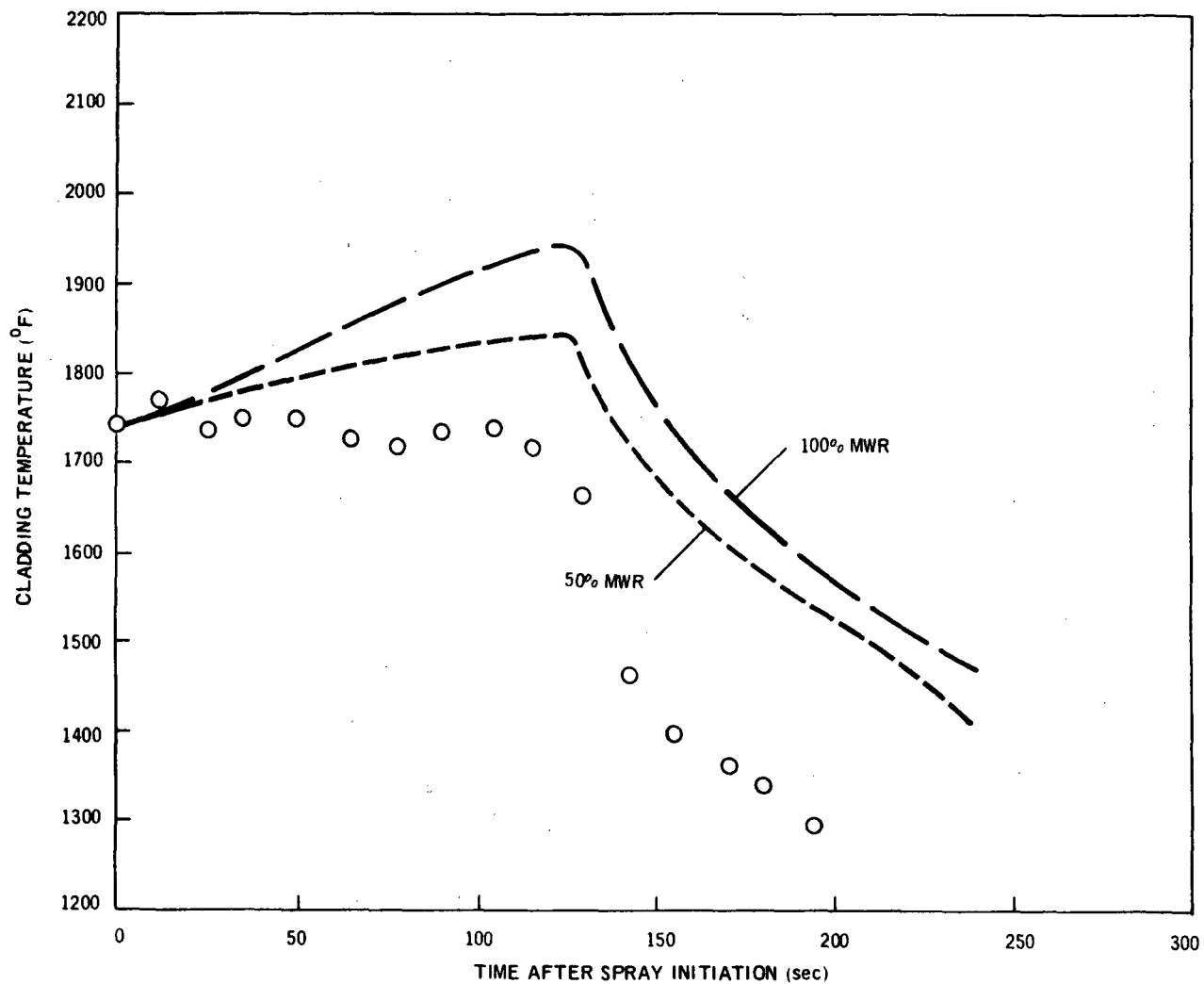

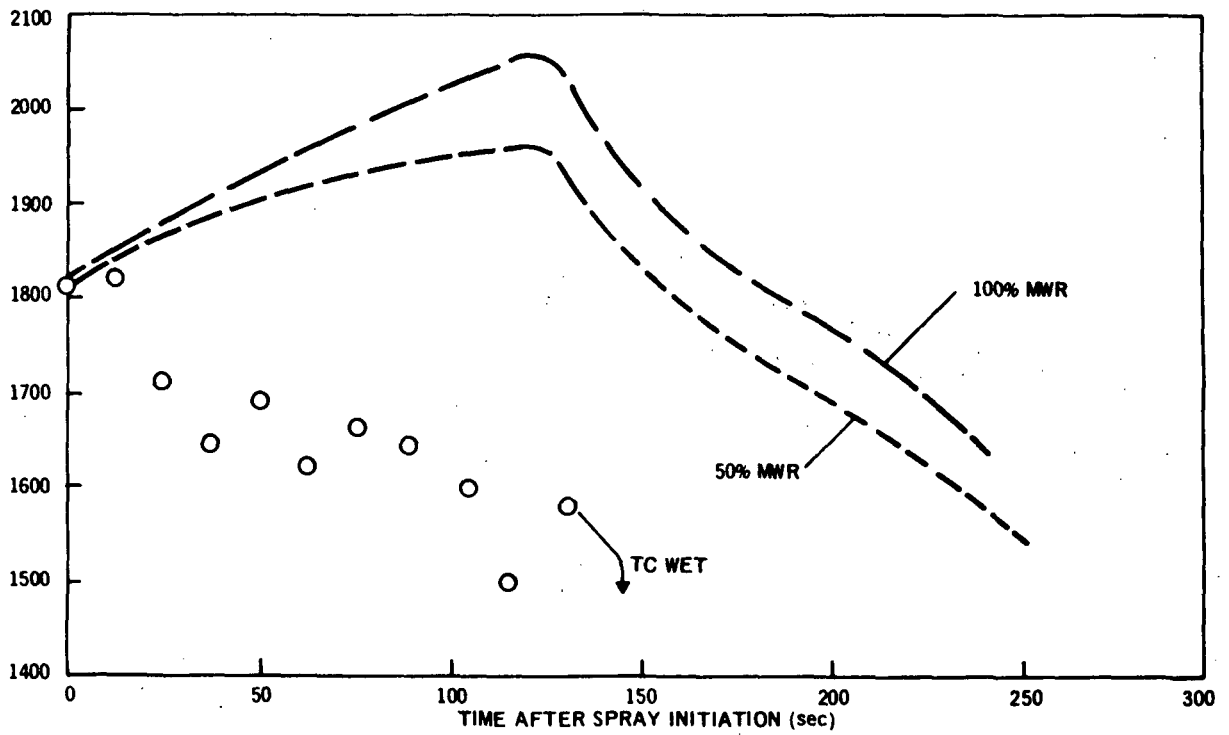*Figure A-16   Bundle Zr3M Rod 1 Midplane Thermal Response Prediction*

Figure A-17   Bundle Zr3M Rod 2 Midplane Thermal Response Prediction

Figure A-18   Bundle Zr3M Rod 4 Midplane Thermal Response Prediction

Figure A-19 *Bundle Zr3M Rod 22 Midplane Thermal Response Prediction*

Figure A-20 *Bundle Zr3M Rod 11 Midplane Thermal Response Prediction*

Figure A-21   Bundle Zr3M Rod 23 Midplane Thermal Response Prediction

Figure A-22   Bundle Zr3M Rod 24 Midplane Thermal Response Prediction

Figure A-23   Bundle Zr3M Rod 17 Midplane Thermal Response Prediction

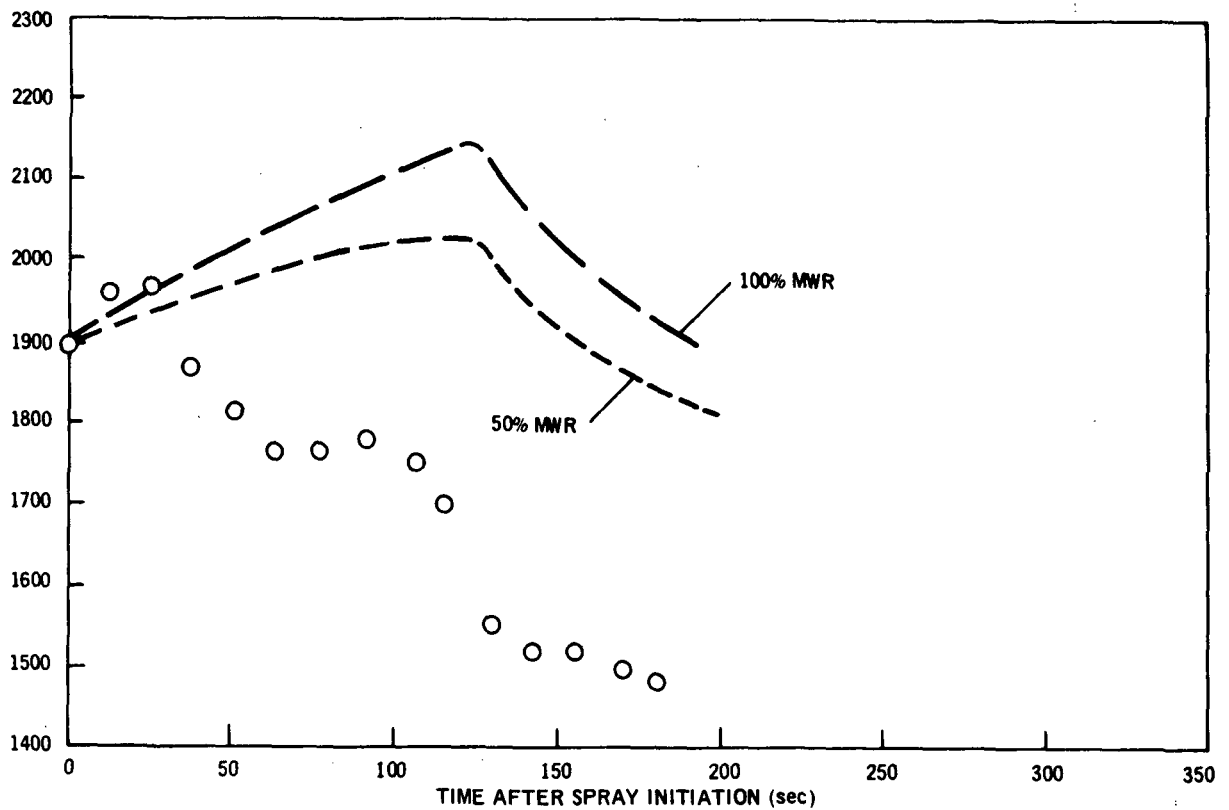*Figure A-24   Bundle Zr3M Rod 25 Midplane Thermal Response Prediction*

Figure A-25   Bundle Zr3M Rod 26 Midplane Thermal Response Prediction

Figure A-26   Bundle Zr4M Rod 1 Midplane Thermal Response Prediction

Figure A-27   Bundle Zr4M Rod 2 Midplane Thermal Response Prediction

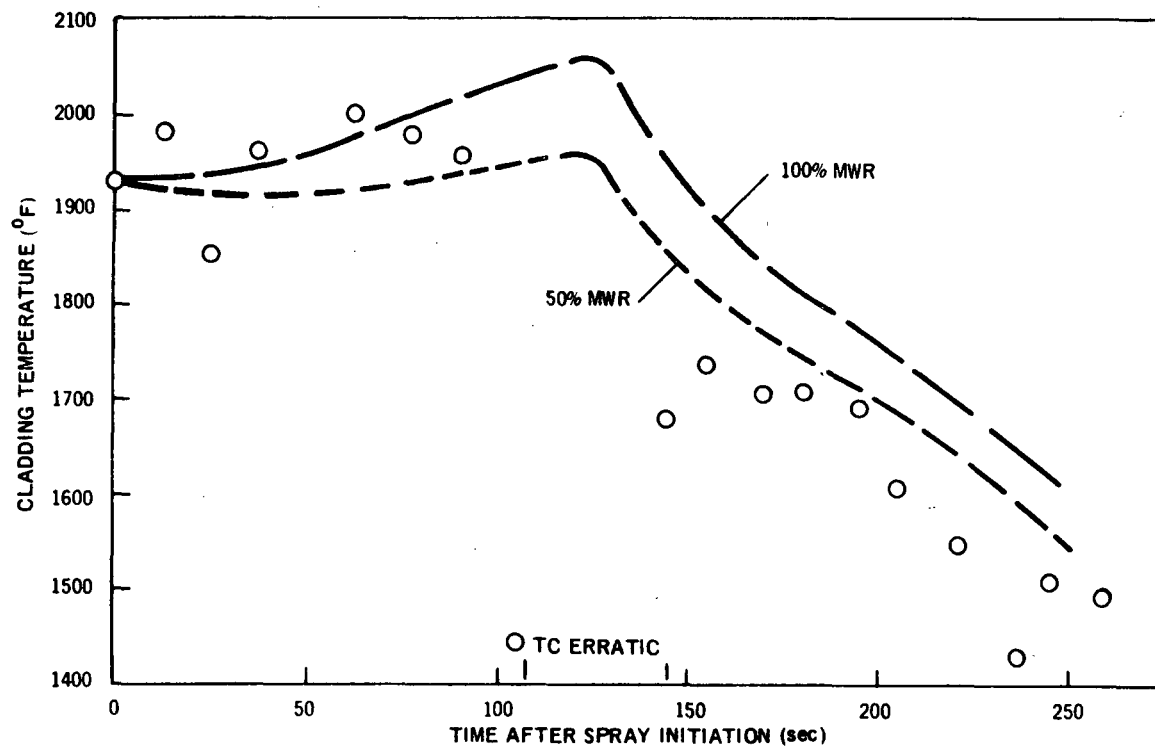Figure A-28   Bundle Zr4M Rod 4 Midplane Thermal Response Prediction

Figure A-29   Bundle Zr4M Rod 8 Midplane Thermal Response Prediction
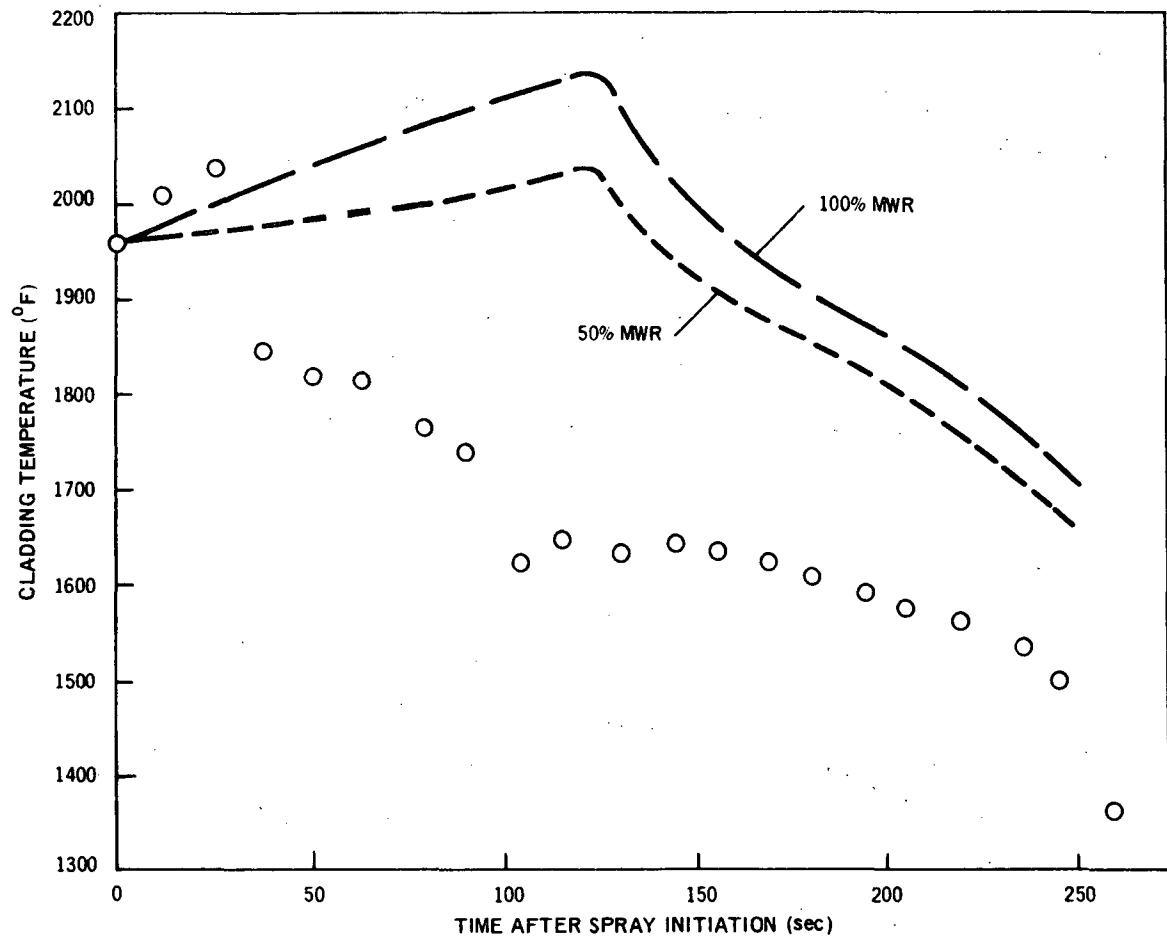
Figure A-30   Bundle Zr4M Rod 15 Midplane Thermal Response Prediction
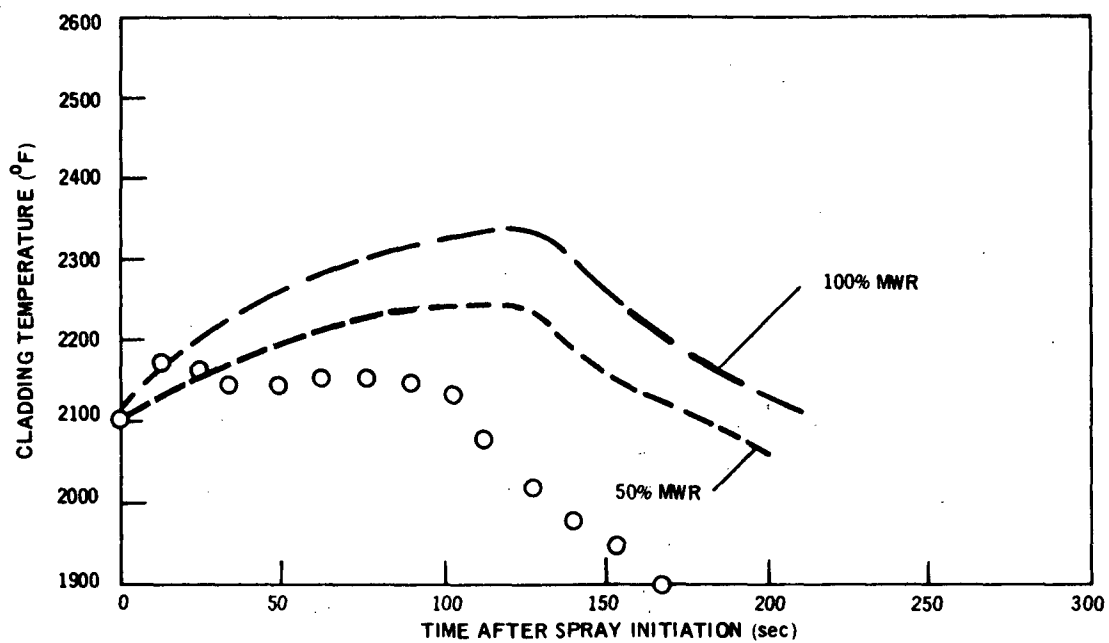
Figure A-31   Bundle Zr4M Rod 9 Midplane Thermal Response Prediction
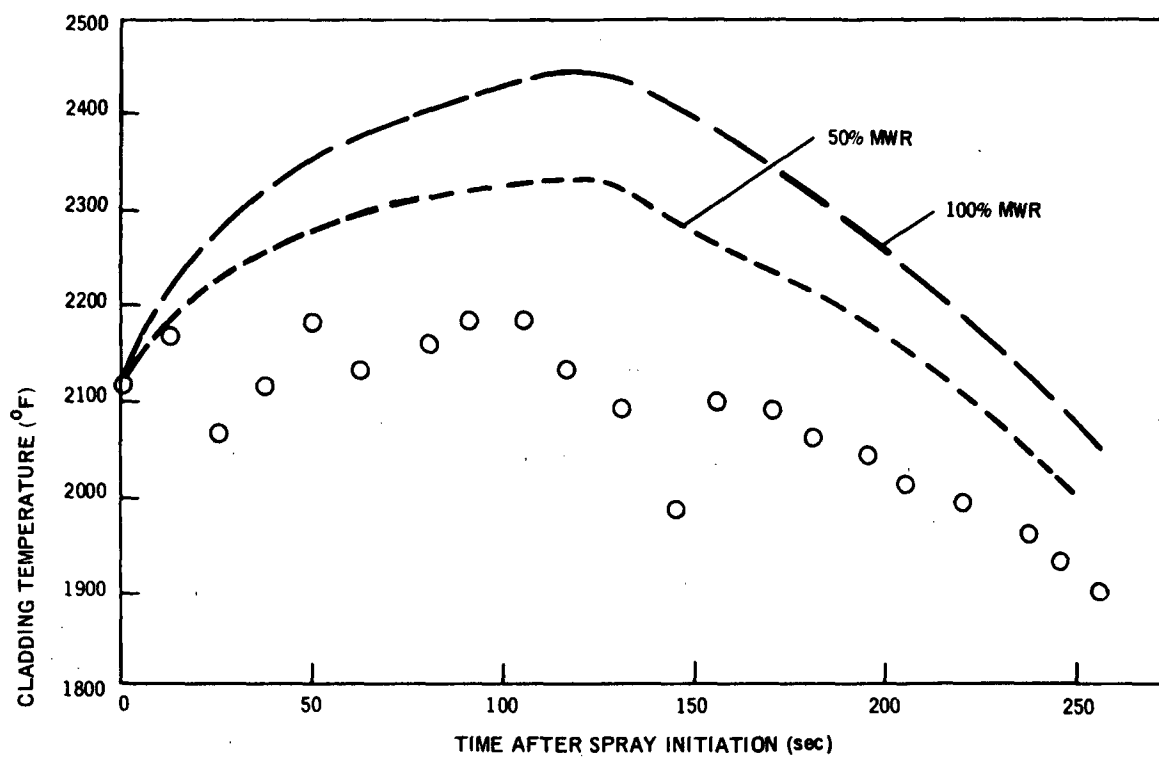

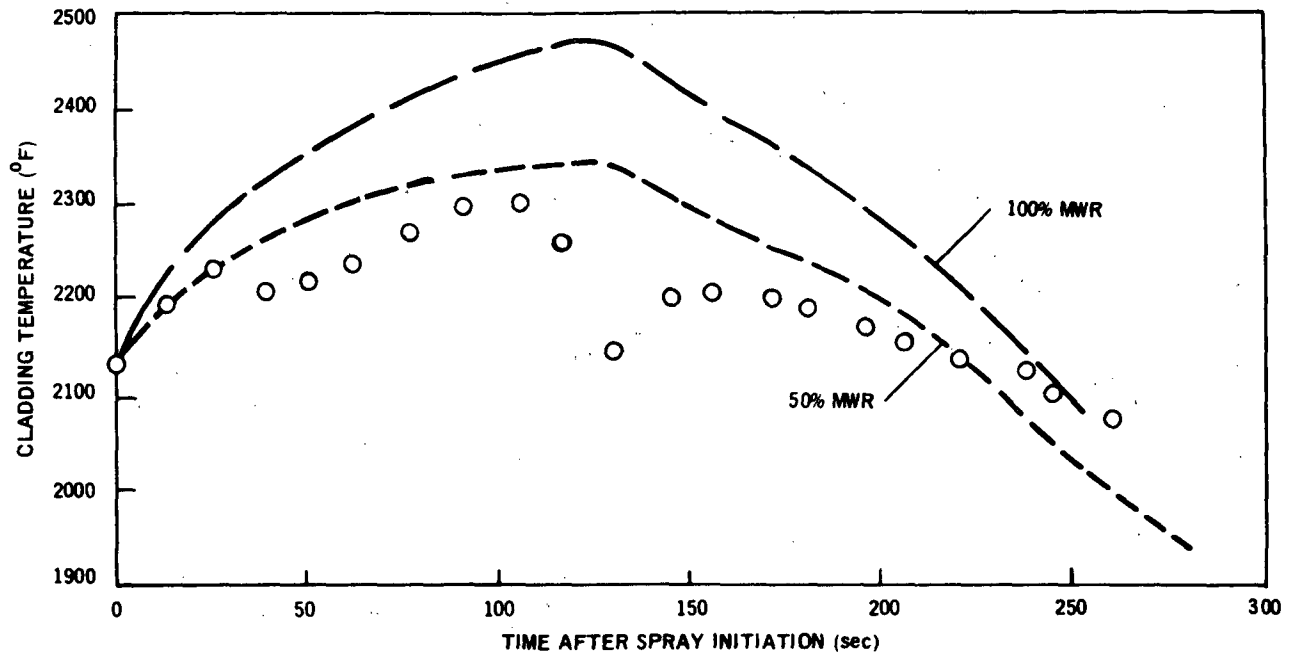Figure A-32   Bundle Zr4M Rod 10 Midplane Thermal Response Prediction

Figure A-33   Bundle Zr4M Rod 11 Midplane Thermal Response Prediction

Figure A-34   Bundle Zr4M Rod 12 Midplane Thermal Response Prediction

Figure A-35   Bundle Zr4M Rod 13 Midplane Thermal Response Prediction

Figure A-36   Bundle Zr4M Rod 16 Midplane Thermal Response Prediction

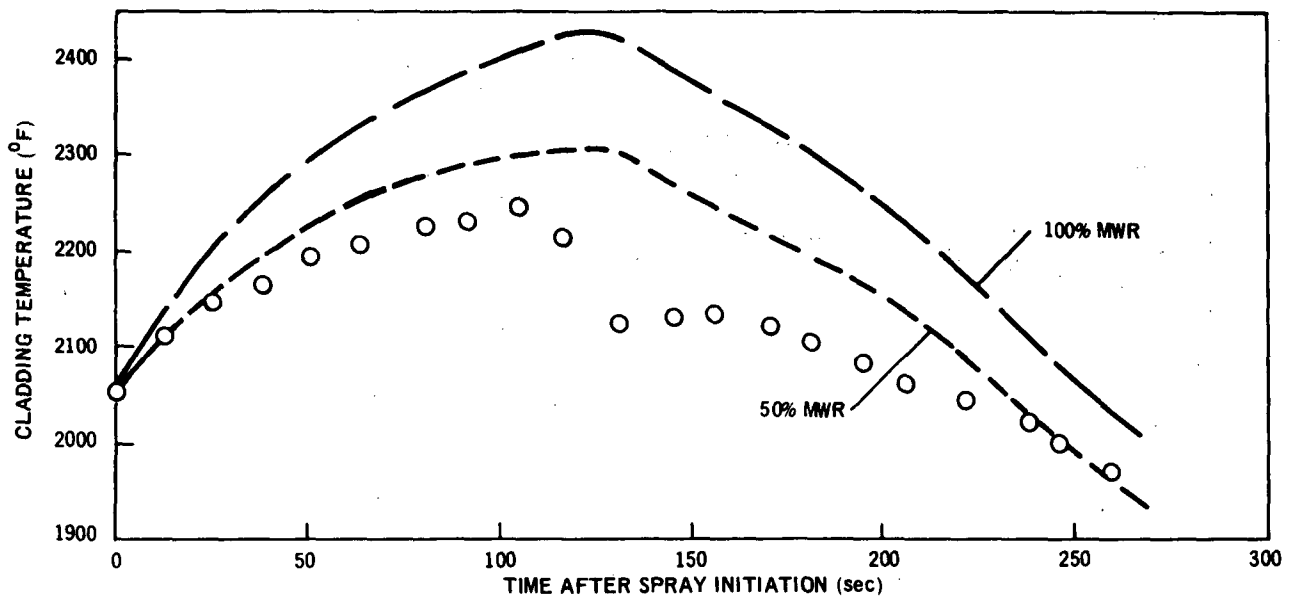*Figure A-37   Bundle Zr4M Rod 23 Midplane Thermal Response Prediction*

Figure A-38   Bundle Zr4M Rod 27 Midplane Thermal Response Prediction

Figure A-39   Bundle Zr4M Rod 39 Midplane Thermal Response Prediction
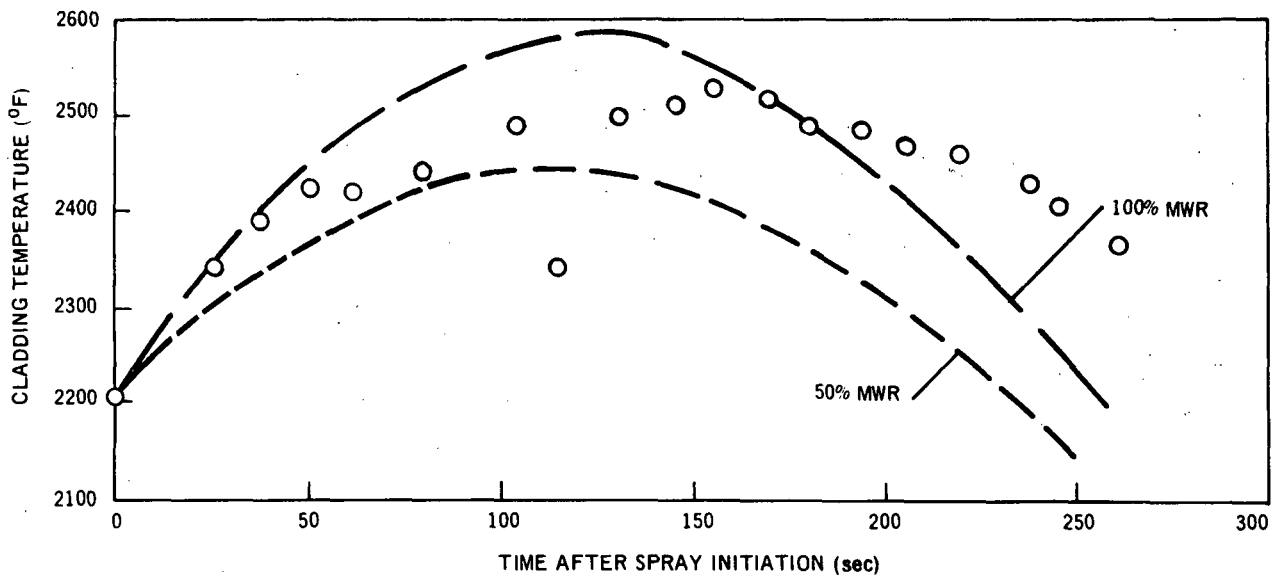
Figure A-40   Bundle Zr4M Rod 18 Midplane Thermal Response Prediction
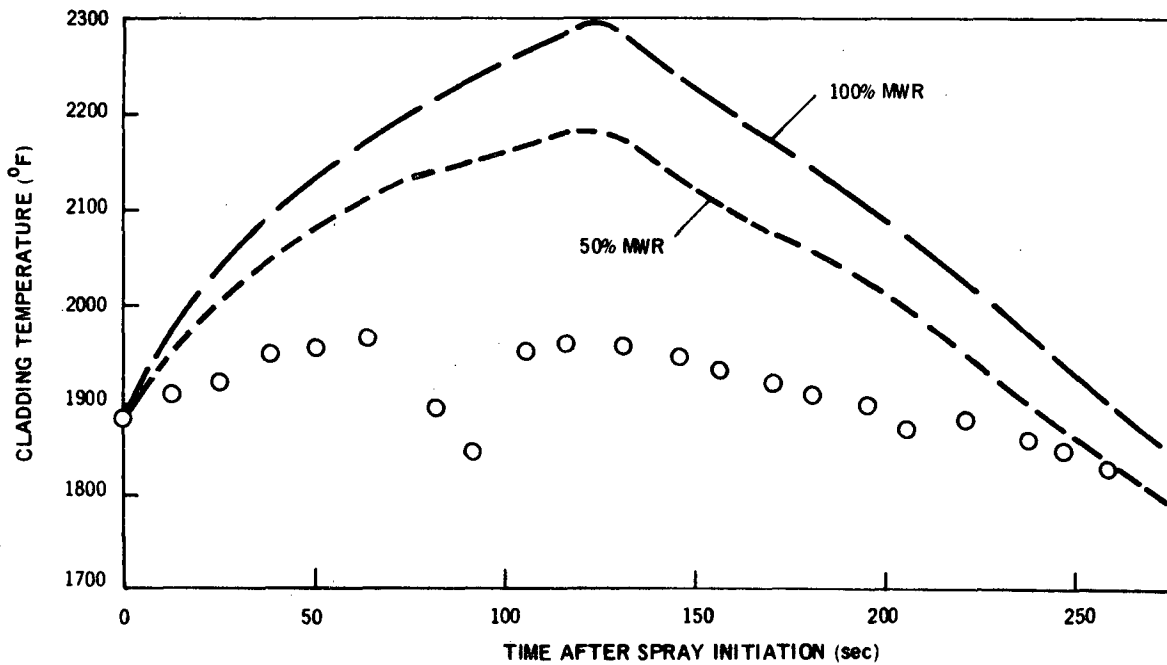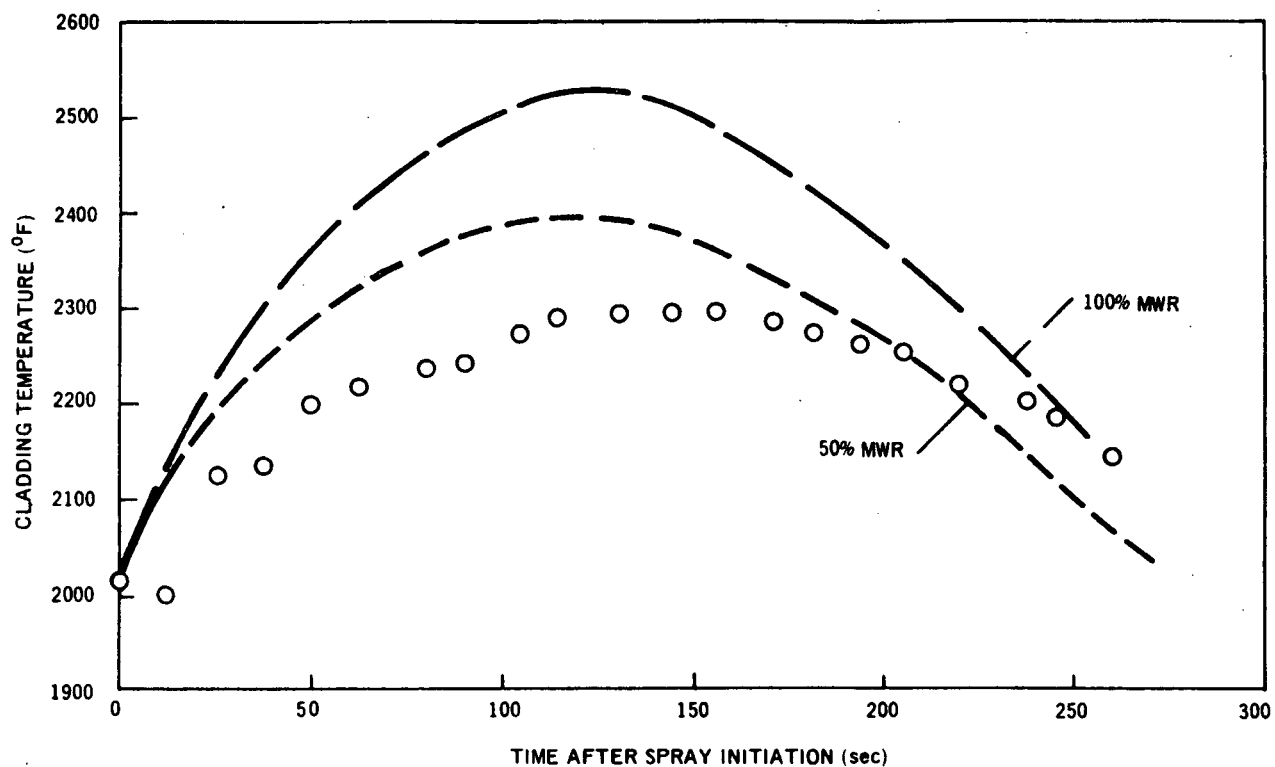
Figure A-41   Bundle Zr4M Rod 19 Midplane Thermal Response Prediction
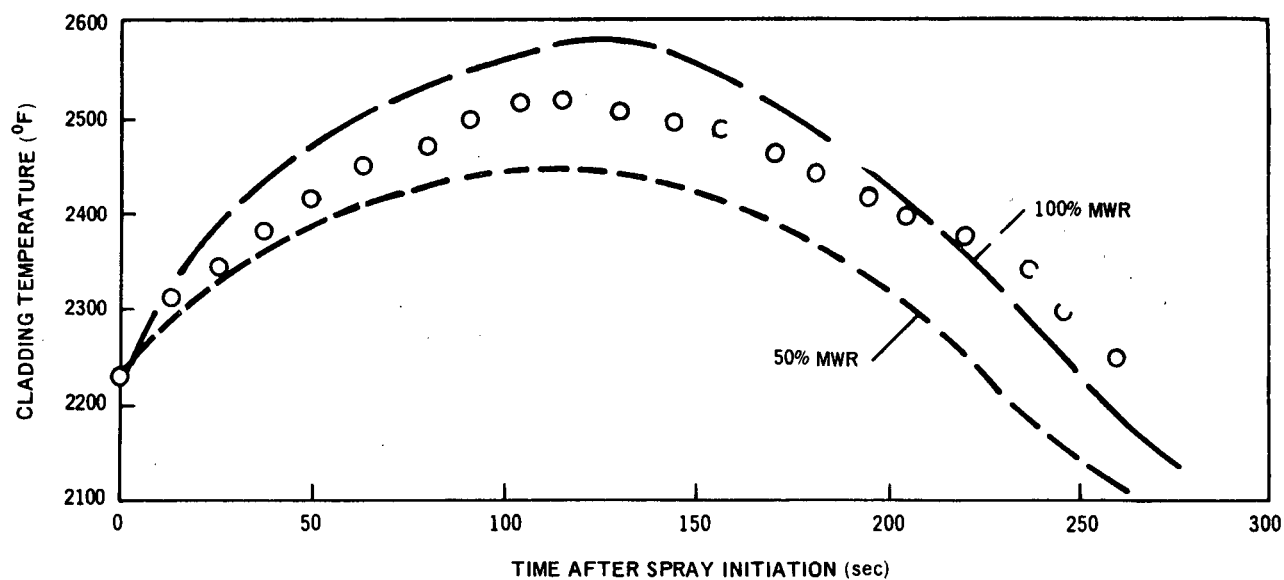
Figure A-42   Bundle Zr4M Rod 24 Midplane Thermal Response Prediction
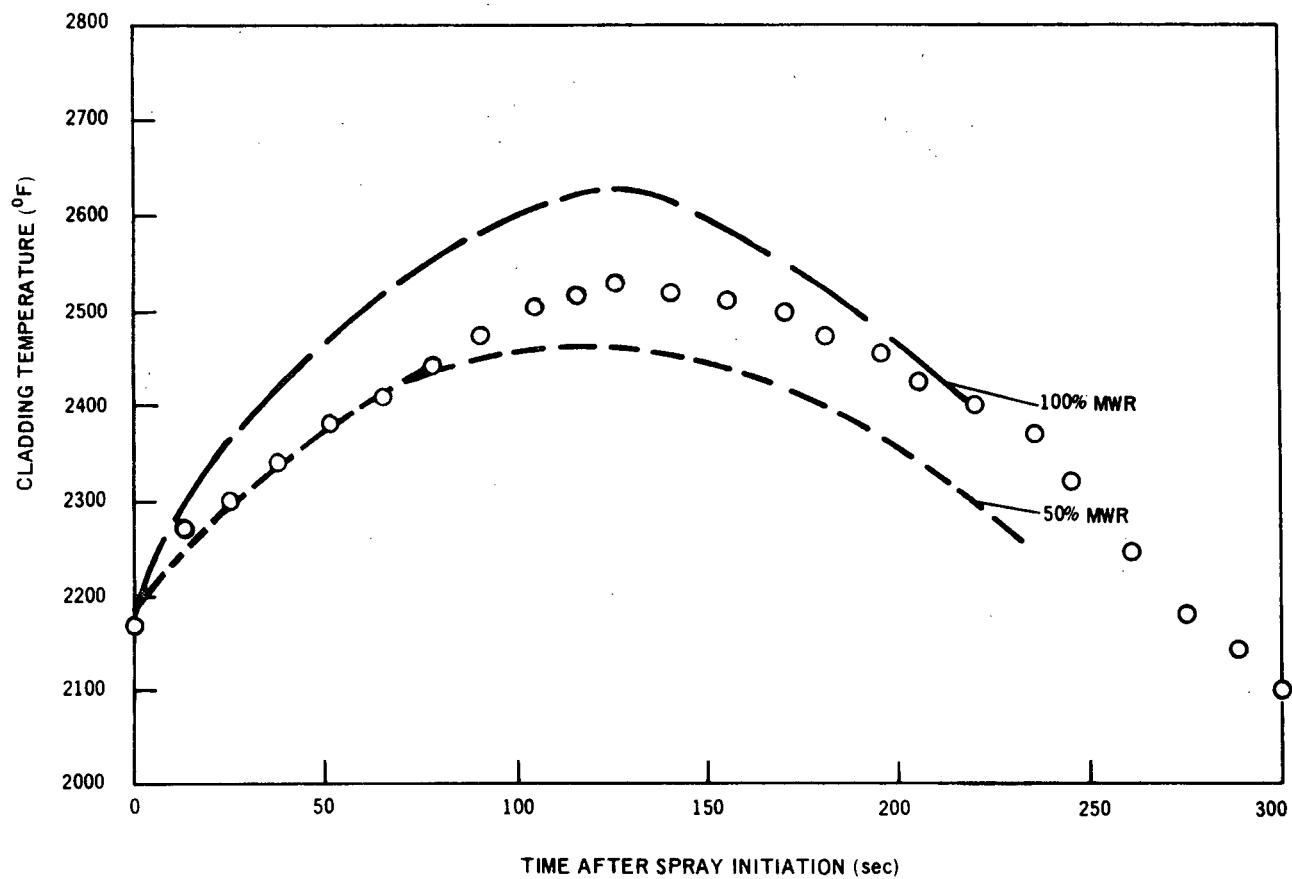
Figure A-43   Bundle Zr4M Rod 25 Midplane Thermal Response Prediction
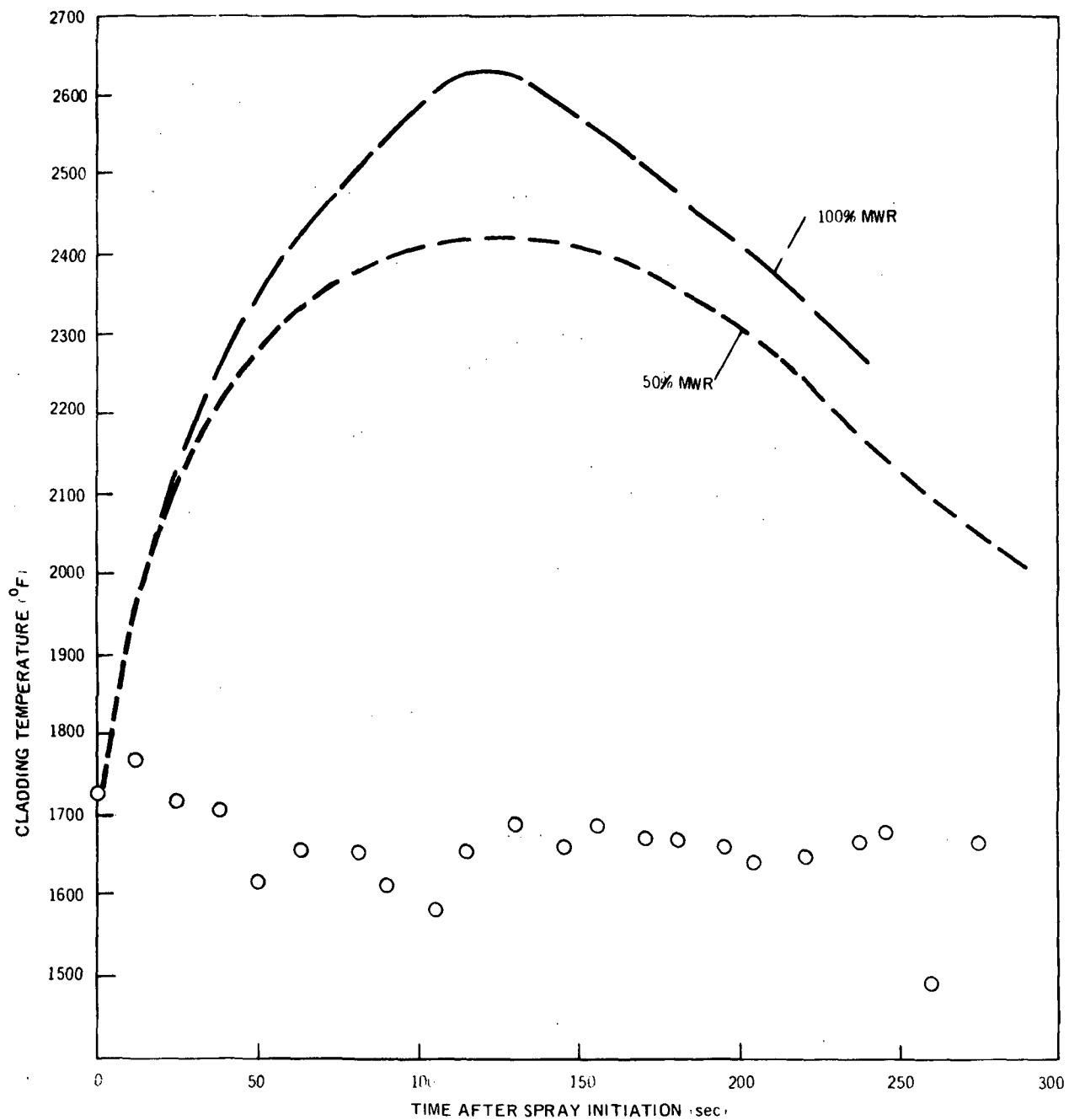
Figure A-44   Bundle Zr4M Rod 26 Midplane Thermal Response Prediction
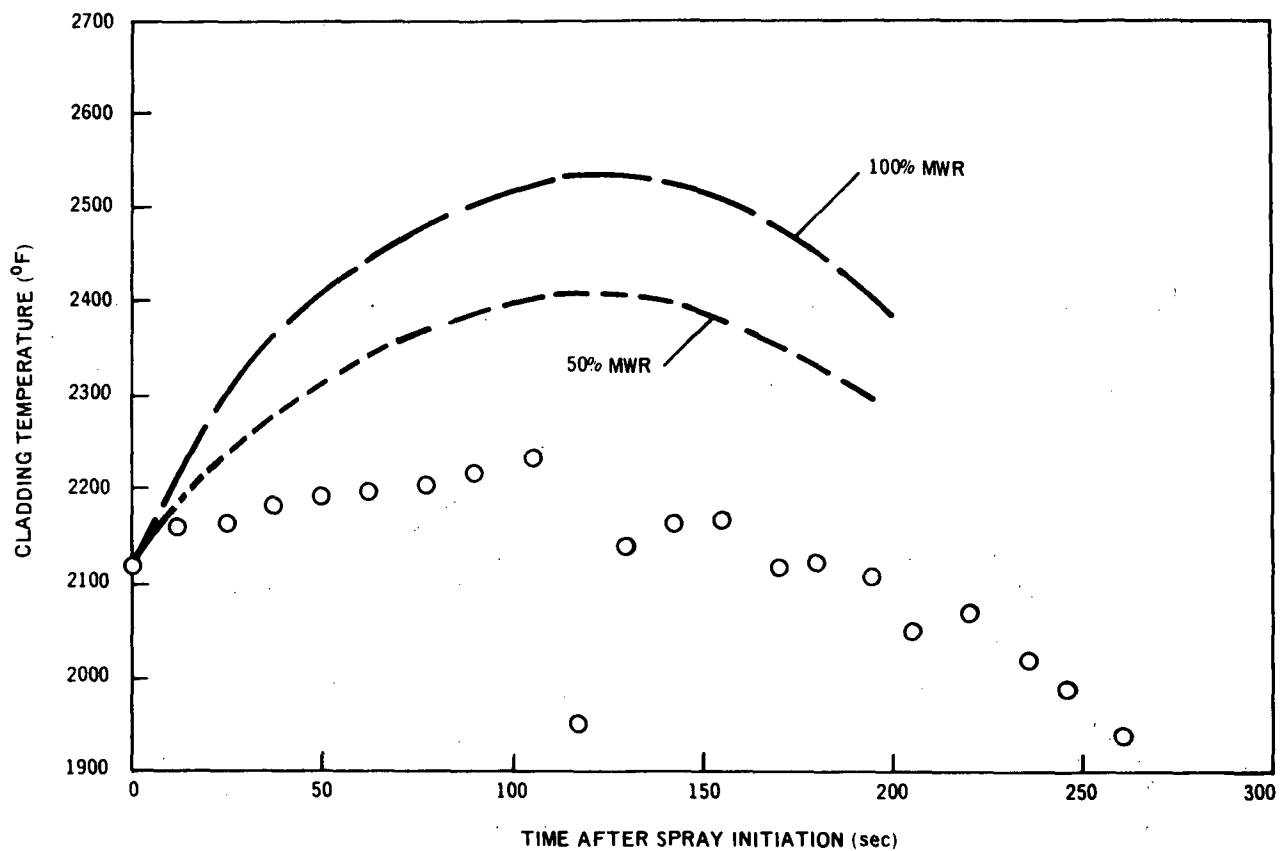
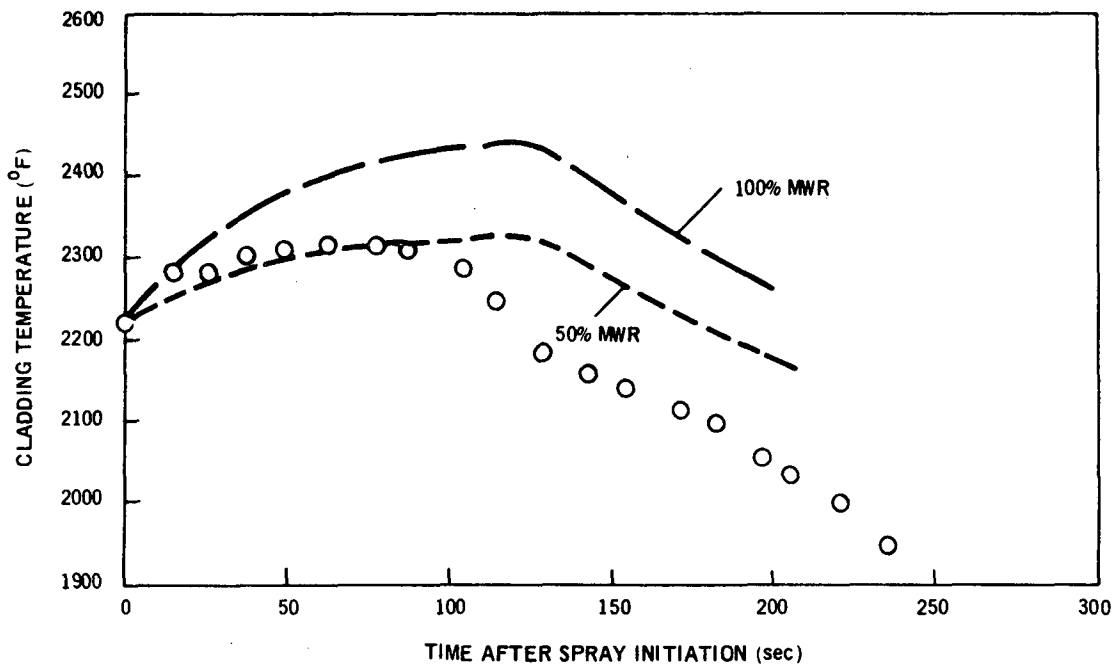Figure A-45   Bundle Zr4M Rod 31 Midplane Thermal Response Prediction
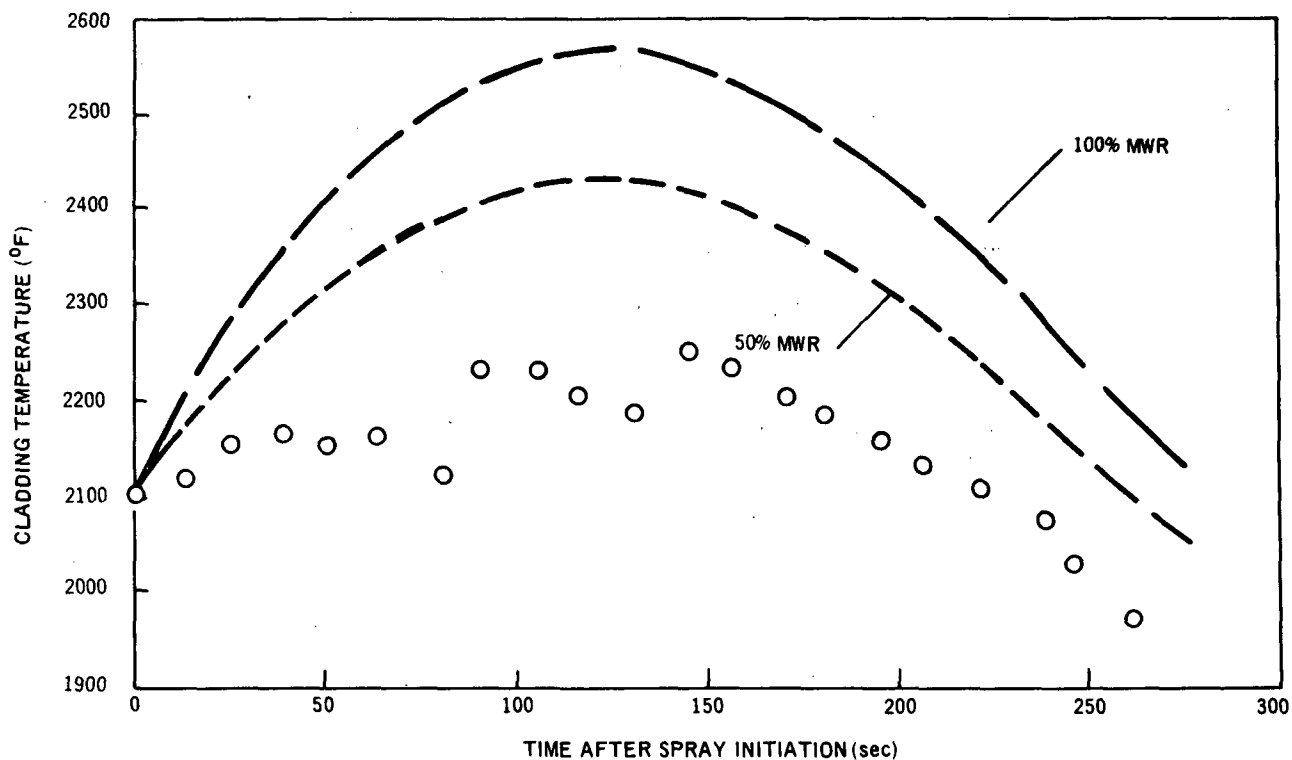
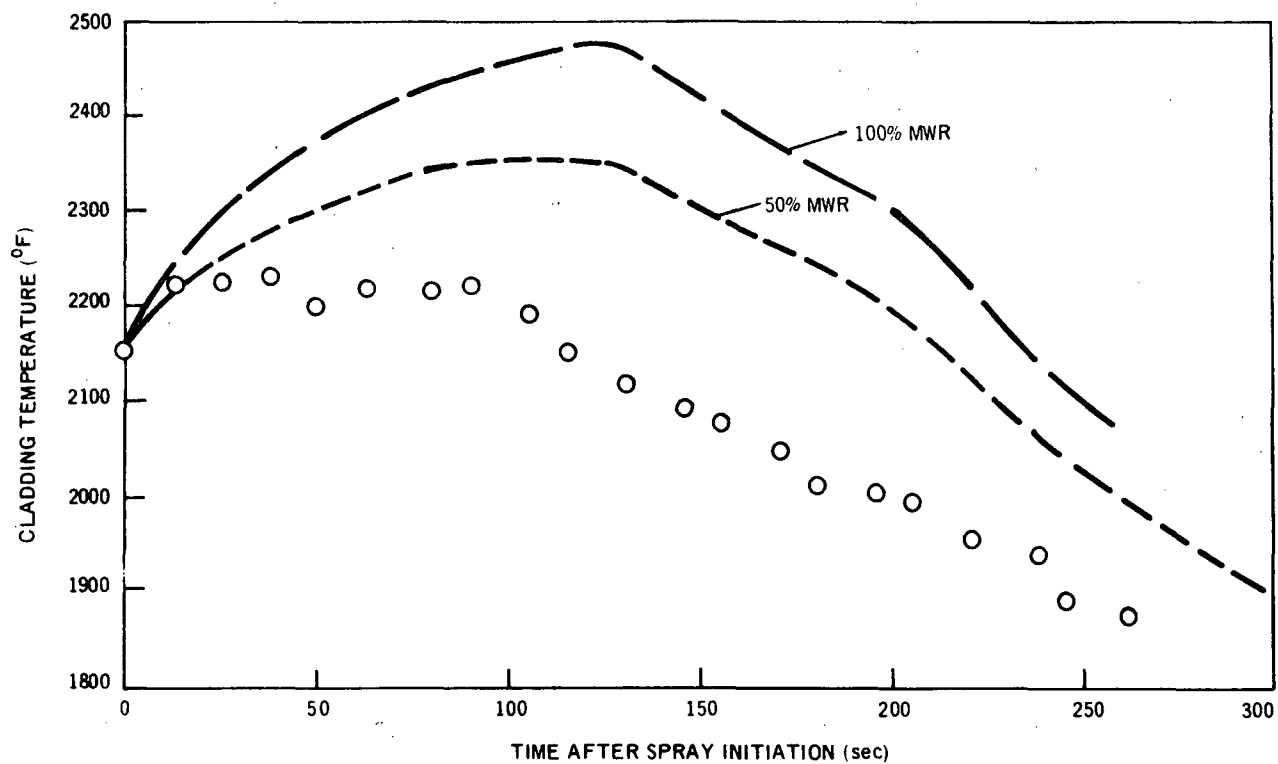Figure A-46   Bundle Zr4M Rod 32 Midplane Thermal Response Prediction

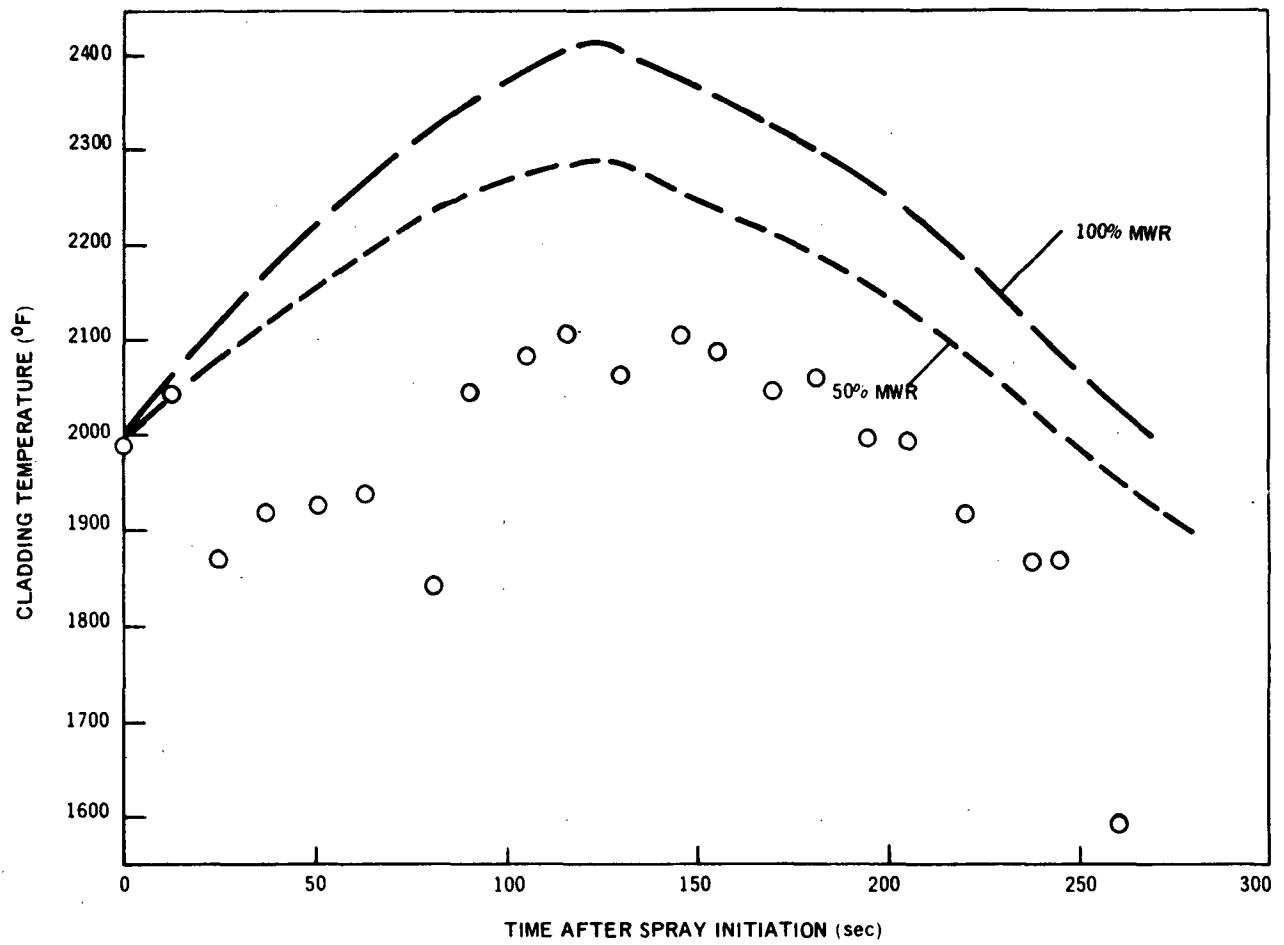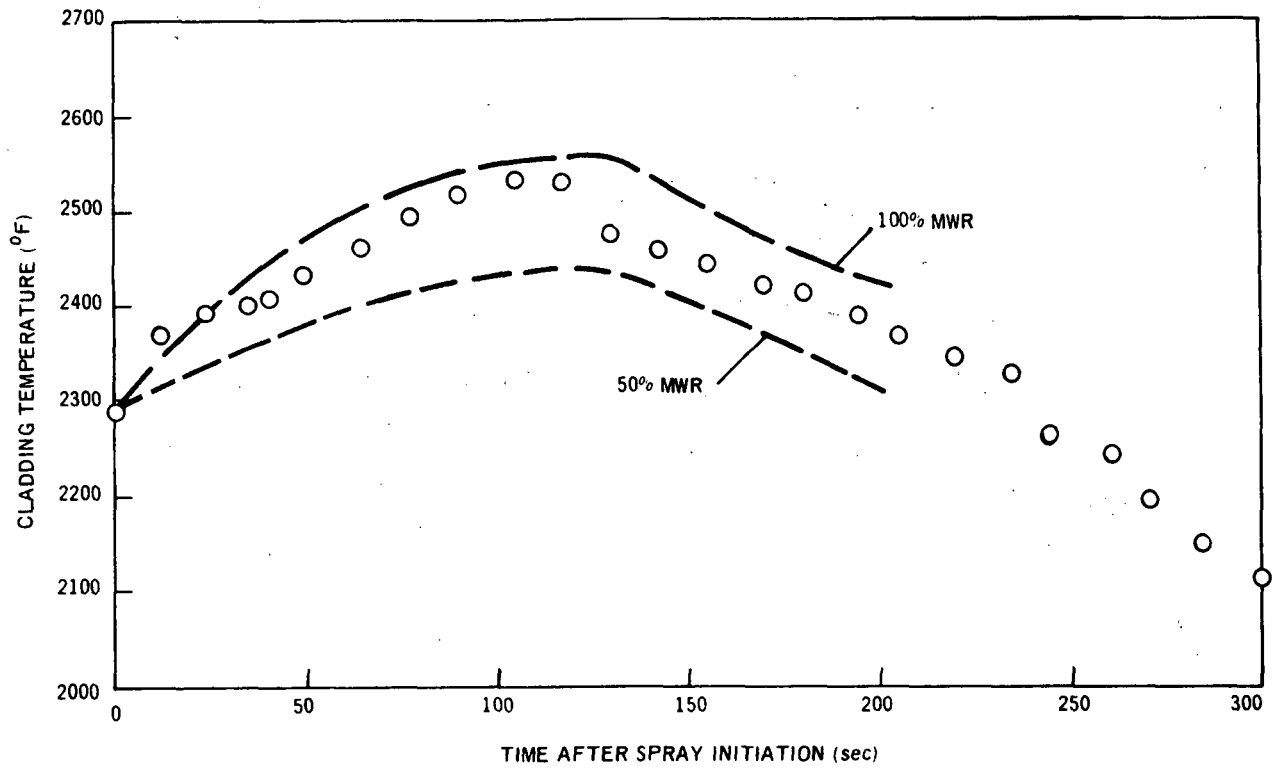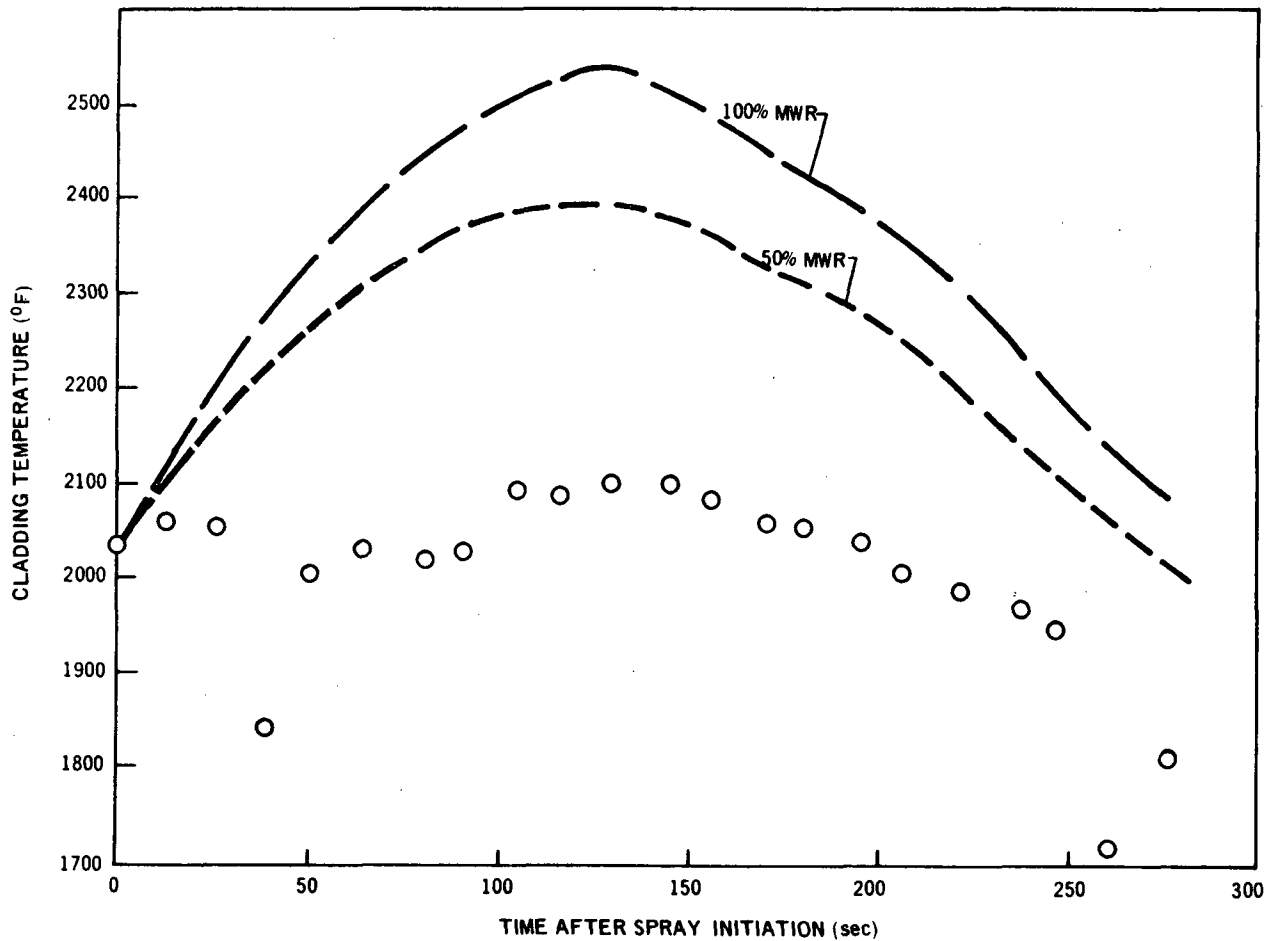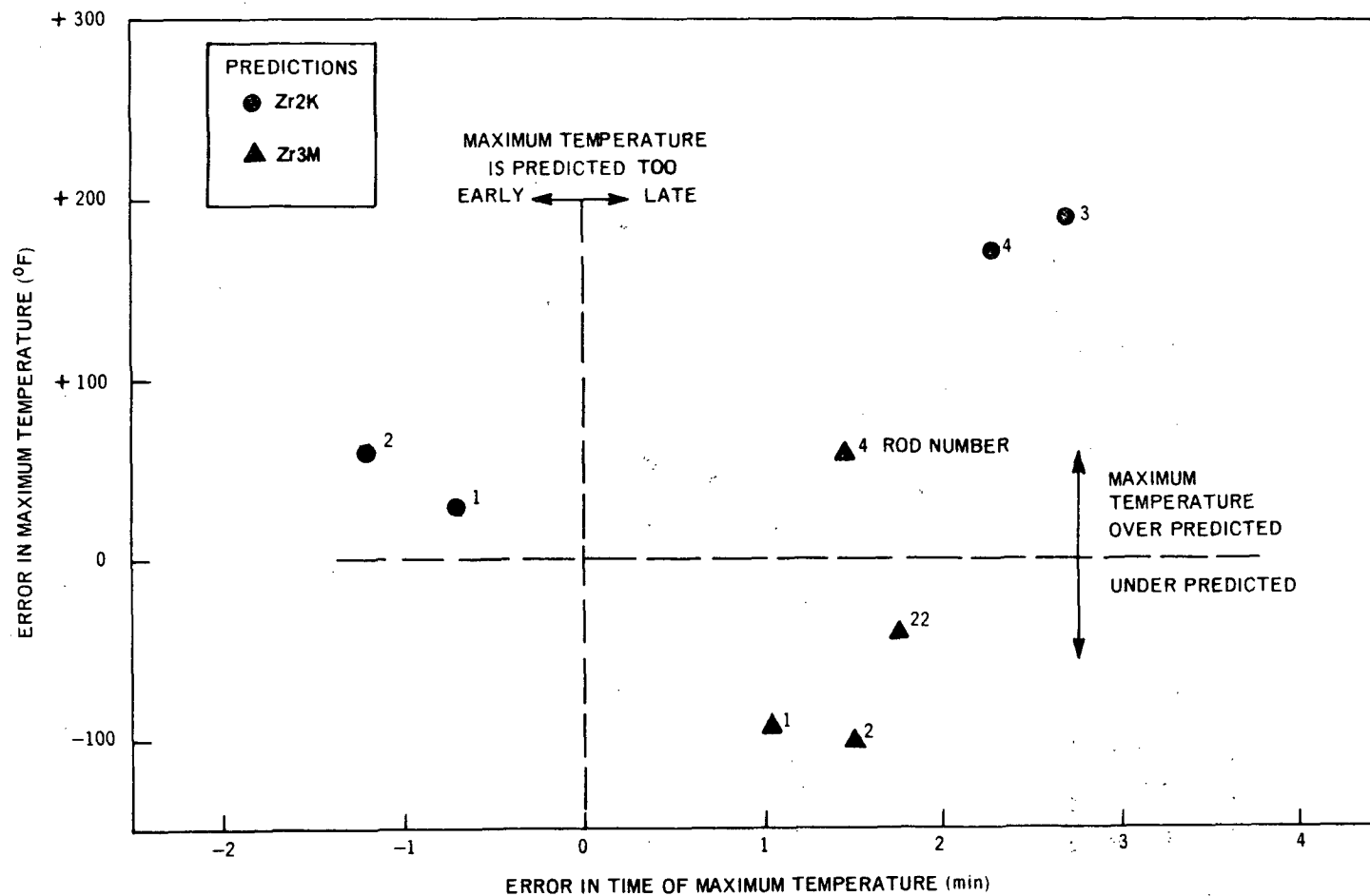Figure A-47   Bundle Zr4M Rod 33 Midplane Thermal Response Prediction

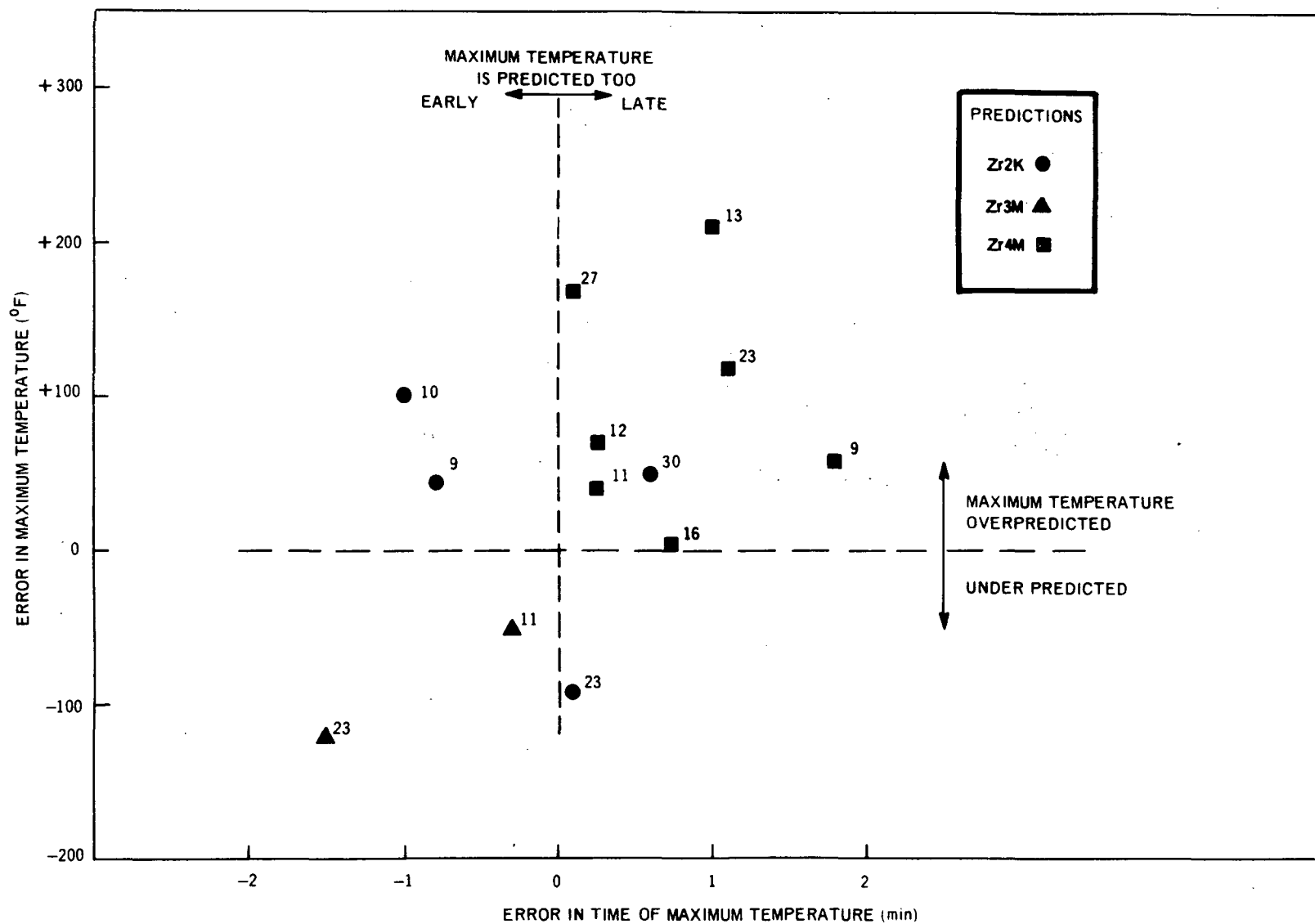Figure A-48   Outside Rod Prediction Map

Figure A-49   Inside Rod Prediction Map

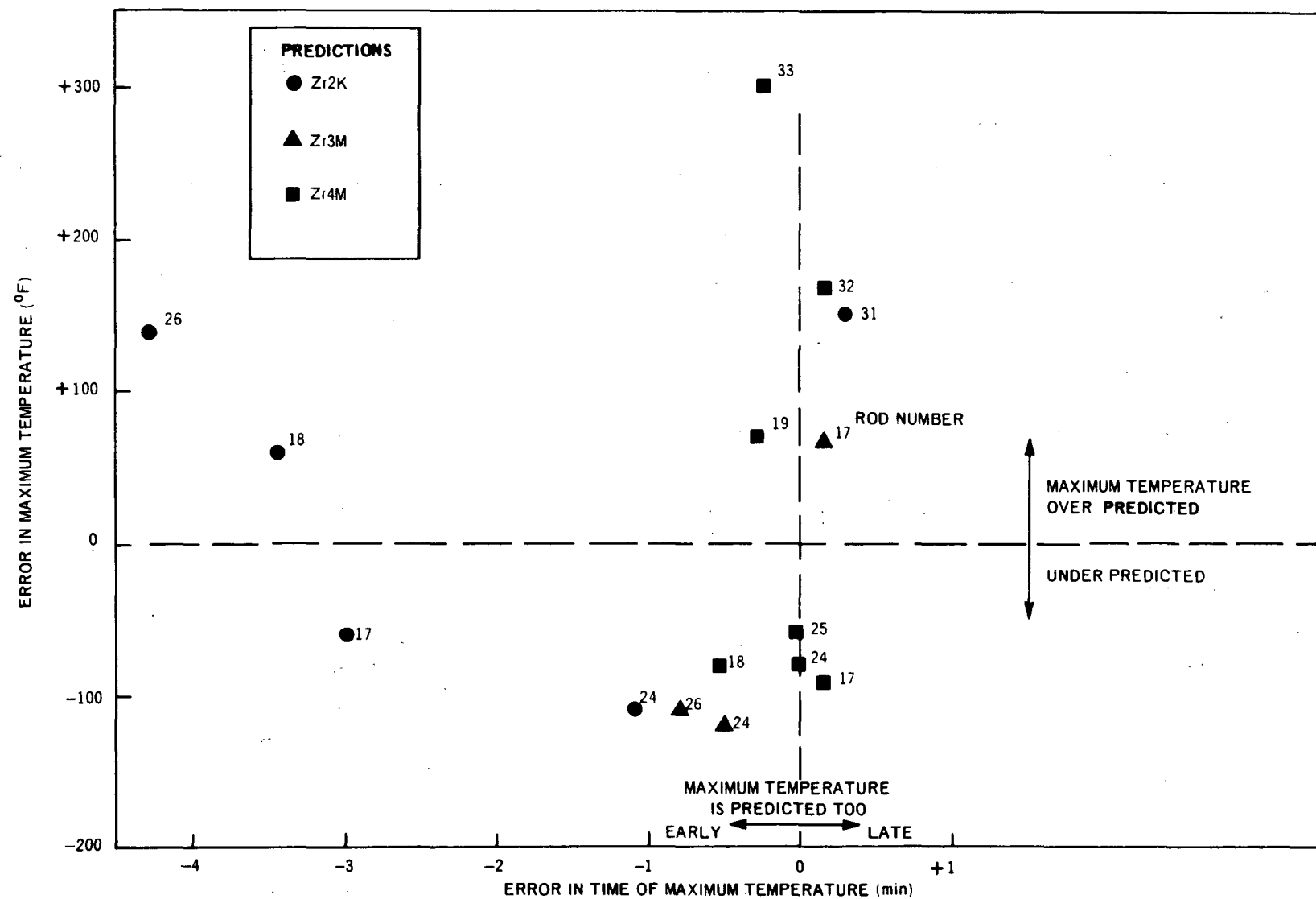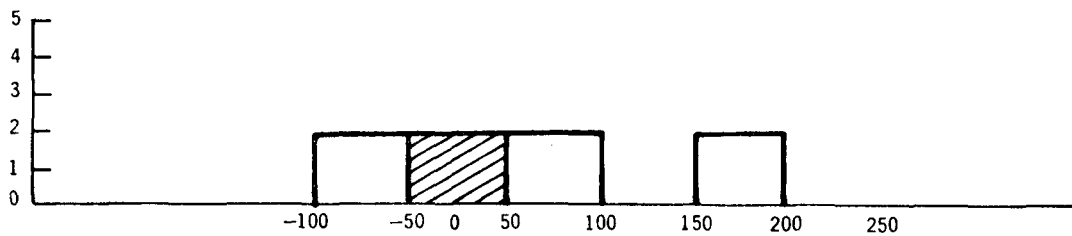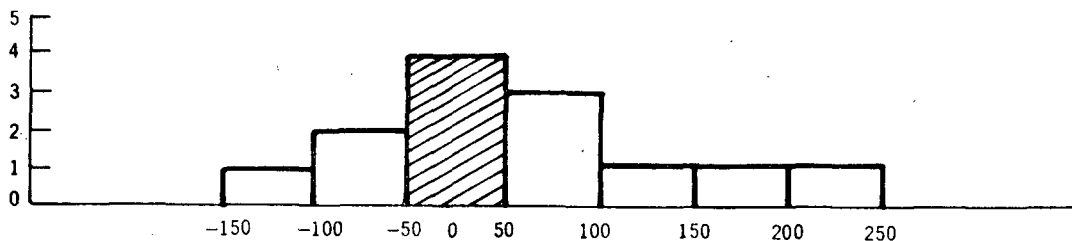Figure A-50 Central Rod Prediction Map
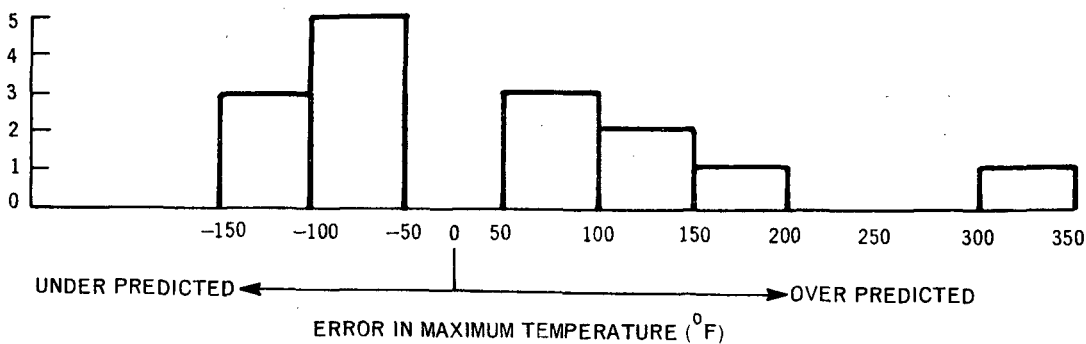
(a)   Outside Rods

(b)   Inside Rods

(c)   Central Rods

Figure A-51   Statistical Representation of Errors in Maximum Temperature Resulting
from Current Model Heat Transfer Coefficients and 50% Metal-Water Reaction

APPENDIX B
UNCERTAINTIES IN LOSS-OF-COOLANT TEST PREDICTIONS

None of the parameters used in calculating the thermal response of a Zircaloy-clad bundle under loss-of-coolant conditions is known exactly. Each of the significant variables (local power, metal-water reaction rate, convection, and radiation) is uncertain to some degree. The significance of these uncertainties is considered in this appendix. Specifically, the uncertainty in the calculated maximum temperature of an individual rod as a function of the calculated temperature is estimated. For the assumptions made (local power uncertain by ±10%, metal-water reaction rate at 0.5 ± 0.5 times that of Baker, convection coefficient = 1.0 ± 0.5 Btu/h ft² °F, and radiation heat transfer uncertain by ± 10%) the uncertainty in the calculated maximum temperature is estimated to be approximately 170°F at 2000°F and approximately 220°F at 2300°F (Figure B-4).

Energy Balance

An energy balance at the location and time of maximum temperature on a central rod is

$$P + M = C + R \tag{1}$$

where

P	=	Energy input rate due to decay power
M	=	Energy input rate due to the metal-water reaction
C	=	Energy removal rate by convection to the coolant
R	=	Energy removal rate by thermal radiation

Since the energy balance is written at the location and time of maximum temperature, there is no axial conduction and no storage term.

The terms M, C and R are functions of temperature and none can be calculated exactly. The decay power term P also has an uncertainty. We would like to estimate the uncertainty in the maximum temperature of the central rods, given the uncertainties in the individual terms. Accomplishing this, a definite "confidence" in a loss-of-coolant test calculation can be established.

From (1), we can write

$$T = T(P, M, C, R) \tag{2}$$

Uncertainty in Maximum Temperature

We now assume that the independent variables P, M, C, and R are normally distributed and estimate the uncertainty in T as

$$W_T = \left[\left(\frac{\partial T}{\partial P} W_P \right)^2 + \left(\frac{\partial T}{\partial M} W_M \right)^2 + \left(\frac{\partial T}{\partial C} W_C \right)^2 + \left(\frac{\partial T}{\partial R} W_R \right)^2 \right]^{1/2}, \tag{3}$$

where W_X is the uncertainty in the variable X. Thus, given the functional relationship (Equation 2) and estimates of the uncertainties in the individual terms, we can estimate the uncertainty in the maximum temperature T.

Partial Derivatives

Take the partial derivative of Equation (1) with respect to P to obtain $\partial T/\partial P$,

$$\frac{\partial P}{\partial P} + \frac{\partial M}{\partial T} \frac{\partial T}{\partial P} = \frac{\partial C}{\partial T} \frac{\partial T}{\partial P} + \frac{\partial R}{\partial T} \frac{\partial T}{\partial P} .$$

Then

$$\frac{\partial T}{\partial P} = \frac{1}{\dfrac{\partial C}{\partial T} + \dfrac{\partial R}{\partial T} - \dfrac{\partial M}{\partial T}} \tag{4}$$

Now differentiate with respect to M to obtain $\dfrac{\partial T}{\partial M}$,

$$\left(\frac{\partial P}{\partial M} = 0 \right) \frac{\partial T}{\partial M} + \frac{\partial M}{\partial M} = \frac{\partial C}{\partial T} \frac{\partial T}{\partial M} + \frac{\partial R}{\partial T} \frac{\partial T}{\partial M} .$$

Then

$$\frac{\partial T}{\partial M} = \frac{1}{\dfrac{\partial C}{\partial T} + \dfrac{\partial R}{\partial T}} \tag{5}$$

Similarly,

$$\frac{\partial T}{\partial C} = \frac{1}{\dfrac{\partial M}{\partial T} - \dfrac{\partial R}{\partial T}} , \tag{6}$$

and

$$\frac{\partial T}{\partial R} = \frac{1}{\dfrac{\partial M}{\partial T} - \dfrac{\partial C}{\partial T}} \tag{7}$$

It remains to establish the derivatives $\partial M/\partial T$, $\partial C/\partial T$ and $\partial R/\partial T$ so that Equation (3) may be solved.

Metal-Water Reaction Term

If the metal-water reaction proceeds at a rate of one-half that predicted by Baker, the energy addition rate can be shown to be

$$M \cong \frac{C_1}{d} e^{-C2/T^\circ R} \quad Btu/h\text{-}ft^2 \tag{8a}$$

where

$$C_1 \quad \sim 9.95 \times 10^6$$

$$C_2 \quad \sim 41,219$$

$$d \quad = oxide \ thickness, \ inches$$

From Equation (8),

$$\frac{\partial M}{\partial T} = \frac{C_1 C_2}{d(T^\circ R)^2} e^{-C2/T^\circ R} \tag{8b}$$

Convection Term

Taking convection to the coolant at saturation temperature,

$$C = h(T - 212) \ Btu/h\text{-}ft^2 \tag{9a}$$

and

$$\frac{\partial C}{\partial T} = h$$ (9b)

Radiation Term

To exactly evaluate the radiation term, a complex expression must be written. For the purposes of an uncertainty analysis, the radiation term may be approximated as follows,

$$R = h_r (T - 1750) \text{ Btu/h-ft}^2$$ (10a)

and $$h_r \approx 20$$

where the fourth power dependence on T is masked because of the radiation shielding effect caused by the inside rods. Actually, one might expect

$$R \sim T_{central}^4 - T_{inside}^4 .$$

Typically, inside rods are approximately $100°F$ cooler than central rods so that

$$\frac{R \text{ (central rods at } 2300°F)}{R \text{ (central rods at } 2200°F)} = \frac{2760^4 - 2660^4}{2660^4 - 2560^4}$$

$$= 1.14$$

which is quite close to the radio calculated using Equation (10a), i.e.,

$$\frac{R \text{ (} 2300°F)}{R \text{ (} 2200°F)} = \frac{2300 - 1750}{2200 - 1750} = 1.22.$$

Thus, Equation (10a) provides a reasonable, simple approximation for the radiation term. Differentiating Equation (10a)

$$\frac{\partial R}{\partial T} = h_r (\sim 20)$$ (10b)

Uncertainty in Maximum Temperature

Equation (3) can now be completed. The uncertainty in the maximum temperature is from Equations 3-7 and 8b, 9b, 10b:

$$W_T^2 = \left[\frac{W_P}{h + h_r - \frac{C_1 C_2}{d(T°R)^2} e^{-C_2/T°R}} \right]^2$$

$$+ \left[\frac{W_M}{h + h_r} \right]^2$$

$$+ \left[\frac{W_C}{\frac{C_1 C_2}{d(T°R)^2} e^{-C_2/T°R} - h_r} \right]^2$$

$$+ \left[\frac{W_R}{\frac{C_1 C_2}{d(T°R)^2} e^{-C_2/T°R} - h} \right]^2$$ (11)

To attach a physical significance to Equation (11), we might think of the exponential as a "metal-water" coefficient, h_m, that is, a mechanism for adding energy. We then rewrite Equation 11 as

$$W_T^2 = \left(\frac{W_P}{h + h_r - h_m}\right)^2 + \left(\frac{W_M}{h + h_r}\right)^2 + \left(\frac{W_C}{h_m - h_r}\right)^2 + \left(\frac{W_R}{h_m - h}\right)^2 \tag{11a}$$

Note that the power uncertainty W_P is compared to a "net removal coefficient" $h + h_r - h_m$ and the other three uncertainties (in the temperature dependent terms) are compared to coefficients by which energy is removed (in the case of metal-water uncertainty) or by which energy is added (in the case of convection and radiation uncertainties).

Evaluation of Energy Terms

We now return briefly to the energy balance (Equation 1) and evaluate the individual terms at several temperatures so that we may determine the uncertainty in T as a function of T.

Calculate the terms at 2300°F:

From Equation 8a,

$$M = \frac{9.95 \times 10^6}{0.0023} e^{\frac{41,219}{2760}} = 1440 \text{ Btu/h-ft}^2$$

where we estimate the oxide thickness from Figure B-1

From Equation 9a,

$$C = 1.0 (2300 - 212) = 2088 \text{ Btu/h-ft}^2$$

where we have taken a nominal h of 1.0 Btu/h-ft² °F.

From Equation 10a,

$$R = 20 (2300 - 1750) = 11,000 \text{ Btu/h-ft}^2$$

Then from the energy balance

$$P = R + C - M = 11,638 \text{ Btu/h-ft}^2,$$

which is a reasonable heat flux resulting from decay power.

In a similar manner, Figure B-2 can be established. The figure gives the approximate value of the four energy terms as a function of temperature, subject to the approximations and assumptions made previously.

Given an estimate of the accuracies of the individual terms we can estimate the individual uncertainties and the uncertainties in T. The accuracies are estimated as follows (~ 10:1 odds)

Term	Accuracy
P	±10%
M	±100%*
C	±50%**
R	±10%

The uncertainty is the accuracy times the value of the term at a particular temperature.

We can now calculate the uncertainty in T from Equation (11) at various temperatures. The individual uncertainties resulting from each variable (R, M, C, P) are plotted against temperature in Figure B-3. Note that the

* Here we allow the reaction to proceed at from 0 to 1.0 times the rate predicted by Baker. This is not intended to imply that zero metal-water reaction is possible. The assumption is made for the purposes of the present calculation (where a normal distribution is required) only.
** With a nominal h = 1.0, we allow for 0.5 < h < 1.5.

DATA FROM BUNDLES Zr 3M & Zr 4M

ASSUMED ZrO$_2$
THICKNESS vs
MAXIMUM TEMPERATURE

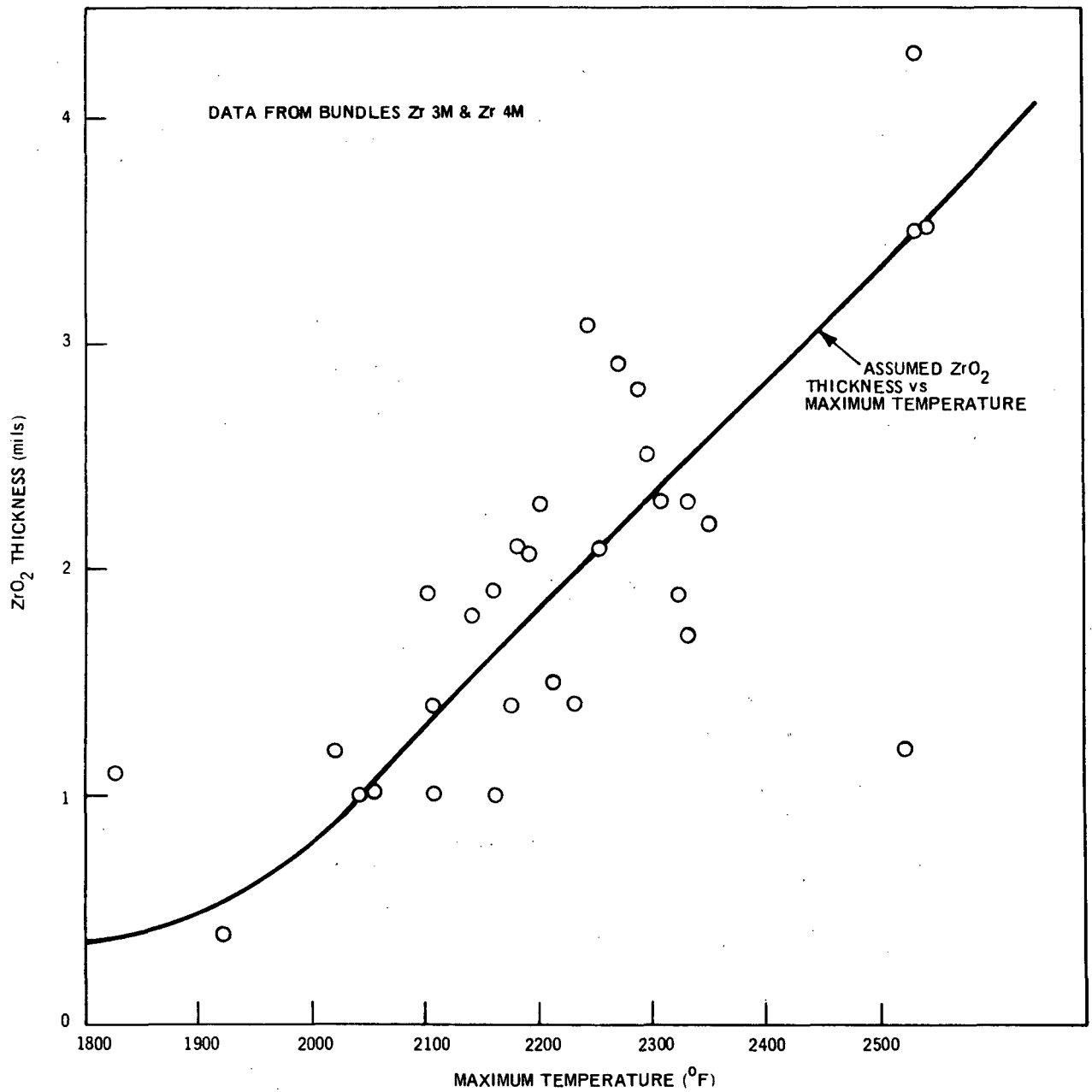ZrO$_2$ THICKNESS (mils)

MAXIMUM TEMPERATURE (^{o}F)

Figure B-1   ZrO$_2$ Thickness as a Function of Maximum Temperature
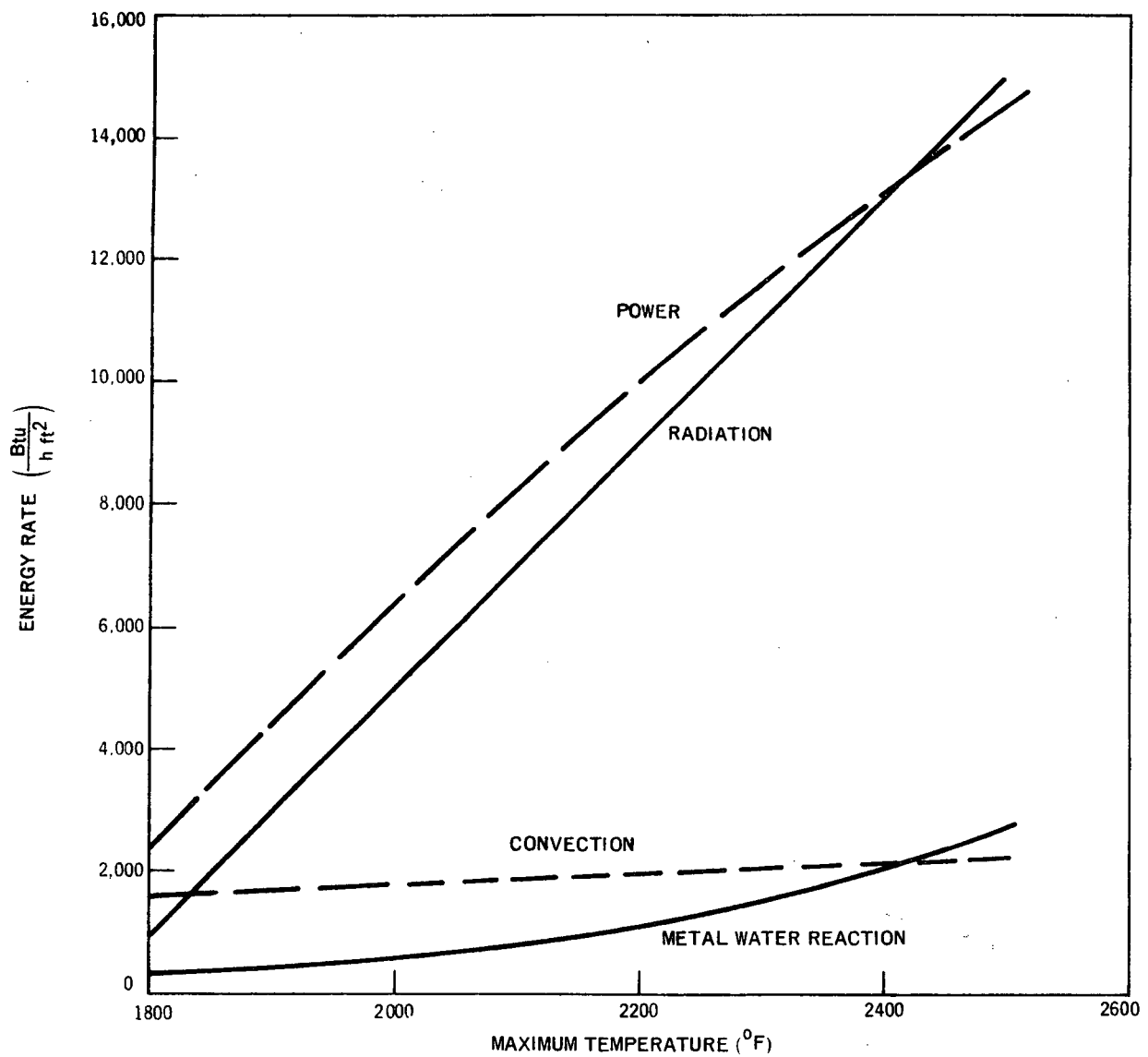
Figure B-2   Approximate Energy Addition and Removal Rates in a Loss-of-Coolant Calculation
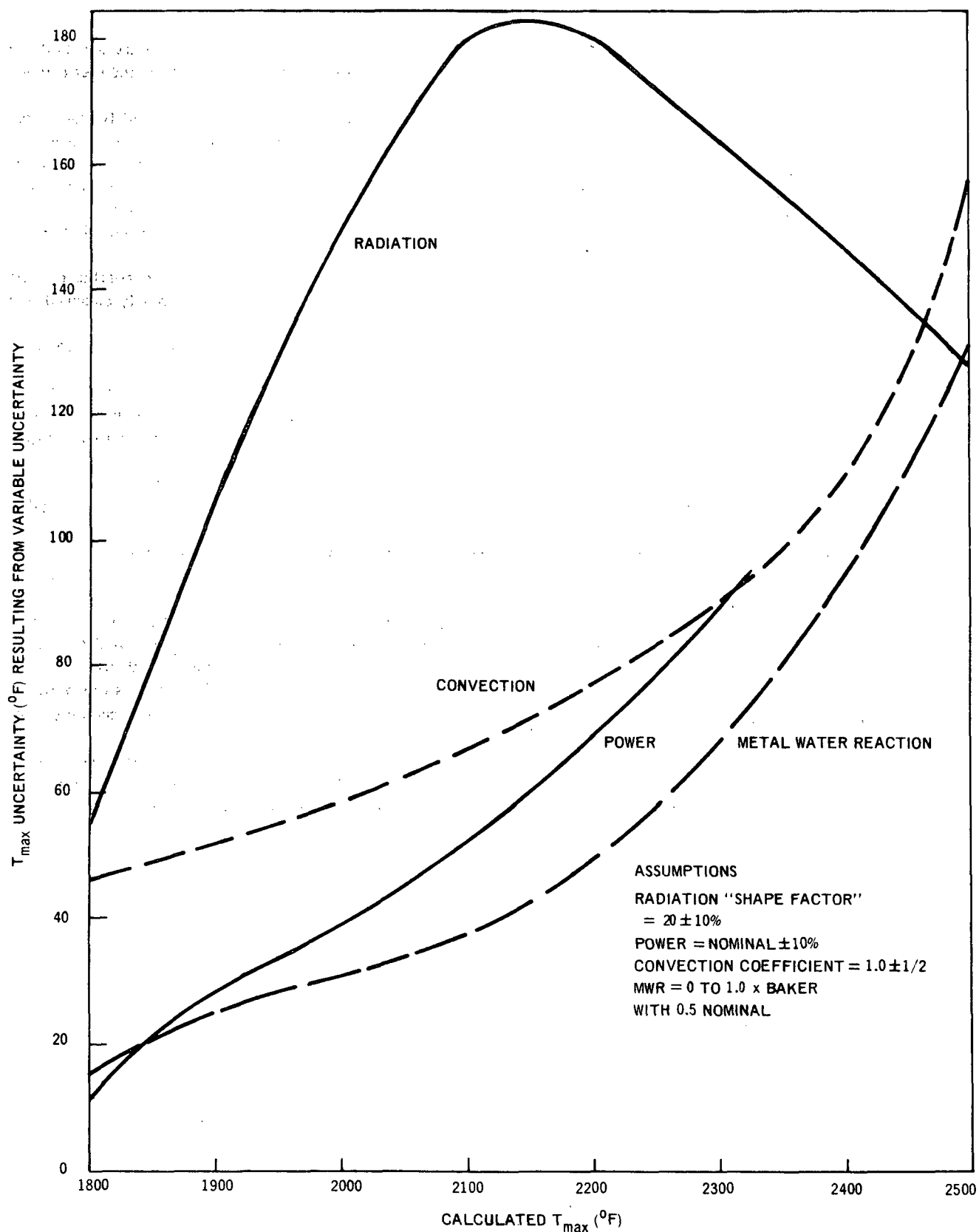
Figure B-3   Uncertainty in T_{max} Resulting from Uncertainties in Each Energy Rate Variable

significance of uncertainties in convection, power and metal-water reaction increase with temperature and that the significance of uncertainty in radiation peaks at ∼ 2150°F. The following physical explanations for these effects are offered:

a. Power — As the calculated maximum temperature is increased, more power is required to satisfy the energy balance (physically, the higher power causes the higher temperature). Thus, W_P (the numerator of the power term in Equation 11) increases. Further, at high temperatures, the metal-water reaction energy addition coefficient (the exponential in the power term) approaches the energy removal coefficient $(h + h_r)$. Thus, with these coefficients nearly balanced, power becomes more important in determining the maximum temperature.

b. Metal-Water Reaction — Since the metal-water reaction rate increases with temperature, an uncertainty in the rate constant becomes more important as the temperature increases.

c. Convection — At high temperatures, the metal-water coefficient approaches the radiation coefficient (the denominator in the convection term becomes smaller). Thus, with these coefficients more nearly balanced, the importance of an uncertainty in the convection term increases.

d. Radiation — The peak in the radiation curve on Figure B-3 is difficult to explain on a physical basis. In Equation (11), W_R increases with temperature, so that at $T < 2100°F$ the uncertainty in T increases with T. However at about 2100°F, the exponential in the denominator of the radiation term begins to dominate the $(1/T)^2$ and the denominator increases rapidly as temperature is further increased. Thus, the peak in the radiation curve on Figure B-3 seems to result from the character of the metal-water reaction. It may be, however, that the approximation made for radiation heat transfer,

$$R = h_r (T - 1750) \tag{10a}$$

becomes quite poor at $T \gtrsim 2200°F$ and that the peak in Figure B-3 results from this approximation.

Total Uncertainty in Calculated Maximum Temperature

We now solve Equation (11) and estimate the uncertainty in a calculated maximum temperature as shown in Figure B-4. Figure B-4 is intended to represent an approximation of the uncertainties in a test case. Figure B-4 does not necessarily apply to a reactor loss-of-coolant calculation for several reasons, the most important of which are:

a. Reactor calculations are made assuming 100% of the Baker rate constant. The actual constant is not normally distributed about this value so that Equation (3) does not apply. Thus, an uncertainty in this term can only cause the calculated temperature to be higher than the actual temperature.

b. Conservative assumptions are made in the reactor calculation regarding the local power. That is, a value higher than that most likely is assumed. Thus, the local power is not distributed normally and an overprediction of maximum temperature, resulting from a power uncertainty, is more likely than an underprediction.
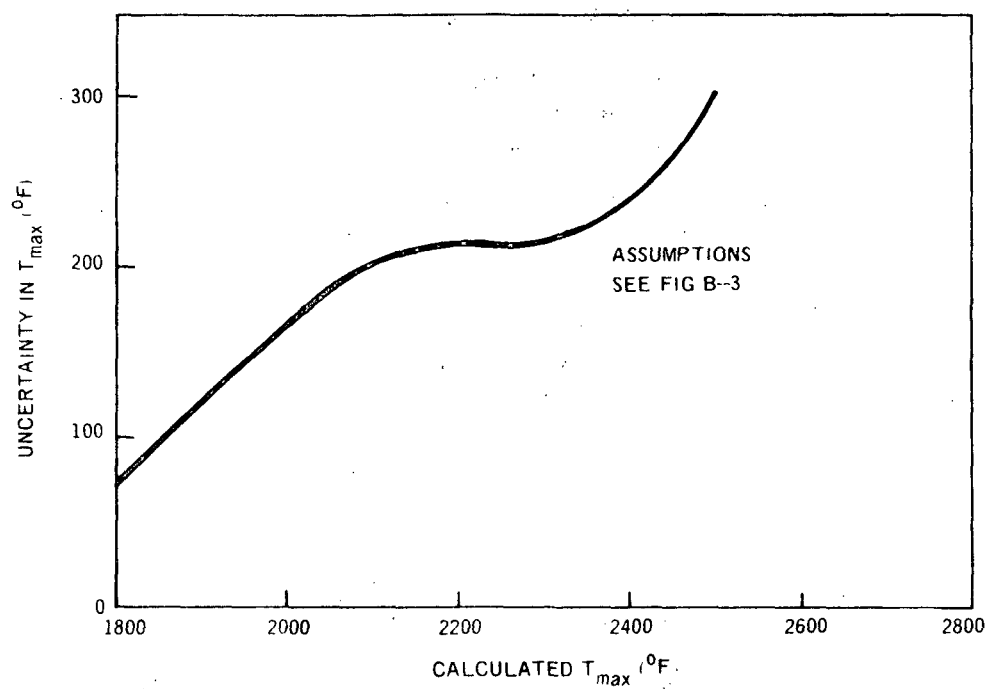
Figure B-4   Maximum Temperature Uncertainties

ACKNOWLEDGEMENTS

EXTERNAL DISTRIBUTION

R. W. Griebe   150
Idaho Nuclear Corporation
P. O. Box 1845
Idaho Falls, Idaho   83401

INTERNAL DISTRIBUTION

NAME	M/C	NAME	M/C
R. G.Bock	583	B. C. Slifer	662
J. D. Duncan (30)	662	G. L. Sozzi	584
C. M. Foster	583	W. A. Sutherland	584
E. J. Hanna	632	H. E. Williamson	155
J. E. Hench (2)	662	NED Library (5)	328
P. W. Ianni	662	VNC Library (2)	VNC-102
J. E. Leonard (2)	583		
D. J. Liffengren (2)	662	**CIRCULATED**	
A. E. Rogers	662		
R. R. Roof (3)	126	A. P. Bray	633
J. P. Rocchio (5)	831	D. H. Imhoff	588
F. A. Schraub	583	J. E. Torbeck	583

very good! print asap — and get strategy for comm w/ry

To Lankins — ASAP

Keep Ernst informed!!,

comment by Ross

be sure and study ALAB675 and talk to Scinto (Ernst) on "credible" or scenario

MEMORANDUM FOR: Roger Mattson, Director
Division of Systems Integration
Office of Nuclear Regulatory Research

FROM: O. E. Bassett, Director
Division of Accident Evaluation
Office of Nuclear Regulatory Research

SUBJECT: ANALYSIS OF HYDROGEN RELEASE RATES FOR DEGRADED CORE ACCIDENTS FOR BOILING WATER REACTORS

As part of the RES programs on severe accidents, source term re-evaluation and rulemaking activities on hydrogen control a number of core heat-up and hydrogen release analyses have been performed using the core melt-down analysis code MARCH and to a much lesser degree the preliminary version of the severe core damage assessment code SCDAP. As you are aware, the earlier calculations done by Battelle Columbus Laboratory (BCL) and published in NUREG/CR-2540 in support of the proposed interim rule on hydrogen control for ice condenser and MARK-III plants were done using the earlier version of MARCH or version 1.1 as it was title. More recently calculations of various core melt sequences have been run by BCL and Oak Ridge National Laboratory (ORNL) with an updated version of the code (MARCH 2.0) for two BWR plant designs. Although significant changes were incorporated in MARCH 2.0 (Appendix A) the ranges of hydrogen flow rates observed in the degraded core studies are similar to those calculated in the core meltdown analyses (0-200 lbs/min.). As discussed below the hydrogen flow rates are very dependent upon accident sequence definition and the assumptions that go into the analyses. The preliminary SCDAP calculations (EGG-NTAP-6148) give somewhat lower hydrogen release rates, however, the calculations are limited to the early phases of core heat-up and stop at the on set of fuel melt. A more recent version of SCDAP corrects this limitation and with completion of coding verification a number of these analysis will be re-done.

The BWR sequences studied at BCL and ORNL included the following accident sequences: S_2E, S_1E, TQUV (done for NUREG/CR-2540); AE, TW, TC, station blackout and scram discharge volume break for the MARK I and TQUV, TPI and TC for the MARK III. The assessment of accident sequences likelihood indicates that transients sequences (in particular TC, TW and TQUV) are more likely than

need a table explaining acronyms.

or restored

pipe break sequences with associated failure of emergency core cooling (e.g. the Grand Gulf RSSMAP study assigns a frequency of 5.4 x 10^{-6} and 1/5 x 10^{-6} for TW and TQUV respectively). The reason for this is the diversity of water supplies potentially available in the event of a pipe break. While a wide variety of partial and complete failure modes for engineered safety systems can be postulated, in PRA's core meltdown sequences are generally analyzed with complete los of function for failed equipment rather than considering a spectrum of degraded modes. In contrast, the degraded core sequences to which the hydrogen rule applies always involve some level of ESF performance since they are by definition eventually arrested. Here again, however, an endless *right'* variety of partial degradation, timing of restoration, rate of restoration, etc., can be postulated. The likelihoods of degraded core sequences have not been estimated. It is generally believed that degraded core sequences are more likely than complete core meltdown accidents. The existence of the TMI-2 accident may provide some evidence that this is tre. It is also not clear whether there are close parallels between the core meltdown sequences and degraded core sequences. For example, TQUV is a core meltdown sequence that is believed to be comparatively likely. There could be an important degraded core sequence that is an analog to TQUV but in which ECC recovery occurs before the core is completely lost. Experience indicates, however, that real accident sequences do not follow the stylized scenarios that are layed out in PRA's. Actual accidents have frequently involved multiple failures, partial operation of systems, and operator actions that have in effect shifted the sequences from one accident pathway to another. It would not be suprising therefore to encounter very complex degraded sequences that involve varied levels of ECC performance, rising and falling water levels, and varied pressure in the RCS.

Two very important considerations that are necessary in a degraded core accident analysis are: (1) at what stage of the accident is the core so severely damaged that it is no longer coolable and (2) at what stage of fuel melt have you gone from a degraded core accident to a core melt accident. If one uses the accident at TMI-2 as the definition of a degraded core accident, then we have limited considerations to senarios where essentially we have no fuel

why so low?

melted (core s̸p̸ats below 4700°), but we stil̸l̸ generate significant quantities
of hydrogen (up to 75% of the cladding).⇀ In the analysis performed with MARCH
1.1 and 2.0, melting is initiated at 4130°F and fuel slump is set to occur
when 75% of the fuel reaches melt temperature. This is inconsistent with a
degraded core accident sequence since a large coherent pool of molten fuel
cannot be cooled by transferring heat from the surface. Once melting begins,
the uncertainty in the geometry of the fuel becomes great for large fractions
of core melting, it is not possible to predict whether the core is uncoolable.

Recently, BCL reviewed several previous MARCH analysis considering 10% fuel
melting as a reasonable upper bound for the extent of melting in a degraded
core accident. For these sequences, the maximum values ranged from 6 lbs/min.
to 50 lbs/min. How reasonable this number is an upper limit is uncertain, for
sever reasons. The number of sequences was limited and did not include partial
ECC performance sequences that could lead to protracted core degradation and
limited fuel melting but provide a continued source of water to produce steam
to feed the metal water reaction and the possibility of enhanced released
rates upon quenching was not considered. These calculations were performed
with the version of MARCH which does not include explicit treatment of the BWR
channel box. The cladding was artifically thickened in the analyses to account
for channel box zirconium. Based on analyses by ORNL where the channel boxes
are modeled explicity this may lead to an overestimation of the rate of oxida-
tion by approximately 25%. This overestimate is undercertain for at least two
reasons (1) the uncertainty in the temperature lag between the channel box and
cladding and (2) the uncertainty in the time-temperature lag between the fuel
and cladding at temperatures above 2500°F. It is generally accepted that the
channel boxes will be somewhat lower in temperature and the reaction rate will
be lower and in the second consideration, if the fuel on an average follows
the cladding at temperature *by a few hundred degrees* above 2500°F, then you may get more oxidation
occurring before you reach your calculated fuel melt temperature and terminate
the analysis.

There are additional counter acting forces, which are not modeled in MARCH.
Once local melting of zirconium occurs the rate could be reduced by runoff to

ask
Norm
Tauber
or
Bill
Belkoor

*about severe heatup experiments done 10-12 yrs
ago (BWR-FLECHT) @ GE with elect
htrs and Zr channel boxs*

(e.g. by spallation),

colder regions or increased by the exposure of oxidized surface to the steam. Consideration of these effects can be done by the analyst in the selection of MARCH inputs. The latest version of SCDAP includes modeling of all these phenomena.

Another illustrative case of the effects of accident sequence definition and analysis assumption is in the loss of injection case (TQUV) recently reportly by ORNL (NUREG/CR-3179). This study was done with the improved BWR models (channel boxes, control blades, SRVs, properties) in MARCH 2.0. In this sequence the reactor vessel injection capability by the ECCS systems and the RCIC is lost at the time of scram. Without CRD hydraulic system injection, the core is uncovered at time 28 min, core melting begins at time 97 min. with core slump at 143 min. 17.9% of the Zr in the cladding and 6.7% of the ZR in the control boxes is reacted at the time of core slump. If there is also a SORV, then core uncovery occurs at 17 min. core melt at 73 min, slump at 111 min and 28% of the clad and 10.4% of the control boxes are reacted. With operator action to enhance the injection capacity of the CRD hydraulic system, there is a temporary period of core uncovery but melting is averted and the core is recovered. Without operator action the effect of the CRD hydraulic system is to dely but not prevent core melting and slump. The following table shows the fraction of ZR reacted for the cases without operator action but with CRD flow.

Case	Core Uncovery (min	Melting (min)	Slump (min)	% Clad	% Box
No operator action 6.1	37	105	276	20.7	6.1
Same, with SORV	19	80	206	45.5	12.3

The actuation of the automatic depressurization system (ADS) would have a significant effect on the couse of this accident. Without a SORV the release rate can be relatively high (a few hundred lbs/min.) however this would be for short periods of time as the safety releif valves would provide periodic blowdowns during this period after core uncovery. In the case of a SORV there would be lower rates of release, but they would be continuous.

Because of the noted uncertianties in degraded core sequence analysis and because of the large quantity of hydrogen produced in the TMI-2 accident, a

total production equivalent to 75% reaction of the clad is reasonable bound
for degraded core sequences. There appears to be little basis for reducing
this number for BWRs at this time. In terms of the rate of release of
hydrogen for degraded core accidents, there could be a basis for reducing the
rate below those ranges in NUREG/CR-2540 if a maximum level of core melting is
associated with degraded core accidents. A range of 25-75 lbs/min might be
reasonable, however, this should probably be verified by some additional
analysis with different levels of ECC performance using both MARCH and SCDAP.
We would also recommend a review meeting of these analysis upon their com-
pletion.

APPENDIX A

MARCH 2 IMPROVEMENT

An improved zircaloy-steam model has been incorporated in MARCH 2. Some of the features which have been included are:

1. Improved physical modeling for solid-state oxidation (Urbonic-Heidrick) to account for the high temperature ZrO_2 phase transformation,

2. Improved geometric modeling for gaseous diffusion oxidation,

3. Chemisorption/dissociation retardation due to high hydrogen partial pressures,

4. Laminar and turbulent flow conditions,

5. Automatic timestep contraction and expansion within a MARCH timestep.

6. Explicit treatment of the BWR channel boxes, control blades, SRVs and improved thermal-hydraulic property tables.

0.738 in. PITCH

ROD NUMBER

0.562 in. O.D. RODS

0.400 in. R
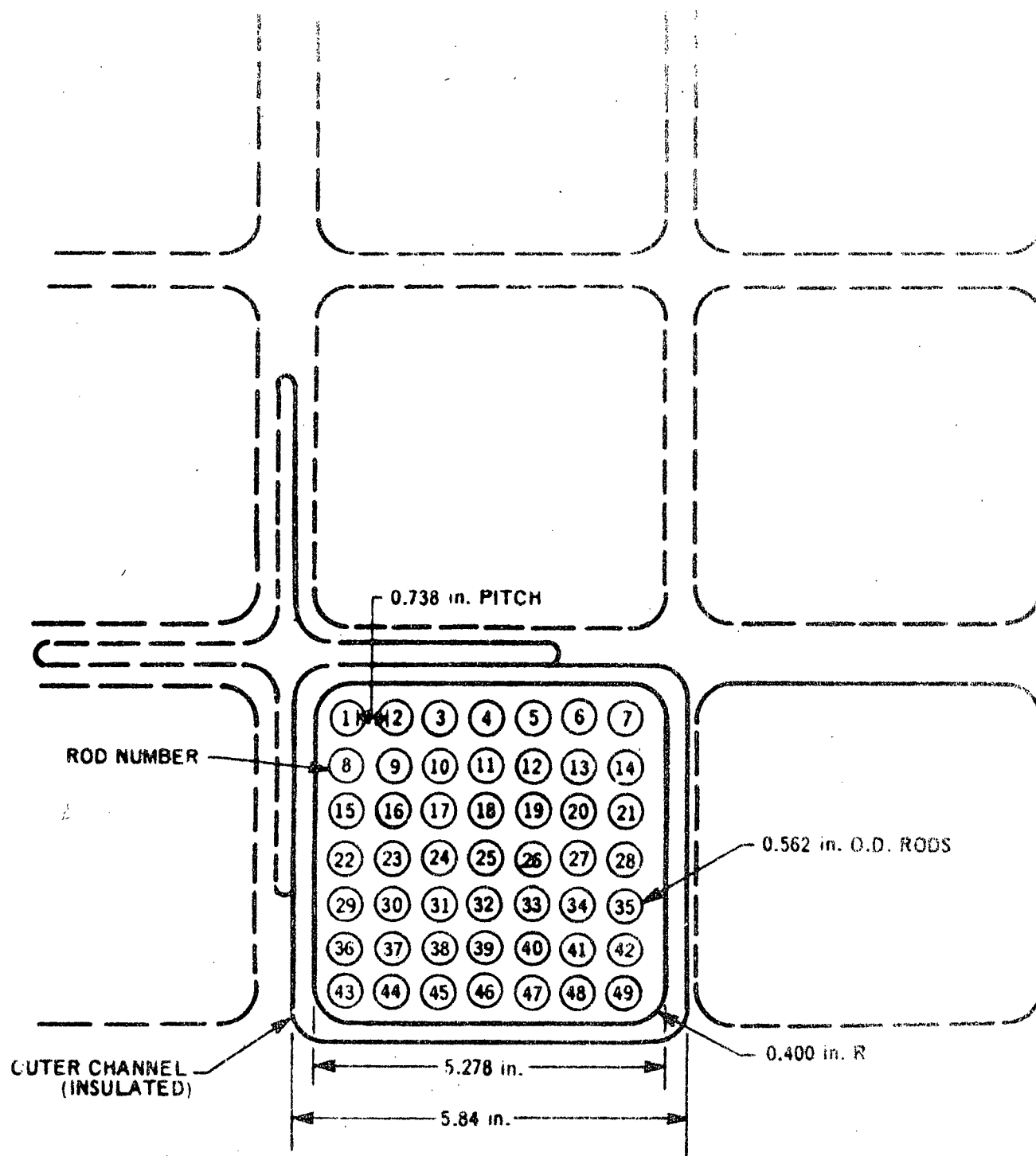
OUTER CHANNEL
(INSULATED)

5.278 in.

5.84 in.

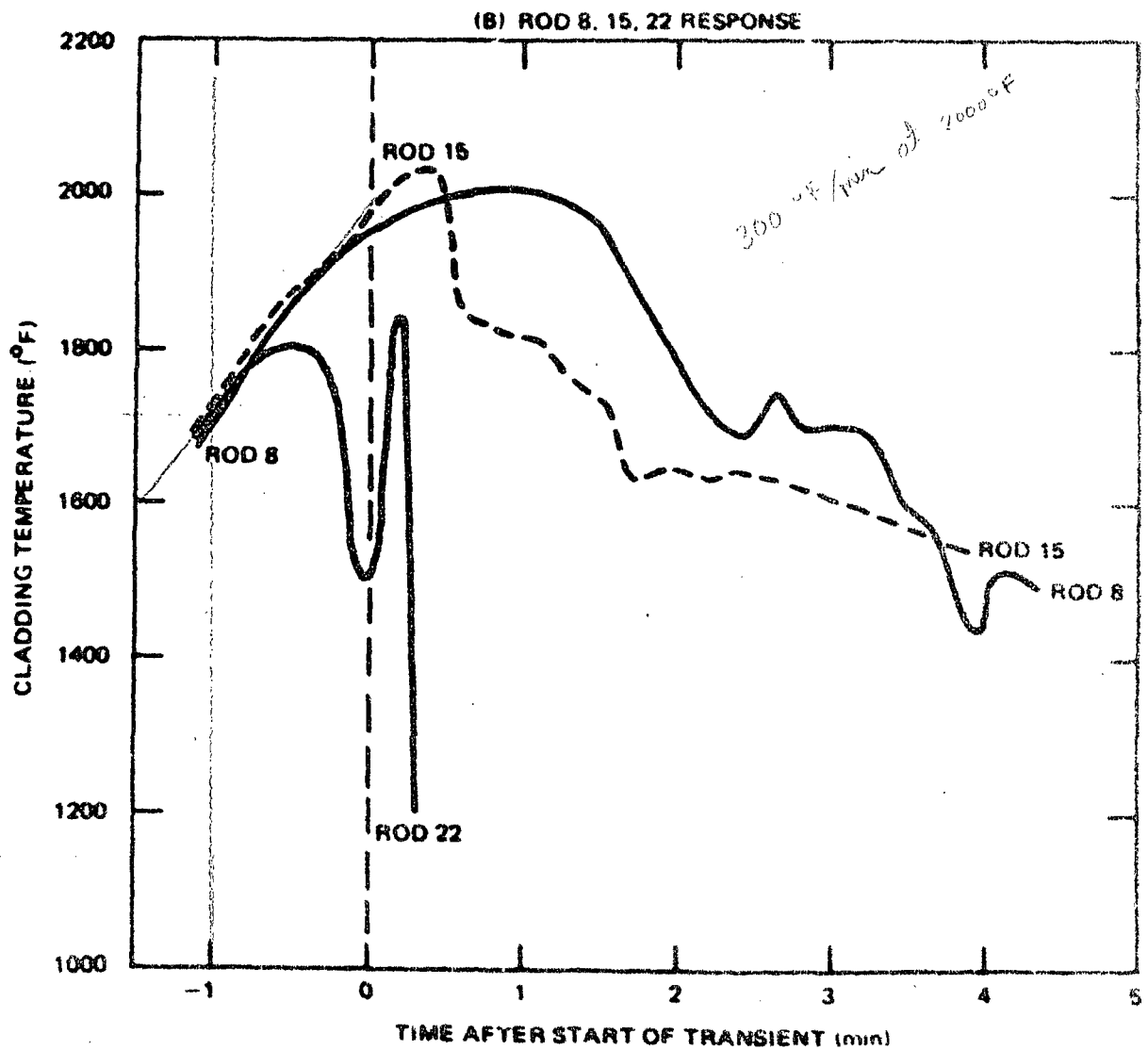Figure 2.   Comparison of Test Section and Reactor Geometry
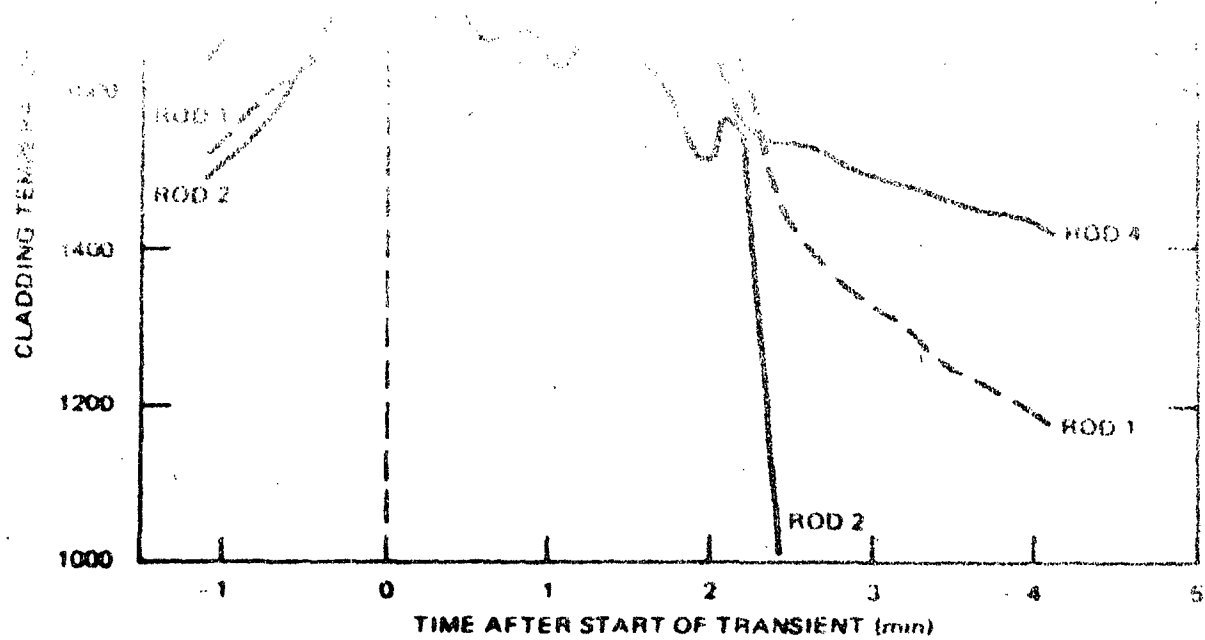
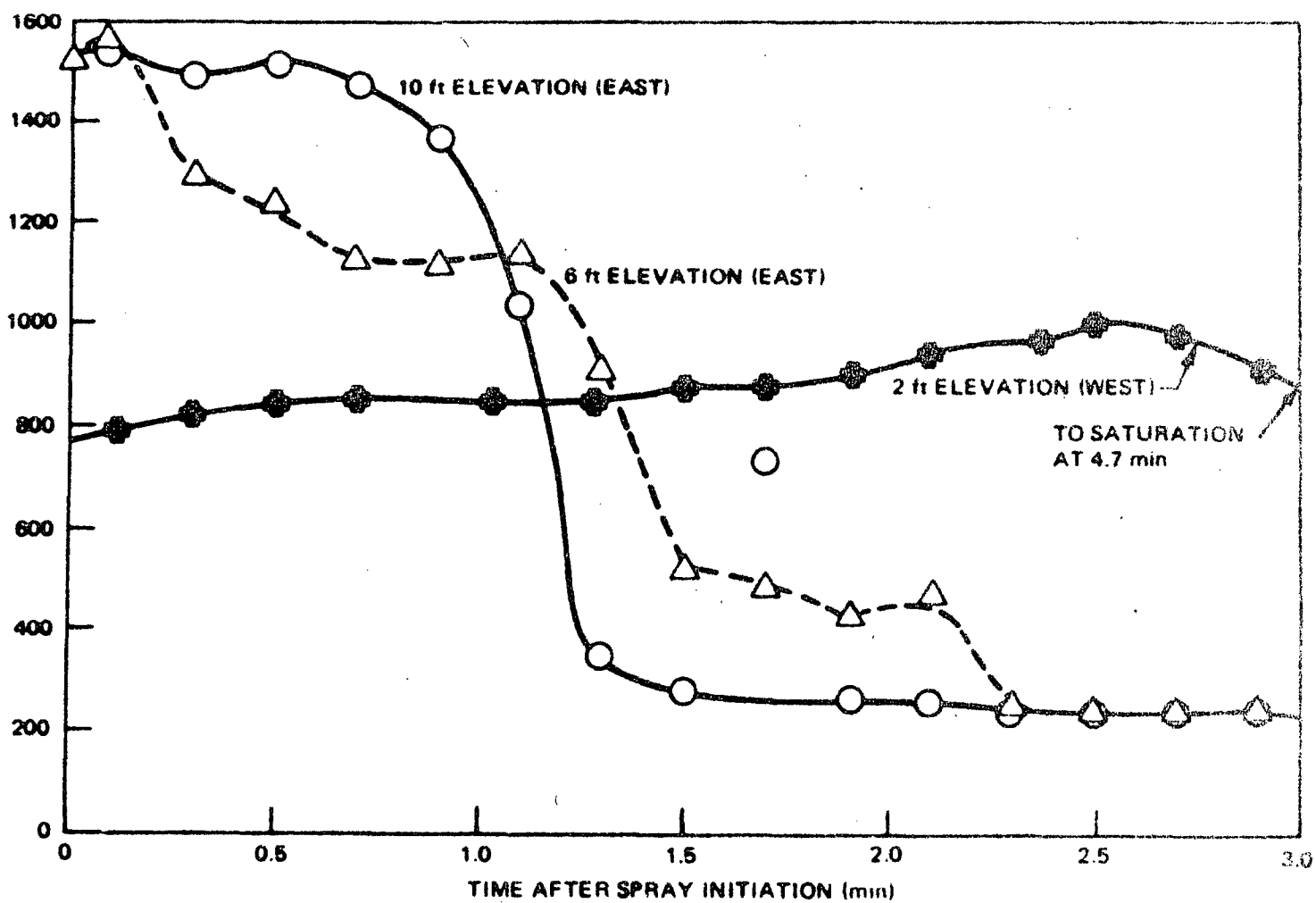Figure 15. Midplane Thermal Response of Outside Rods in Bundle Zr-4 Spray Transient

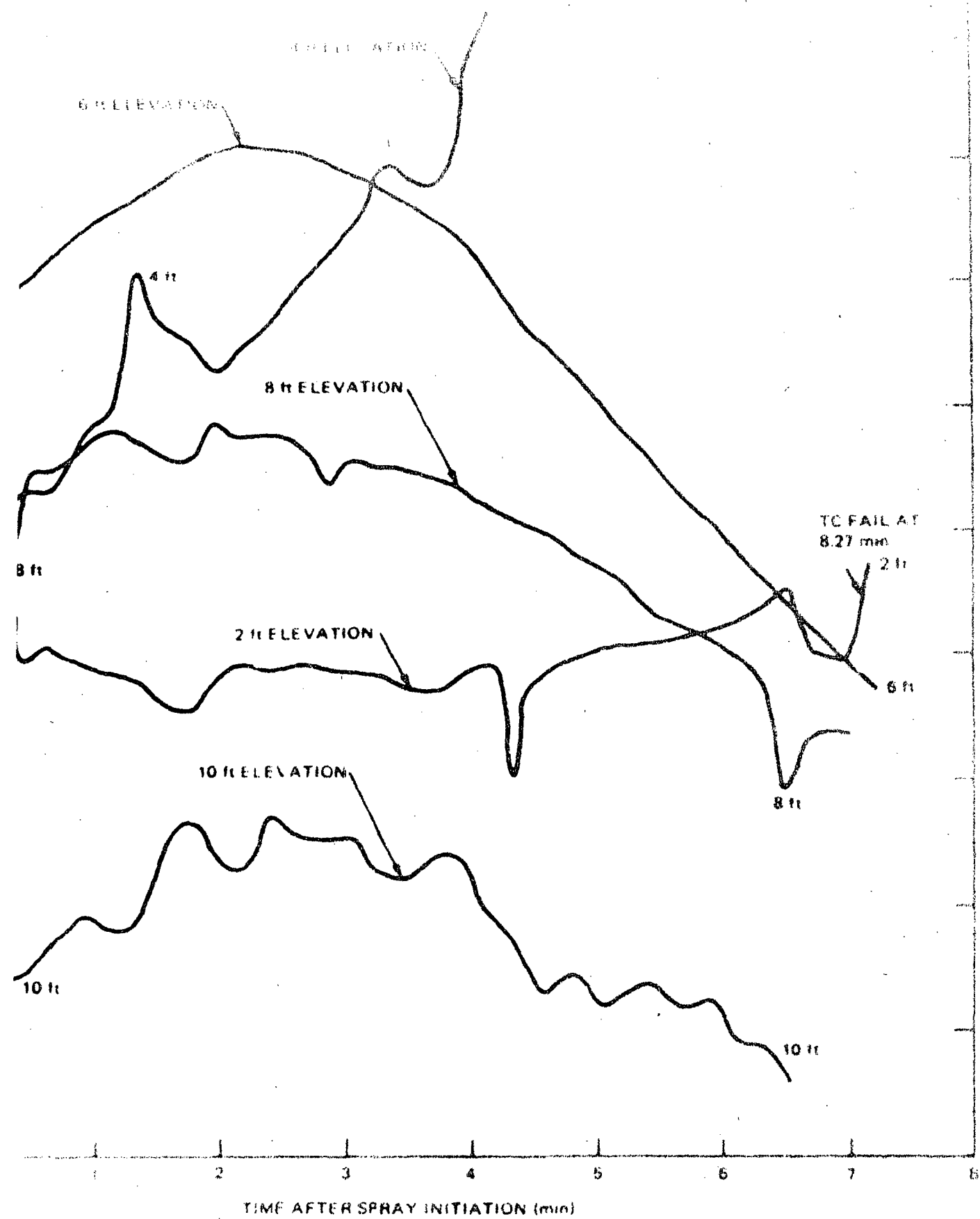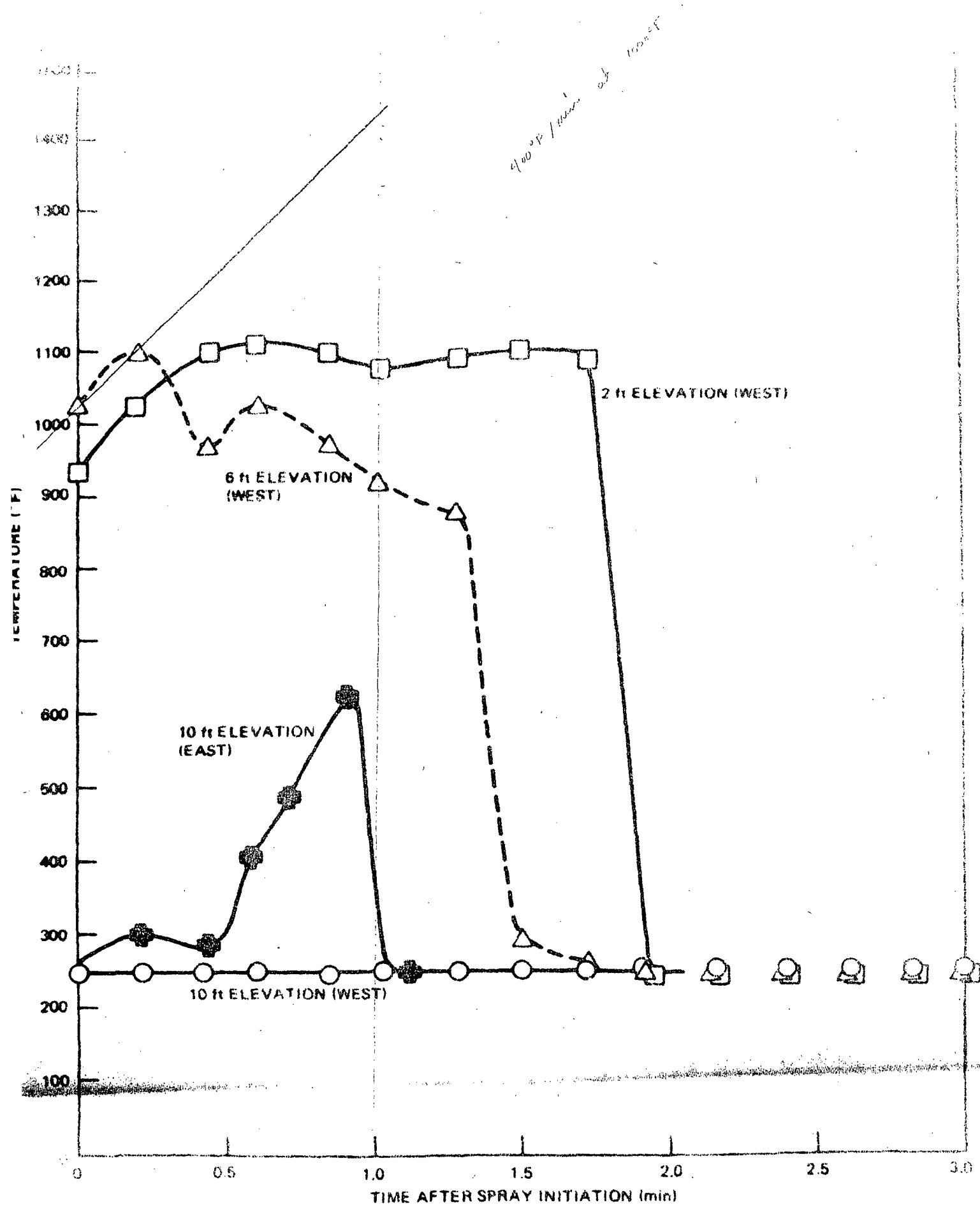Figure 24.   Zr-3 Channel Cooling

Figure 19   Rod 25 Response During Zr-4 Transient

Figure 25. Zr-4 Channel Cooling